Università degli Studi “Roma Tre” Department of Science

PhD Thesis in

Sciences of Material and Nanomaterials XXXVII Cycle

DESIGN AND SYNTHESIS OF POLY(2-OXAZOLINE)S-BASED ADSORBENTS FOR WASTEWATER REMEDIATION

Supervisor

PROF. TECLA GASPERI

Candidate

LUCA STEFANUTO

Coordinator

PROF. MARCO BARBIERI

July 2025

ABSTRACT

Wastewater contamination by a wide range of organic and inorganic pollutants, including pharmaceuticals and heavy metal ions, poses significant risks to human health and ecological systems. This doctoral thesis presents the design, synthesis, and characterization of novel, highly efficient adsorbents based on poly(2-oxazoline)s for wastewater remediation. The core strategy involved designing polymers to selectively interact with different classes of pollutants and immobilizing these polymers onto solid supports, such as Graphene Oxide and cellulose, to ensure water insolubility and facilitate their recovery and regeneration after adsorption experiments.

Specifically, a novel 2-oxazoline monomer bearing a diphenyl moiety was synthesized and subsequently polymerised via Cationic Ring-Opening Polymerisation to yield the homopolymer. This new polymer demonstrated remarkable efficacy in adsorbing hydrophobic organic pollutants from spiked aqueous solutions, exhibiting a direct correlation between removal efficiency and the pollutant's hydrophobicity. To address acidic pharmaceutical contaminants, a novel composite material was developed by covalently linking a pre-synthesised poly(2-oxazoline) bearing amine moieties onto Graphene Oxide following a "*Grafting To*" methodology. The resulting GO-pAmOx, after characterization with TGA, ATR-FTIR, AFM, and TEM-EELS analyses, was employed in separate adsorption experiments against the most common pharmaceutical compounds detected in wastewater, demonstrating superior adsorption capacities selectively for acidic drugs (ketoprofen, aspirin, and ibuprofen) compared to unmodified GO. A phenomenon attributed to the specific acid-base interactions between the polymer's amine moieties and the drugs' carboxyl groups. For the removal of heavy metal ions, a "*Grafting From*" methodology was successfully employed to synthesize cellulose-poly(2-oxazoline) composite materials starting with three different decorated 2-oxazoline-based monomers. After confirming the successful growth of the corresponding poly(2-oxazoline) polymer onto cellulose with ATR-FTIR and TGA, these composite materials were separately employed in adsorption experiments targeting harmful heavy metal ions, demonstrating not exclusively the higher efficiency of the composite with the poly(2-oxazoline) decorated with carboxyl group, but also the higher efficiency of all the composites respect to native cellulose against the majority of heavy metal ions employed.

In conclusion, this research successfully demonstrates the versatility of the poly(2-oxazoline)s for realizing specialized, high-performance adsorbents. By rationally designing monomers and selecting suitable solid supports, this work presents three distinct, reusable, and effective systems for the selective removal of hydrophobic pharmaceuticals, acidic organic compounds, and heavy metal ions from aqueous environments, paving the way for the development of advanced materials for targeted environmental remediation.

Summary

1. Introduction

Water is indispensable to both humans and wildlife, and the functioning of the world depends upon the availability of clean water.[1] While approximately 71% of the Earth's surface is covered by water, the vast majority is saline, with freshwater resources (constituting a mere 3% of the total amount) disproportionately sequestered in ice caps and glaciers (68.7%), subterranean aquifers (30.1%), and surface water bodies (a scant 0.3%).[2] Nowadays, a continuous increase in water demand is observed as a consequence of demographic growth, escalating industrial requirements, and evolving standards of living.[3] Indeed, the Organization for Economic Co-operation and Development (OECD) projected in 2012 a global increase in water demand of 55% between 2000 and 2050, mainly as a function of burgeoning needs of manufacturing (+400%), thermal power generation (+140%), and domestic consumption (+130%).[4] Moreover, it was estimated that 1.8 billion individuals will reside in regions experiencing scarcity by 2025, while two-thirds of the world's population will be inhabiting water-stressed areas.[5] Decreasing water quality, caused by increasing and newly emergent pollutants, also became an important reason for restricting the availability of water suitable for safe utilisation by both natural systems and human populations, aggravating the water scarcity problems.[6] These contaminants encompass a broad spectrum of species, ranging from inorganic heavy metals to a diverse array of organic compounds, including personal care items, endocrine disrupting substances (EDCs), polycyclic aromatic hydrocarbons, herbicides, insecticides, and synthetic dyes. Exposure to these pollutants can engender severe and far-reaching health consequences.[7]

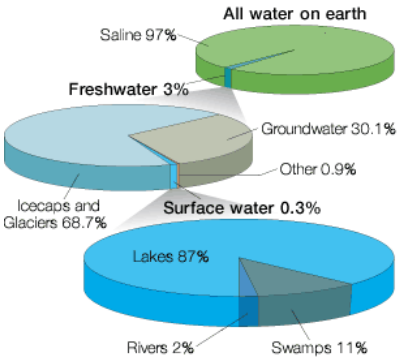

Figure 1 Amount of water present on Earth.

1.1 Water pollution

Aquatic pollution, the contamination of water bodies encompassing lakes, rivers, oceans, aquifers, reservoirs, and groundwater, is predominantly anthropogenic in origin and exerts deleterious effects on legitimate water uses, thereby reducing the capacity of these systems to provide essential ecosystem services.[8] The aetiology of aquatic pollution can usually be attributed to four principal sources: sewage, industrial effluents, agricultural runoff, and urban stormwater. Furthermore, releasing inadequately treated wastewater into natural waters can instigate the degradation of these aquatic ecosystems. The ecological ramifications of aquatic pollution are profound. Contaminants can disrupt the natural balance, leading to the decline of aquatic species and the degradation of habitats. This affects the overall health of the environment and can have cascading effects on human health and economic activities that rely on clean water. Pollutants can be broadly categorised into inorganic compounds such as heavy metal ions, and organic molecules.

1.1.1 Inorganic pollutants

Notably, heavy metals such as lead (Pb), mercury (Hg), nickel (Ni), cadmium (Cd), chromium (Cr), and arsenic (As), while detectable even in trace concentrations, pose significant hazards and may be released into aquatic environments as a consequence of insufficient and inadequate wastewater treatment. Major sources of these pollutants include: plating and electroplating industry, battery manufacturing, pesticide production, mining, rayon industry, metal rinse processes, tanning, fluidized bed bioreactors, textile production, metal smelting, petrochemicals, paper manufacturing, and electrolysis applications.[9] The non-biodegradable nature and potential carcinogenicity[10–13] of heavy metals underscore the critical health risks posed to living organisms by their in water at concentrations exceeding permissible limits. Major sources and effects of the most harmful and commonly detected heavy metal ions are presented in **Table1**.

Table 1 : Toxic Elements Commonly Present in Municipal and Industrial wastewaters.

Element	Source	Adverse Effect
Arsenic (As)	Pesticides, Chemical wastes, Mining biproducts	Enzyme-inhibitor, Carcinogenic
Cadmium (Cd)	Industrial discharge, Metal plating, Ni-Cd batteries, Mining waste	Causes high blood pressure, kidney malfunctioning, anaemia, disorder of bone marrow
Chromium (Cr)	Metal plating industries, Tanning process.	Carcinogenic
Lead (Pb)	Plumbing, mining, coal, gasoline	Causes anaemia, kidney malfunctioning, nervous disorder
Mercury (Hg)	Mining, industrial waste, coal.	Highly toxic

The heavy metal ion toxicity depends on their concentration, oxidation state, and the possibility to react forming toxic metalloorganic compounds. Specifically,

- Arsenic (As) can exist in four valence states: -3, 0, +3 and +5. As (V) is generally stable form in the oxygenated environment, and As (III) compounds are highly toxic. Under natural conditions, the highest concentrations of arsenic are found in groundwater because of the influence of rocks such as arsenopyrite (FeAsS). Arsenic is structurally similar to phosphorus; its presence interferes with the process of phosphorylation in the human body.[14] Arsenic is also known to cause lung cancer in humans, dermatitis and hair loss. Additionally, due to its strong affinity for sulfhydryl groups and its lipid solubility, it tends to bioaccumulate in the liver and kidneys.
- Cadmium (Cd), once in the human body, replaces calcium in the bones. Symptoms similar to those of rheumatism set in. Subsequently, the bones softened and became susceptible to fractures. In Addition, this heavy metal ion displaces zinc in many vital enzymatic reactions, resulting in disruption or cessation of activity. This normally leads to gastroenteritis.[15]
- Chromium (III) is an essential element in human nutrition and is necessary for glucose metabolism,[16] Chromium occurs as Cr (VI) and Cr (III) with the former being the more soluble form. While Chromium (VI) has been shown to be carcinogenic to humans also by inhalation in occupationally exposed populations.

- Lead (Pb) tends to concentrate in the bones. It remains in the bones in a relatively inert form, causing no ill effects. However, when the body feels a shortage of an essential element like calcium or phosphorus, the blood leaches out these minerals from the bones and supplies it to the relevant organ. In this process, lead becomes labile and enters the bloodstream, subsequently accumulating in the tissue where it induces toxic effects.[17]
- Mercury (Hg) exists in elemental, inorganic and organic forms which include compounds where mercury is bonded to a structure containing carbon atoms. In particular, methyl mercury is easily absorbed through the gut and deposits in many tissues not crossing the blood-brain barrier as efficiently as elemental mercury. However, on entering the brain it is progressively demethylated to elemental mercury. Toxicity varies with dosage: large acute exposures to elemental mercury vapor induce severe pneumonitis, which in extreme cases can be fatal.[18] Low-grade chronic exposure to elemental or other forms of mercury induces subtler symptoms such as neurological dysfunctions.

1.1.2 Organic pollutants

An important source of anthropogenic pollution is represented by pharmaceuticals, hormones, consumer product chemicals and other organic compounds (OWC)s, employed in human activities. Critically, organic pollutants are often unregulated in drinking water, and existing toxicity data are frequently inadequate to assess potential risks from chronic low-dose exposure.[19] The manufacturing and consumption of these organic compounds have substantially increased over the past few decades and due to this increased production and employment, the concentration of pharmaceuticals in wastewater has escalated rapidly. Analgesics and anti-inflammatories are the major contributors of pharmaceuticals in wastewater, which are heterogeneous in nature and used to achieve anodyne (i.e., relief from pain or to reduce fever). Pharmacological active contaminants are persistent in aqueous media and show resistance to degradation.[1] For instance, studies in southwestern India have reported the presence of common non-steroidal anti-inflammatory drugs (NSAIDs), such as ibuprofen, aspirin, and ketoprofen, in three selected wastewater treatment plants (WWTPs) effluent and river water (Gurupura River) at concentrations ranging from 5–22, 125-184 and 3-41 μg L^{-1}, respectively,[20] thereby highlighting the limitations of conventional wastewater treatments.[21] Despite negligible detectable amounts in the environment, NSAIDs have prolonged ecotoxic effects on the biotic components of ecosystems.[22] According to Feng et al.,[23] ingestion of NSAIDs is greater than 30 million doses per day and is vastly increasing day by day. Contaminants in the form of NSAIDs can cause major organ disorders in living organisms through the usage of untreated water. Invertebrates and vertebrates when exposed to NSAIDs can form induced oxidative stress in their bodies which includes changes in the activity of antioxidant enzymes (catalase, superoxide dismutase, glutathione-S-transferase, etc.), the total number of proteins as well as lipid peroxidation.[24] According to the research conducted by Selderslaghs et al.,[25] the presence of diclofenac and ketoprofen resulted in cardiovascular defects and cardiac anomalies in freshwater fish *Clarias gariepinus* and *Danio rerio*.

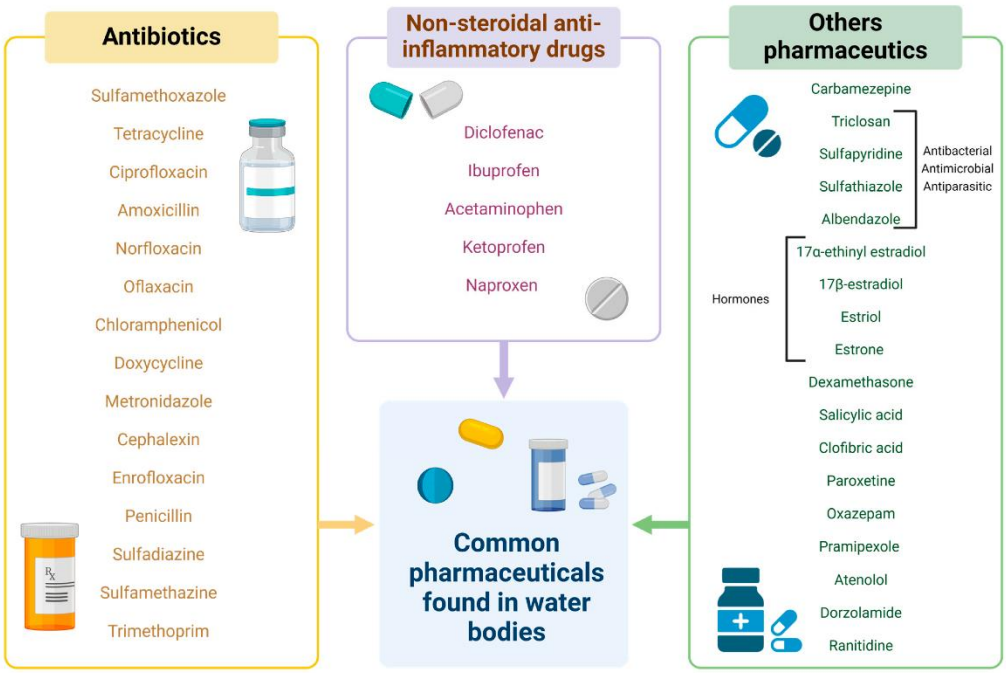

Figure 2 Common pharmaceutical pollutants found in water bodies.[26]

Therefore, the development of novel, highly efficient, reusable, and biocompatible systems for the removal of inorganic and organic pollutants, even in traces, is not only crucial, but also compulsory for safeguarding human health and ecological well-being. The available data on the environmental presence of pharmaceuticals is unsatisfactory in terms of understanding which compounds present the highest threats to the environment. As such, it is necessary and recommended to perform more representative acute and chronic toxicity tests of pharmaceuticals in a representative range of aquatic organisms. A study reported cyto-genotoxic effects on *zebra mussels* due to short-term exposure to a nonsteroidal anti-inflammatory drugs (NSAIDs) mixture that caused an increase in oxidative stress, which in turn led to genetic damage.[27] With the increasing evidence of the negative effects of pharmaceuticals on the environment and aquatic life, more attention has been paid to this issue.[28] Efforts to mitigate aquatic pollution necessitate the implementation of stringent regulations, the deployment of advanced wastewater treatment technologies, and the execution of public awareness campaigns to curtail the release of harmful substances into the environment. Sustainable practices in agriculture, industry, and urban planning are also paramount in addressing the root causes of water pollution and protecting our invaluable water resources for future generations. In contemporary wastewater treatment plants (WWTPs), the predominant mechanisms for removing pollutants revolve around precipitation of the target substances and in biochemical processes. For instance, the electrocoagulation (EC) process is widely employed for the precipitation of heavy metal ions. Conversely, organic compounds are typically targeted using biochemical approaches. Essentially, the most prevalent systems are designed to eliminate soluble organic pollutants, suspended solids, and flocculated matter. This results in the production of high-quality effluent that meets the standards for environmental discharge,[29] even if these pollutants have been detected in manly aquifers in traces.

1.2 Wastewater treatment methods

Municipal wastewater is mostly treated in sewage treatment plants which use various treatment processes including physical, chemical and biological. Wastewater treatment and discharge are done according to regional and national regulations and standards. Wastewater treatment is done with the purpose of producing a pollutant-free and toxicity-free effluent that can safely be discharged into the environment.[30] Three main stages are involved in wastewater treatment: primary or physico-chemical, secondary or biological and tertiary or advanced treatment.[31] Briefly:

- *Primary treatment* involves physical separation of heavy solid particles gravimetrically, oil and other lighter floating materials mechanically. Wastewater is passed through several tanks and filters that separate water from contaminants. The resulting "sludge" is then fed into a digester, in which further processing takes place.
- *Secondary treatment* involves the removal of dissolved and suspended biological components by means of an indigenous microbial population, which is removed prior to release of the treated water into the environment or tertiary treatment stage. It is carried out in secondary treatment chambers such as aeration tanks or bioreactors. In the presence of sufficient oxygen supplied through aeration pumps, the indigenous microflora degrades the soluble organic fractions.
- *Tertiary treatment* includes advanced wastewater treatment methods focusing on the elimination of toxic compounds to meet stringent water quality standards.[32,33]

An ideal scheme of Wastewater Treatment Plant stages is reported in **Figure 3**.

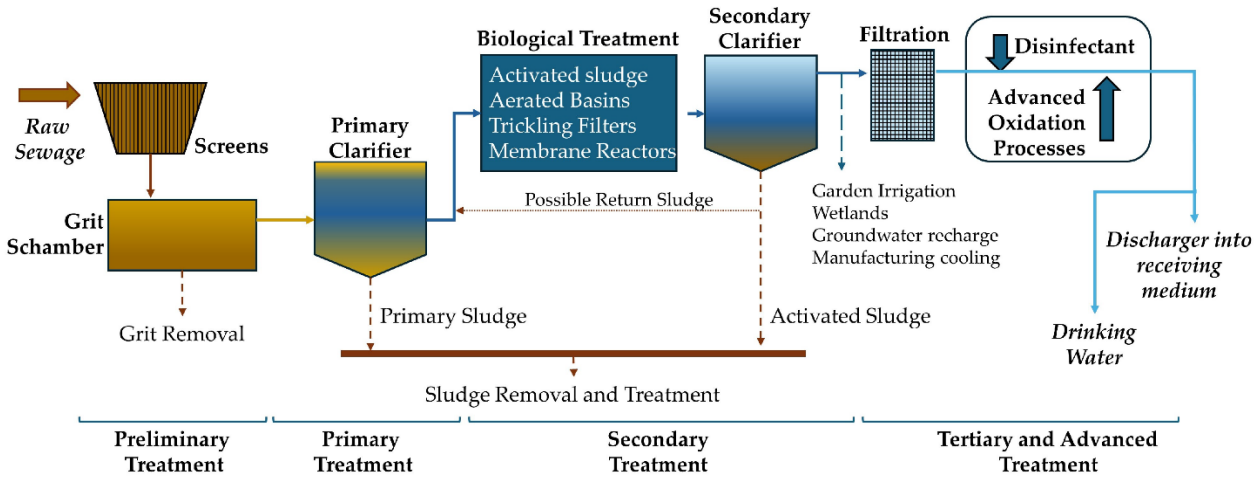

Figure 3 Wastewater treatment plant stages, from preliminary to advanced treatment processes.[34]

Contemporary strategies for mitigating aquatic pollution, specifically heavy metal ions, encompass a diverse array of methodologies including electrocoagulation (EC), adsorption utilising both synthetic and natural adsorbents, magnetic field implementation, advanced oxidation processes (AOPs), and membranes technologies.[9] For the removal of organic pollutants in WWTPs, prevalent mechanisms include biological

approaches, membrane Bio-Reactor (MBRs), attached growth systems, constructed wetland, algae photobioreactors, and stabilization ponds.[35] The most common processes include, but are not limited to:

- *Electrocoagulation (EC):* is an economically viable water treatment technology that effectively removes suspended solids to sub-micrometre levels, destabilises emulsions (e.g., oil, grease, latex), and oxidizes/eradicates heavy metals without requiring filters or additional separation chemicals. Fundamentally, an electrocoagulation reactor comprises an electrolytic cell equipped with an anode and a cathode. Upon connection to an external power source, the anode undergoes electrochemical corrosion through oxidation, whereas the cathode experiences passivation. During electrolysis process, consumable metal plates (typically made of iron or aluminium), release ions that neutralise particle charges thereby initiating coagulation. The released ions facilitate the removal of undesirable contaminants either through chemical reaction and precipitation, or by encouraging colloidal materials to coalesce, which can subsequently be extracted via flotation.[36,37] Electrocoagulation eliminates the necessity for moving parts, thereby simplifying the overall process and reducing maintenance requirements. Additionally, the sludge produced by EC exhibits better settleability, acid resistance, stability, featuring larger floc sizes and containing less bound water, which enables quicker separation through filtration along with easier dewatering.[38–40] However, in less economically developed countries, electricity costs present a significant limitation to the application and implementation of this process. Hence, to address such issues, researchers have explored the integration of solar power as an energy source for EC-based wastewater treatment, yielding remarkably promising results.[41] By incorporating renewable energy, EC can further enhance both economic and environmental sustainability in wastewater treatment.

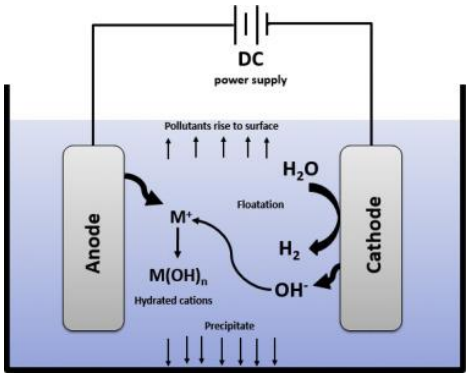

Figure 4 Schematic representation of basic Electrocoagulation cell.[36]

- *Membrane bioreactors (MBRs):* These systems represent a combination of membrane processes (such as micro or ultrafiltration) with biological treatment, most notably the activated sludge process.[42] An MBR consists of a specifically-designed bioreactor chamber that cultivates a sustained, biologically active environment, enabling the proliferation of bacteria and protozoa which metabolise organic compounds within the raw wastewater. The biological activity results in the production of a stabilised waste sludge containing the oxidised material. The efficacy of MBRs surpasses that of conventional biological systems owing to the exceptionally high microbial population maintained in close proximity of the membrane surface, which facilitates the comprehensive removal of pollutants, prior to the filtration stage. Additionally, due to the inherent sieving action of the membrane, pollutants with molecular weights exceeding the membrane's cut-off are

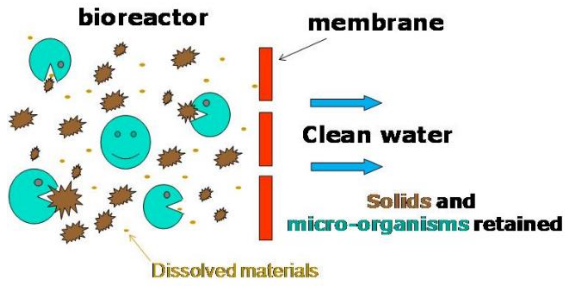

Figure 5 Schematic representation of membrane bioreactor process.

effectively retained, thereby ensuring contact with the resident degrading microbial communities inside the reactor for complete degradation (pollutants' residence time range from hours to days). Among the significant advantages of these systems, are the notably reduced reactor volume required and the consistently higher quality of the effluent compared to traditional treatment methods,[43] coupled with markedly lower levels of bacterial contamination.[44] Nonetheless, a persistent challenge encountered in MBR operation is membrane fouling, which can lead to substantial flux decline and ultimately compromise water quality. Severe fouling episodes often necessitate intense chemical cleaning or membrane replacement,[45] procedures that inherently elevate operational costs and impact the economic sustainability of such treatment plants.

- *Advanced Oxidation Processes (AOPs):* These processes are characterised by the in-*situ* generation of highly reactive oxidative species, predominantly hydroxyl radicals (·OH), which are capable of oxidising a broad spectrum of contaminants within aqueous matrices. The formation of hydroxyl radicals is typically facilitated through the use of one or more primary oxidants (such as ozone, hydrogen peroxide, or molecular oxygen) in conjunction with energy sources (e.g. ultraviolet irradiation) or suitable catalysts.[46] These reactive oxygen species possess an extraordinarily high oxidative potential, enabling the degradation of virtually any organic or inorganic pollutant present. A prototypical example of an AOP is the *Fenton Process*, which employs a combination of hydrogen peroxide and ferrous ion (Fe^{2+}) as a catalyst to produce active radicals; ferrous ion is oxidised by hydrogen peroxide to ferric ion (Fe^{3+}), simultaneously generating a hydroxyl radical and a hydroxide ion (**Eq.1**). Subsequently, ferric ion (Fe^{3+}) is reduced back to ferrous form (Fe^{2+}) by an additional molecule of hydrogen peroxide, yielding a hydroperoxyl radical and a proton (**Eq.2**). The overall, net reaction can be summarised as the disproportionation of hydrogen peroxide, producing two distinct oxygen-radical species (**Eq.3**).

$$F_e{}^{2+} + H_2O_2 \rightarrow F_e{}^{3+} + HO^{\bullet} + OH^- \quad (1)$$

$$F_e{}^{3+} + H_2O_2 \rightarrow F_e{}^{2+} + HOO^{\bullet} + H^+ \quad (2)$$

$$2\,H_2O_2 \rightarrow HO^{\bullet} + HOO^{\bullet} + H_2O \quad (3)$$

The oxidative degradation of organic pollutants through Fenton's reagent proceeds rapidly and exothermically, often resulting in mineralisation to carbon dioxide and water. However, the application of the Fenton process requires meticulous control of the reaction mixture, particularly the pH, to mitigate the formation of undesired precipitates and complexation reactions. Indeed, at lower pH values ferrous ion (Fe^{2+}) tends to form stable complexes, reducing catalytic efficiency, whereas at higher pH levels, iron precipitates as ferric hydroxide ($Fe(OH)_3$), diminishing the availability of catalytic iron.[47,48] Additional drawbacks of Fenton oxidation include high chemical consumption, the inherent instability of the Fenton's reagent, parasitic side reactions, and loss of oxidant, difficulty in optimising the reagent concentrations. Furthermore, the process requires the neutralisation of the treated effluent prior to disposal, adding to operational complexity and cost.[49]

- *Adsorption:* The adsorption process remains one of the most versatile and effective techniques for water treatment, owing to its simplicity, high efficiency, and capacity to remove a broad spectrum of pollutants.[50] Fundamentally, adsorption involves a mass transfer process in which solute or removable species migrate from the aqueous phase onto the surface of a solid adsorbent. This mechanism typically proceeds through three sequential steps: (i) initial migration of the adsorbate to the border shell of the adsorbent, (ii) intraparticle diffusion into the porous structure of the material, and finally (iii) adsorption or desorption of solute. The rate-determining steps are chiefly influenced by the physio-chemical characteristics of the adsorbate, the adsorbent, and the surrounding matrix.[32] A diverse array of adsorbents have been investigated and tested for the removal of various contaminants, they include:

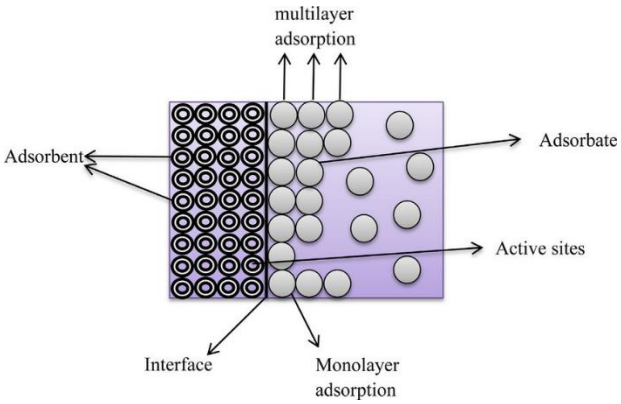

Figure 6 Schematic diagram of the adsorption process.[51]

Activated Carbon. Extensively employed for organic pollutant adsorption due to its high surface area and porosity, its properties can be further tailored through surface modifications aimed at enhancing contaminant affinity.[51] Its primary mode of action involves the diffusion of pollutants onto the surface and thereafter into pores of the activated carbon; for example, hydrophobic pollutants such as toluene and chlorinated solvents show better removal efficiency than hydrophilic or highly water-soluble pollutants.[52] In addition, the system's efficiency is heavily dependent on factors such as particle size, pH of the pollutant containing wastewater, concentration and molecular weight, adsorbent dose and presence of other co-contaminants in the wastewater.[44]

Lignocellulosic Materials. Lignocellulose, recognised as the most abundant biodegradable, bio-based polymers globally, consists mainly of lignin, hemicellulose, and cellulose (**Figure7**).

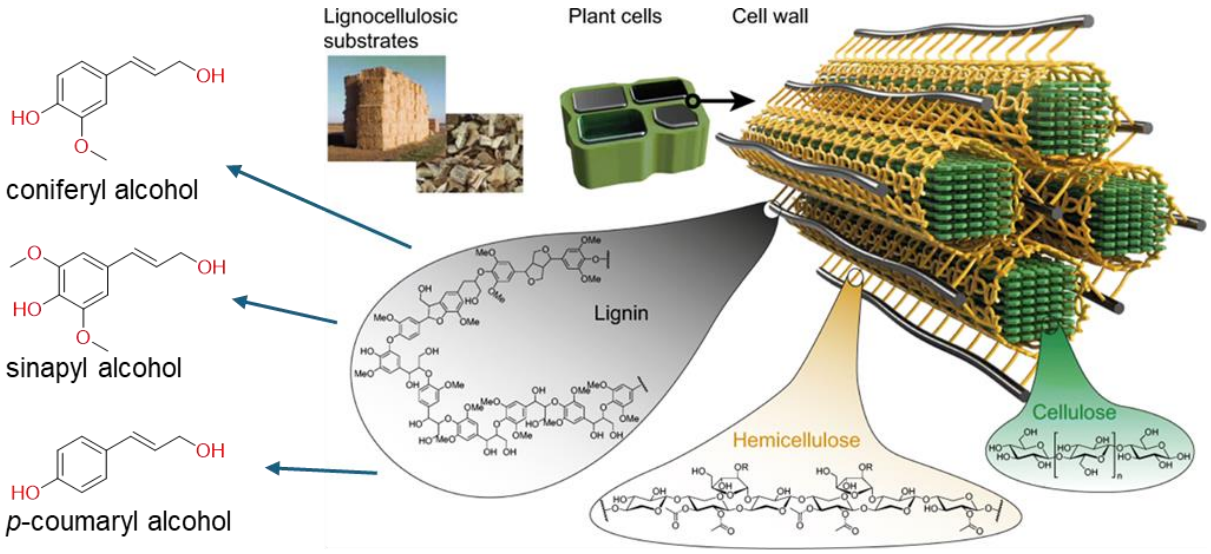

Figure 7 Components and structure of lignocellulosic plant cell walls.[53]

Each component has its own characteristics and exhibits distinct physical and chemical properties but shares a surface rich in active functional groups. These material and their composites are widely used for the removal of toxic dyes and organic molecules.[54] Lignin is a natural aromatic polymer composed of three basic chemical structure units monolignols (*p*-coumaryl alcohol, coniferyl alcohol, and sinapyl alcohol), which are interconnected via arylalkyl ether linkages such as β-O-4, α-O-4 and 4-O-5.[55] Its physicochemical properties vary depending on the source and the processing methods, which define lignin classification as follows: industrial pre-hydrolysed lignin, enzymatically hydrolysed lignin, sulphate lignin, alkali lignin, sulfonate lignin, etc. These natural polymers can be chemically modified (e.g., oxidation, sulphonation, carboxylation, alkylation, amination) or hybridised with metallic composites and graphene oxide to enhance their affinity for specific pollutants, leveraging the active functional groups present in this natural polymer, such as hydroxyl, carbonyl, carboxyl, and aromatic functionalities for targeted binding.[56–58] Empirical evidence indicates that nanocomposites, hydrogels, nanoparticles, and hybrid lignin systems exhibit significantly increased adsorption capacities.[59] Likewise, cellulose is an abundant, environmentally friendly, and biocompatible natural polymer that has been widely used in clothing, household paper, pharmaceuticals and other advanced functional materials. Its surface active hydroxyl groups combined with its unique structural properties, make it highly suitable for chemical modifications,[60–62] such as carboxyl,[62] sulfonic,[63] and cyclodextrin groups [64] to improve the removal of specific contaminants. Modified cellulose adsorbents with carboxyl and sulfonic groups exhibit superior adsorption performance compared to native cellulose adsorbents.[59]

Graphene and related two-dimensional materials. Pristine graphene is a remarkable carbon nanomaterial, consisting of two-dimensional layers of a single atom thick planar sheet of sp^2 bonded carbon atoms, arranged in a tightly packed honeycomb lattice crystal.[65] This structure imparts graphene high hydrophobicity due to the absence of functional groups.[66] Its exceptional mechanical strength, coupled with its chemical and thermal stability, make it an ideal candidate for employment in water depuration systems, particularly as a filter membrane. Graphene can be prepared through different methods (**Figure 8**), each producing varying purity levels tailored for specific applications. *Mechanical exfoliation,* commonly known as Scotch tape or peel-off method, was pioneered by Novoselov and Geim. This technique involves peeling layers of graphene using adhesive tape;[67–69] multiple layers of graphene remain on the tape after peeling off, but with recurrent peeling, it splits open into a handful of graphene flakes. Another synthesis approach involves the *thermal decomposition* of silicon carbide (SiC), where, at elevated temperature, silicon atoms are desorbed leaving behind carbon atoms that form few graphene sheets.[70] *Chemical Vapor Deposition* (CVD) is a bottom-up synthesis technique that facilitates large scale production of high-quality graphene.[71] This process entails combining a gas molecule with a surface substrate inside a reaction chamber under controlled temperature, pressure, and gas flow rate conditions.[72] The process comprises two main steps: formation of carbon through pyrolysis of a gaseous precursor (a mixture of H_2 and CH_4), and the subsequent formation of graphene's carbon lattice using the segregated carbon on a metallic catalyst's surface, typically Nickel.[73] The decomposition of hydrocarbons makes the

carbon atom to dissolve in the Ni film where the solid solution is formed. Ni has high solubility at high temperature and the solid solution of Ni is cooled down in argon atmosphere to form Ni-C precipitate which etches graphene.[74]

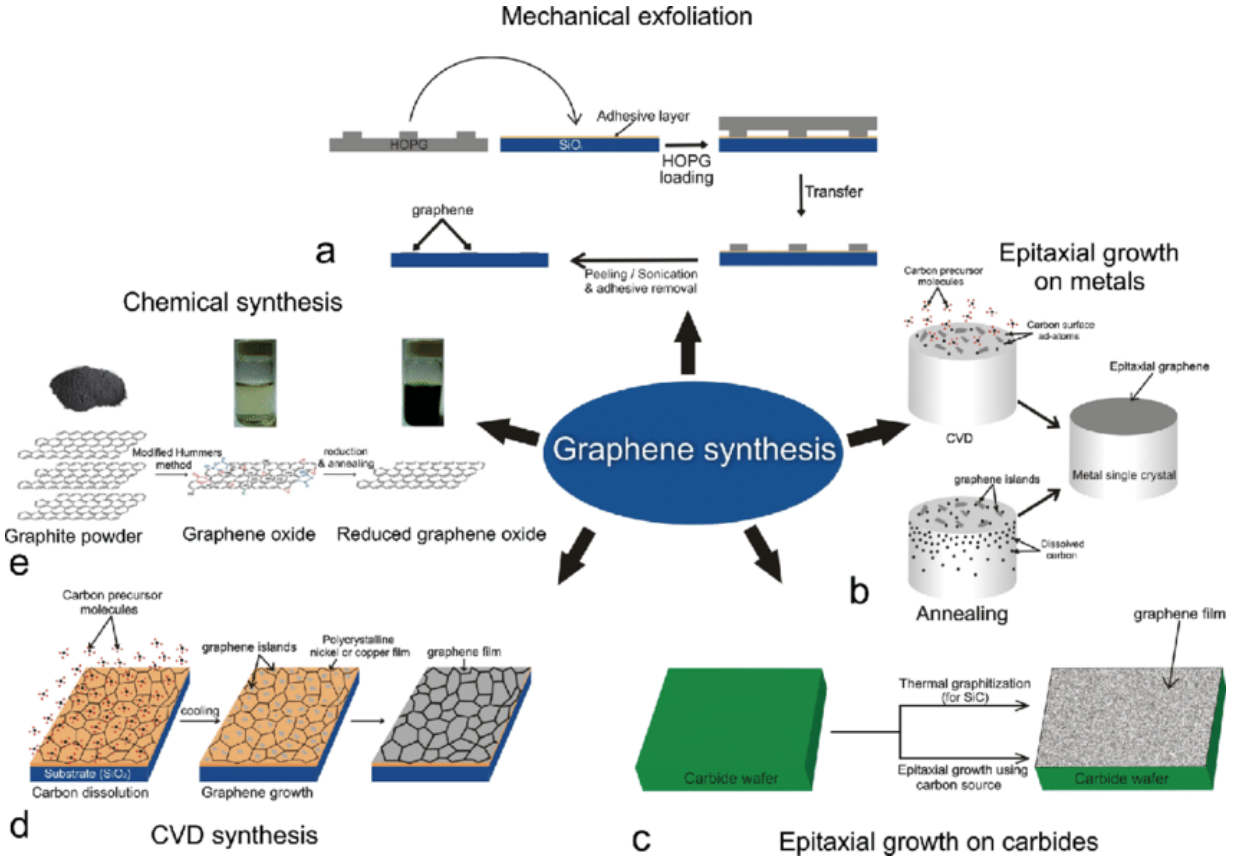

Figure 8 Schematic of various graphene synthesis techniques. (a) Graphene flake synthesis by mechanical exfoliation form Highly Oriented Pyrolytic Graphite (HOPG). (b) Epitaxial graphene growth on metal single crystals. (c) Epitaxial growth of graphene on carbide wafers by graphitization or deposition. (d) CVD synthesis of large area graphene on metal (Ni or Cu) foils. (e) Chemical synthesis of graphene from graphite oxide.[75]

More interesting than a simple layer of graphene is Graphene Oxide (GO), wherein each carbon grid is decorated with hydroxyl, epoxy, carboxyl, and carbonyl groups. These functional groups enhance GO's dispersibility in several organic solvents and water,[76] while also facilitating chemical transformation to optimise and tailor its adsorption capability against pollutants.[77] The standard procedure for GO preparation involves the oxidation of graphite using the Hummers' method.[78] All these quite recent advancements in graphene synthesis and functionalisation underscore its potential as a versatile material in nano scientific applications, particularly in environmental remediation.

Nanomaterials. Nanomaterials, characterised by a high-surface-to-volume ratio, exhibit superior performances in pollutant adsorption. They are broadly categorised into inorganic nanoparticles and polymeric nanomaterials. Inorganic nanoparticles are renowned for their distinctive optical, magnetic, catalytic, thermodynamic, and electrochemical properties, alongside notable bioactivity.[79] Examples include particles derived from non-metallic sources such as aluminium hydroxide and oxides of iron, zinc, silica, and calcium, as well as metal and metal alloys (e.g. silver, gold, aluminium, etc.), which have been explored for diverse biomedical applications.[80] Polymeric nanomaterials represent an innovative class of

materials, distinguished by their properties such as elasticity, mechanical resistance, crystallinity and attributes previously unseen in conventional materials.[81] Covalent Organic Polymers (COPs) comprise networks of porous organic molecules interlinked by covalent bonds between monomers.[82] These materials have recently emerged as new, versatile, and functionalised adsorbents due to their affordability, reusability,[83] and robust structural properties.[84] Furthermore, COPs demonstrate exceptional stability under various harsh conditions including high temperatures, even in boiling water.[85] Supporting COPs on cost-effective backbone material provides an optimal solution for developing economically viable purification process.[86] These attributes make COPs highly suitable for advanced nanotechnological applications, particularly in the field of environmental remediation.

In contemporary wastewater treatment, the employment of the above-described adsorption methods with composite materials - comprising a solid-state support and a biopolymer capable of selectively interacting with specific classes of pollutants – has garnered significant interest. Indeed, recent research efforts have focused on developing cost-effective and efficient adsorbents. Notably, several studies have explored unconventional, affordable adsorbents, including biosorbents, natural materials, and agricultural and industrial waste products. Desirable characteristics of an ideal adsorbent include non-toxicity, high efficiency, versatility, chemical and mechanical resistance, and reusability. In light of these criteria, non-toxic and biocompatible polymers such as poly(2-oxazoline)s became as highly promising candidates, owing to their straightforward synthesis, biocompatibility, and cost-effective production.[87–91] Furthermore, enhancing previously described materials, particularly lignocellulosic substrates and graphene oxide, through covalent bonding onto biocompatible polymers, like poly(2-oxazoline)s, is anticipated to significantly augment their adsorbent capacities of pollutant removal but also contributes to the development of sustainable and economically viable water treatment solutions.

1.3 Chemistry of poly(2-oxazoline)s

Poly(2-oxazoline)s (PAOx, **5**) constitute a prominent class of polymers within the broader family of pseudo-polypeptides. These five-membered heterocyclic monomers **1** are either commercially available or accessible through straightforward, multi-step syntheses from simple organic compounds. Since their initial discovery in 1966,[92–94] poly(2-oxazoline)s have garnered significant interest owing to their remarkable versatility in enabling the preparation of materials with precisely tailored properties; such attribute has spurred substantial research into the potential of these compounds as biomaterials, especially due to the accessible of the corresponding polymer via Cationic Ring-Opening Polymerisation (CROP). The principal advantage of the CROP of 2-oxazoline monomers **1** lies in the ability to conduct the polymerisation under conditions that suppress undesired side-reactions, such as the termination of chain growth and/or chain-coupling (**Scheme 1**), thereby affording well defined polymers with narrow molecular weight distributions. The CROP of 2-oxazolines follows a typical chain-growth polymerisation mechanism, which proceeds via the following steps:

- *Initiation*: typically occurs by an exothermic nucleophilic attack of the cyclic iminoether **1** on an electrophilic species **2** (the initiator), resulting in the formation of an oxazolinium cation **3**. During this

stage, the nature of the counter ion present influences the equilibrium between the cationic molecule and the covalent molecule of the 2-oxazoline monomer, affecting the efficiency of initiation.

- *Propagation:* this occurs via a two-step process. The initial step involves the addition of the monomer **1** to the oxazolinium ion **3** formed during initiation, governed by a propagation rate constant. Because of the slow rate, this step can be a determining step, if the initiation process is fully efficient.[95] After achieving the total initiation efficiency and completing the first step of propagation, the second step is taking place. This step is determined by the increased propagation rate constant established by the neighbouring dipole-ion polarization effect. The conclusion made at this step can be summarized as the cationic species playing an enormous role and should be treated as the responsible individual for the propagation process.
- *Termination*: termination ensues upon the addition of an external nucleophile stronger than the monomer, effectively quenching the polymerisation process. It is also possible to introduce designed end-chain moieties through the addition of specific terminating agents, allowing for further functionalization or tailored end-group properties.

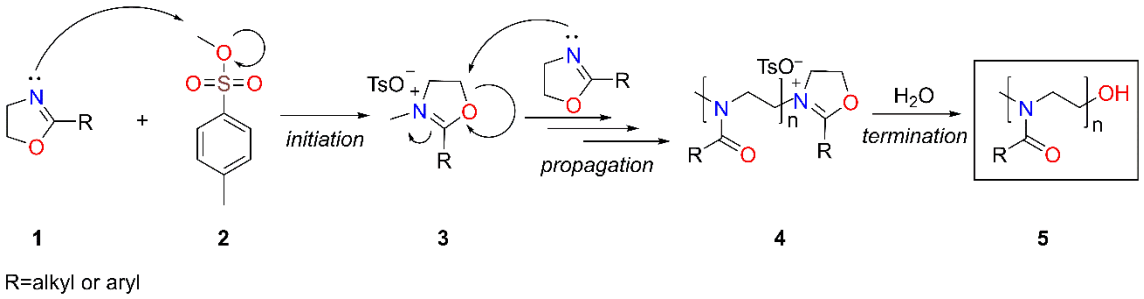

Scheme 1 Reaction scheme for methyl tosylate (**2**)-initiated CROP of 2-oxazolines (**1**), with water as quenching agent.

Notably, also the initiation step exhibits a highly regioselective character, occurring exclusively at the nitrogen atom of a 2-oxazoline monomer **1**, while the oxygen atom, being considerably less nucleophilic, remains inert.[96] The high regioselectivity facilitates straightforward access to a diverse array of well-defined PAOx **5**, allowing precise control over end-group functionalities and enabling the systematic variation of the side chain substituents,[87,97,98] These modifications are predominantly introduced during the synthesis of the 2-oxazoline monomeric precursors, thereby yielding functionalised PAOx **5** with tailored properties. An especially noteworthy feature of this polymer class is the thermoresponsive behaviour in aqueous solution. This property has rendered PAOx **5** a highly attractive candidate for developing smart materials, whose solubility can be modulated by temperature changes. Such properties have led to extensive utilization of PAOx in medical and biological applications - including drug delivery systems and bio-inspired sensors - owing to their bio-compatibility and transition temperature values that closely approximate physiological conditions.[88,99,100] This tuneable thermoresponsiveness underscores the significant potential of PAOx **5** in advancing the field of nanoscience and functional materials.

1.4 Thermoresponsive polymers

A thermoresponsive polymer is a class of smart materials that has the possibility of inducing a modification in the polymer hydration with a change in temperature, which is often naturally present or easily and inexpensively applicable. The ability to control various properties of polymer systems by an external stimulus is highly desirable for performing functions on demand, by simply altering external environmental conditions. Such a possibility of inducing a specific behaviour in response to a trigger paves the way to find increasing applications in diverse areas such as drug delivery,[101,102] tissue engineering,[103–105] gene delivery, and sensors.[106] In the 1960s, Heskins and Guillet demonstrated for the first time the thermally induced polymer solubility transitions of poly(*N*-isopropylacrylamide) (PNIPAm, **6**), which loses its strong hydration in pure water when the temperature is increased, showing a sol-gel transition.[107] Based on their response to change in temperature, thermoresponsive polymers are categorised into two classes: polymer that become insoluble above a lower critical solution temperature (LCST, **Figure 9a**) and polymers that precipitate and undergo phase change below upper critical solution temperature (UCST, **Figure 9b**).

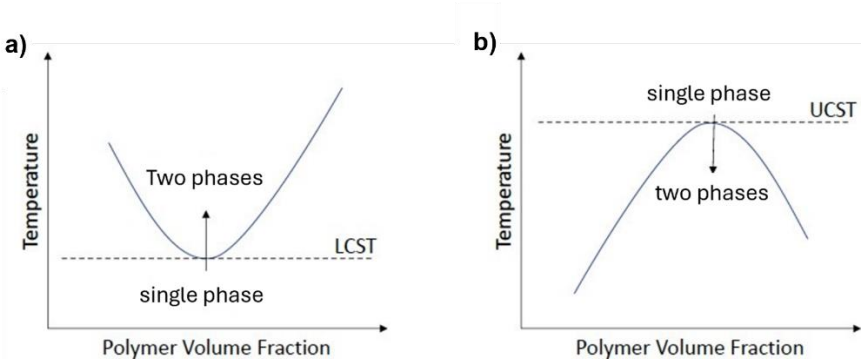

Figure 9 curves for thermoresponsive polymer in solution phase transitions: a) Lower Critical Solution Temperature (LCST) and b) Upper Critical Solution Temperature (UCST).

Specifically, water-soluble thermo-responsive polymers change from hydrophilic to hydrophobic by heating the system above transition temperature in the case of an LCST behaviour. For a polymer in aqueous solution, LCST is the point in the phase diagram at which the entropy of the water in the system increases due to the less ordered arrangement of water molecules and becomes greater than the enthalpy of water hydrogen bonded to the polymer.[108] When the temperature of an aqueous solution of thermoresponsive polymer exhibiting LCST behaviour is increased, the polymer chains show coil-to-globule-to-aggregate transition arriving at the final cluster. On the other hand, polymers with a UCST show the opposite dual behaviour, with a phase separation occurring upon cooling below the phase transition temperature: they pass from soluble to poorly soluble or insoluble.[109] In this case, the lowering of the temperature induces a reduction in the enthalpy of the entire process, therefore the entropy of the system governs the LCST, and the enthalpy of system governs the UCST.[110] Among water-soluble thermo-responsive polymers, those showing an LCST are the most widely studied. The phase separation occurs due to the breakage of the hydrogen bonds between the polymer chains and the water molecules, while the polymer-polymer interactions become thermodynamically favoured. Consequently, the LCST behaviour arises from a peculiar balance between the hydrophilic and the hydrophobic

portion of the polymer and, the LCST is highly dependent on the ability of a polymer to form hydrogen bonds with water.[111] Poly(*N*-isopropylacrylamide or PNIPAm (**6**) **Figure 10a**) is the first studied thermo-responsive polymer exhibiting an LCST in water, which is particularly exploited for biomedical applications. This is not only due to an LCST of 32 °C, close to the human body temperature, but in particular to the low sensitivity of its phase transition to the environmental conditions. Indeed, slight variations in pH, concentration or the chemical environment only cause a little variation in the transition temperature.[112] Conversely, the addition of salts and surfactants was found to have a significant impact on the LCST, which causes an increase and/or a decrease of the phase transition temperature. The most important limitation of the use of PNIPAm (**6**), is the broad hysteresis between the heating and the cooling behaviours, justified by the formation of intramolecular hydrogen bonds after the polymer collapse above the transition temperature.[113,114] Additionally, acrylamide monomers notoriously show acute cytotoxicity, which requires a careful purification of the synthesised polymer, especially when aimed at biomedical applications.[115,116] The discovery of the smart-behaviour properties such as thermoresponsivity, pH-responsivity, and redox responsivity of PAOx, **5** in recent years has attracted the attention of many studies. The thermosresponsive PAOx, which can react to a change in temperature, primarily includes poly(2-ethyl-2-oxazoline) or pEtOx (**7**) **Figure 10b**), and poly(2-isopropyl-2-oxazoline or PiPOx (**8**) (**Figure 10c**).[117] Due to this property, PAOx (**5**) are used in cell sheet engineering over a wide temperature range.[89] Redox and pH transformations are also essential for many industrial and biological processes. PAOx (**5**) shows hydrophilic behaviour at low temperatures and becomes hydrophobic at higher temperatures.[99]

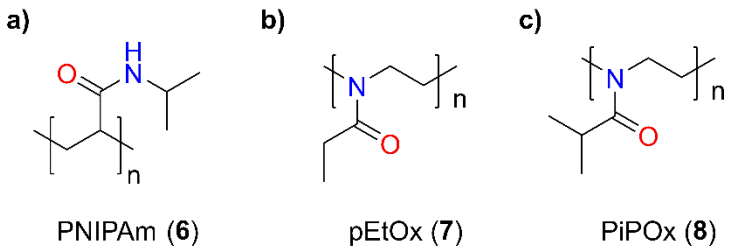

Figure 10 Structures of PNIPAm (a), PEtOx (b), and PiPOx (c).

Specifically, pEtOx (**7**) has hydrophilic characteristics with a lower critical solution temperature (LCST) of 60 °C and PiPOx (**8**) around 37 °C that is very close to the human body temperature. For this reason, the phase transitions of this polymer are under extensive investigation.

2. Aim of this work

As detailed in the preceding introduction, heavy metal ions and a diverse spectrum of organic pollutants, including pharmaceuticals, personal care products, cosmetics, and pesticides, constitute a significant fraction of hazardous chemicals present in wastewater and pose considerable risks to both human and ecological well-being. Although pollutant removal methodologies are widely applicable, their limited effectiveness in eliminating trace contaminants underscores the need for the development of more innovative and sustainable technologies. In this context, the overarching aim of the present Doctoral Thesis is the design and synthesis of alternative highly efficient adsorbents capable of selectively interacting with either inorganic or organic pollutants in aqueous media. Such a target will be achieved by exploiting the inherent versatility of poly(2-oxazoline)s (PAOx, **5**), a biocompatible class of polymer, whose lateral chain functionalities can be precisely tailored via facile chemical modification. To enhance the water insolubility issues of specific PAOx **5**, and to achieve a facile separation between the adsorbent from the treated aqueous media post-experiment, the designed adsorbent will be incorporated onto a suitable solid support. To pursue the intended goal, this research will involve both the employment of previously prepared 2-oxazolines monomers and novel, specifically decorated 2-oxazoline monomers, designed to target prevalent chemical functionalities present with common classes of pollutants. The newly designed monomers will include aromatic domain to facilitate hydrophobic interaction with pharmaceutical products, amine moieties to establish acid-base interaction as well as hydrogen bonding with acidic organic compounds, and carbonyl/carboxyl functionalities for the chelation of heavy metal ions. Cellulose, lignin, and Graphene Oxide (GO) will be investigated as economical, ecologically sound, robust, and chemically stable solid support alternatives to traditional nanoparticles.

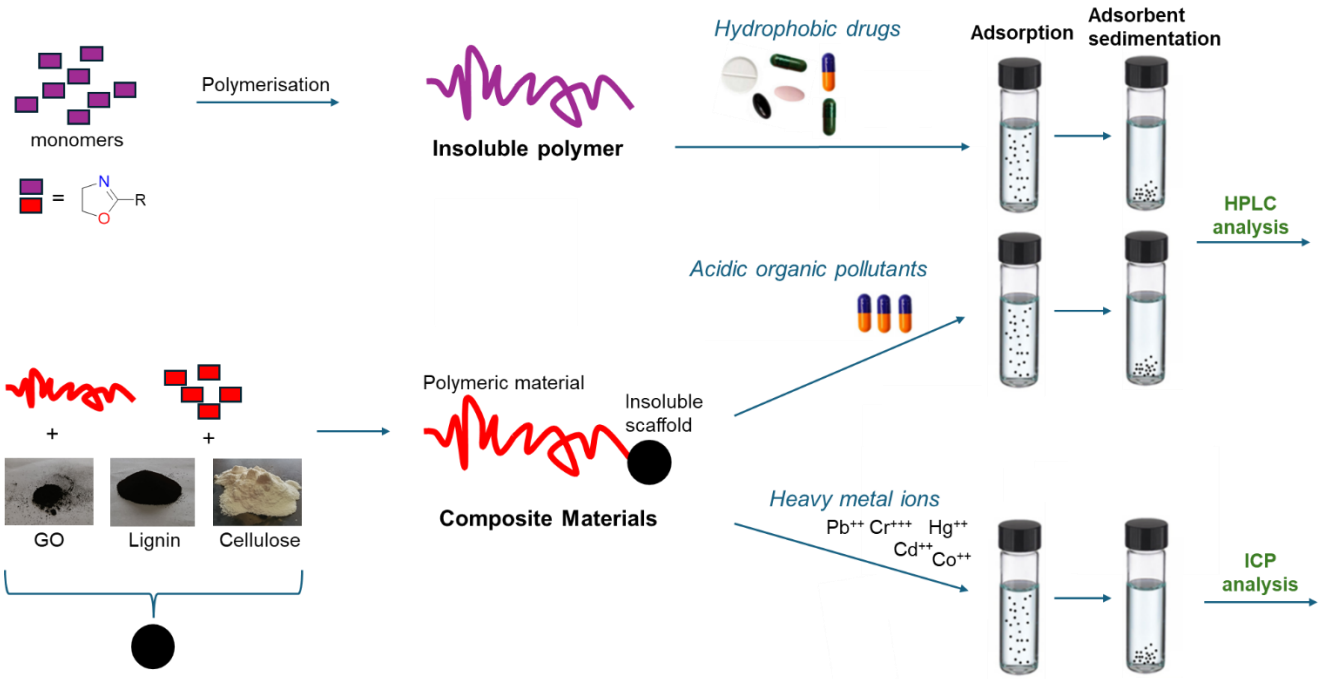

Figure 11 Schematic adsorbents preparation and adsorption procedure for pollutants.

Specifically, the thesis will proceed according to the following structure:

- *monomer synthesis and characterization* (**Chapter 3.1**). The first part will detail the synthesis and full characterization of all monomers via Gas Chromatography-Mass Spectrometry (GC-MS) and Nuclear Magnetic Resonance (NMR);
- *homopolymer preparation and characterization* (**Chapter 3.2**). The preparation and characterization of the corresponding homopolymers will be described in depth. Furthermore, the thermoresponsive behaviour of various chain length PiPOx (**8**) polymers in aqueous solution will be investigated in collaboration with the computational group of Prof. Barbara Capone and Dr. Sara del Galdo;
- *diphenyl-functionalised PAOx for hydrophobic pollutant adsorption* (**Chapter 3.3**). A novel 2-oxazoline monomer bearing a diphenyl moiety will be synthesised, characterised, and subjected to Cationic Ring-Opening Polymerisation (CROP); reaction conditions of both monomer preparation and polymerisation will be fully optimised in terms of temperature, reagent ratios, solvent, and reaction times. The resulting polymer will be then evaluated in adsorption experiments targeting hydrophobic organic pollutants commonly detected in wastewater in stock solutions with concentrations quantified pre- and post-treatment employing High Performance Liquid Chromatography (HPLC);
- *GO-poly(2-oxazoline) composite for acidic pharmaceutical removal* (**Chapter 3.4**). Targeting active principles commonly detected in wastewater, a novel Graphene Oxide (GO) composite with poly(2-oxazoline)s will be prepared, characterised, and its efficacy for removing acidic pharmaceutical products from aqueous solution establishing an acid-base interaction will be assessed. Characterization techniques will include Thermogravimetric Analysis (TGA) to evaluate thermal behaviour post-polymer conjugation, Attenuated Total Reflectance Infrared Spectroscopy (ATR-FTIR) to confirm polymer linkage to GO, and Atomic Force Microscopy (AFM) together with Transmission Electron Microscopy (TEM) to assess composite morphology. The prepared adsorbent will be then employed in several adsorption experiments targeting the acidic pharmaceutical products in stock solutions with pollutant concentrations quantified pre- and post-treatment employing High Performance Liquid Chromatography (HPLC);
- *cellulose-poly(2-oxazoline) composites for Heavy Metal Adsorption* (**Chapter 3.5**). In collaboration with Department of Nanobiotechnology, University of Natural Resources and Life Sciences, Vienna, cellulose composites with the poly(2-oxazoline)s will be prepared for the removal of heavy metal ions, another dramatically important environmental issue. The newly synthesised materials will be characterised using TGA and ATR-FTIR, followed by adsorption experiments targeting harmful heavy metals. Metal concentrations will be quantified before and after treatment with Inductive Coupled Optical Emission Spectroscopy (ICP-OES).

3. Results and Discussion

3.1 Synthesis and characterization of 2-oxazoline monomers

Building upon the established foundation of poly(2-alkyl-2-oxazoline)s (PAOx) and their broad applicability across domains ranging from medicinal chemistry to environmental remediation, extensive literature exists detailing their preparation, derivatisation, and property characterisation.[98,118,119] To meet the specific objectives outlined in this thesis, a range of monomers were carefully selected and designed, incorporating the following key characteristics: (i) an alkyl side chain exhibiting varied solvolytic behaviour in aqueous media, facilitating the precise modulation of polymer-pollutant-solvent interactions; (ii) a protected primary amine or carboxylic acid functionality, capable of being revealed *post-polymerisation*, to enable electrostatic interactions with target analytes in solution (e.g., chelation of heavy metal ions, acid-base interactions for the adsorption of organic pollutants, or the formation of specific hydrogen bonds); and (iii) aromatic groups to encourage π-π stacking interactions with hydrophobic organic pollutants present in aqueous environments. Among a diverse array of potential candidates, a focused subset of 2-oxazoline monomers was strategically chosen, incorporating functionalities designed to interact with specific pollutant classes. For the aim of this Thesis, three monomer scaffolds were selected: 2-isopropyl-2-oxazoline (iPOx, **11**), whose corresponding homopolymer has been extensively studied for its thermoresponsive characteristics [95,99,120] and is decorated by carbonyl moieties that could interact with heavy metals in water medium, *tert*-butyl (3-(4,5-dihydrooxazol-2-yl)propyl) carbamate (AmOx, **18**) whose corresponding homopolymer has amine moieties that could establish acid base interaction with acidic organic molecules and also electrostatic interactions, and ethyl 3-(4,5-dihydrooxazol-2-yl)propanoate (EstOx, **21**) whose corresponding polymer has carboxyl moieties that could chelate heavy metal ions. Furthermore, a novel 2-oxazoline monomer bearing a diphenyl moiety (2-benzhydryl-4,5-dihydro-1,3-oxazole, **13**) was synthesised, hypothesizing a possible π-π stacking interaction between the homopolymer's aromatic domains and aromatic compounds.[121] A modified Witte-Seeliger cyclocondensation reaction served as the general synthetic route for the preparation of 2-oxazoline monomers.[118] Whilst existing procedures detailing the synthesis of (2-alkyl-2-oxazoline)s, specifically those applicable to iPOx (**11**), were successfully adapted, the analogous cyclocondensation reaction to synthesise monomer **13**, and the entirely distinct synthetic pathways were employed to obtain AmOx (**18**) and EstOx (**21**), each required optimisation and refinement to ensure high monomer yield and purity.[90,92,122] Briefly, iPOx (**11**) was efficiently synthesised via the reflux of *iso*butyronitrile (**9**) and ethanolamine (**10**) in the presence of zinc acetate as a catalytic species (**Scheme 2a**). This methodology consistently yielded the desired compound (**11**) in 70% yield following sequential distillations: initially over NaOH to selectively remove residual substrate (**9**), and then over CaH_2 to establish anhydrous conditions and facilitate maximised monomer purity. In contrast, and despite employing a similar cyclocondensation methodology using 2,2-diphenylacetonitrile (**12**) and ethanolamine (**10**) under equivalent reflux conditions, the preparation of monomer **13** necessitated a final purification stage involving silica gel column chromatography to effectively remove unreacted starting

materials and unwanted side-products (**Scheme 2b**). The preparation of AmOx (**18**) followed a distinctly different synthetic strategy, beginning with amino Boc protection of γ-aminobutyric acid (**14**) which, under highly basic conditions (NaOH 5M), was converted into the desired *tert*-butoxycarbamate (**15**). Intermediate **15** was then subjected to activation of the carboxylic acid moiety employing (2-(1H-Benzotriazole-1-yl)-1,1,3,3-tetramethylaminium tetrafluoroborate (TBTU) as a coupling reagent, followed by reaction with 2-chloroethylamine hydrochloride (**16**), resulting in successful installation of the future 2-oxazoline ring within intermediate **17**, purified by column chromatography on silica gel. Exploiting the inherent stability of the Boc protecting group, the final ring-closure reaction was conducted under equivalent strongly basic conditions (saturated NaOH solution in methanol), affording AmOx (**18**) as a white solid product following a standard liquid-liquid extraction procedure (**Scheme 2c**). Lastly, a two-step approach was adapted to achieve synthesis of EstOx (**21**), utilising ethyl succinyl chloride (**19**) and 2-chloroethylamine hydrochloride (**16**). The resulting intermediate (**20**) then underwent a ring-closure reaction facilitated by the addition of anhydrous Na_2CO_3, yielding the desired EstOx product (**21**) (**Scheme 2d**). It is noteworthy that this final step was carefully optimised by conducting the reaction directly on a rotary evaporator, followed by prolonged application of high vacuum, facilitating continuous removal of the by-products (water and CO_2) to drive the reaction to completion. A final purification step, involving a high-vacuum distillation, was employed to obtain the pure monomer product, which was then carefully stored over molecular sieves.

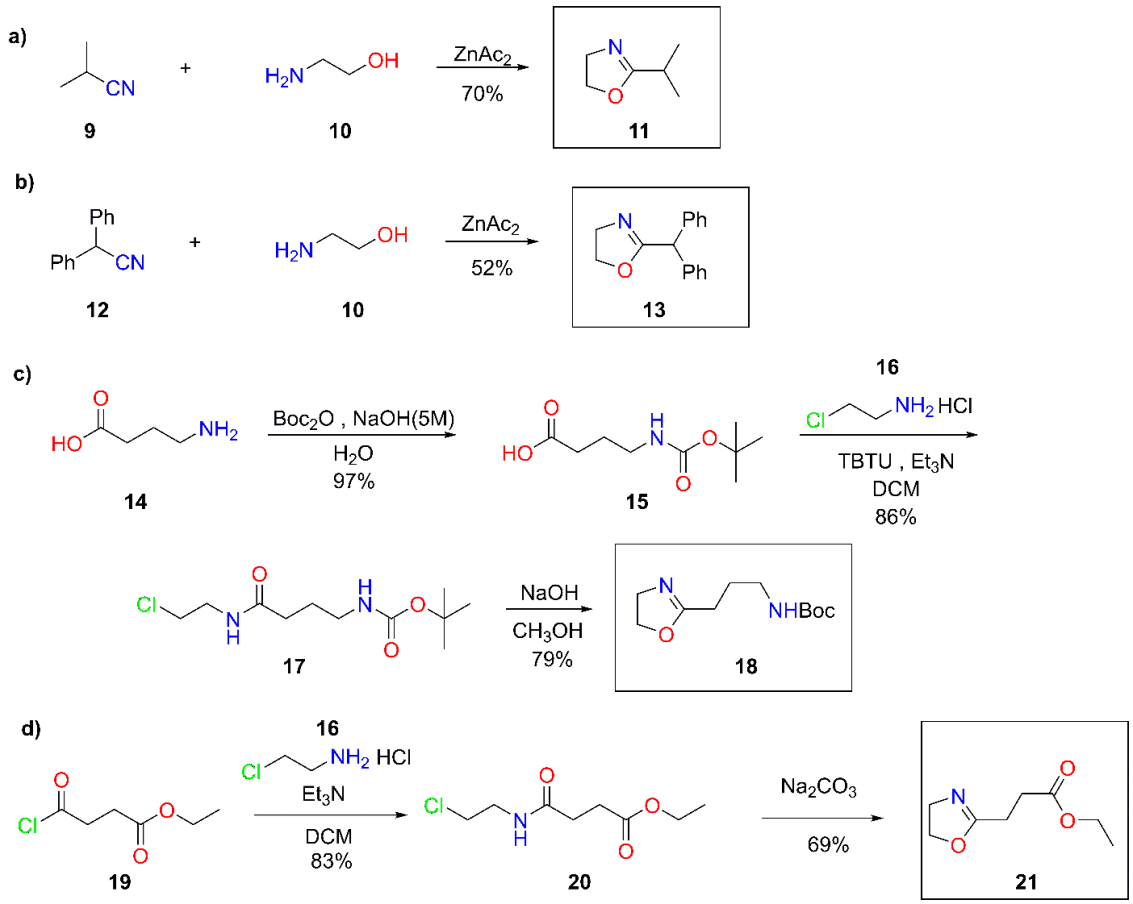

Scheme 2 Synthesis of 2-alkyl-oxazoline monomers.

After synthesis and purification, the four monomers underwent to several analyses to confirm their molecular structures and to ensure the high purity required for subsequent polymerisation reactions. Gas Chromatography-Mass Spectrometry (GC-MS) was employed, as it is a widely used analytical technique for the identification and quantification of trace chemicals in complex or pure mixtures. Specifically, the chromatograms for all the desired monomers displayed a single peak after the purification process. The mass spectra analysis (**Figure 12**) highlights the molecular structure of the monomers: for iPOx (**11**), the molecular ion is observed at *m/z* 113, with its main fragment at *m/z* 98 as the base peak (**Figure 12a**) with a loss of one methyl unit; for compound **13**, the molecular ion is present at *m/z* 237, with main fragments at *m/z* 236 as base peak (loss of an hydrogen), and at *m/z* 167 due to the loss of the 2-oxazoline ring (**Figure 12b**); for AmOx (**18**), the molecular ion is not visible, but fragments are present at *m/z* 155 (cleavage of single bond between the carbonyl carbon and oxygen in the Boc group) and at *m/z* 98 attributable to the cleavage between the second and the third methylene unit of the 2-oxazoline ring (**Figure 12c**); and for EstOx (**21**), the molecular ion is not visible, but the main fragment is observed at *m/z* 126 (cleavage of the single bond between the carbonyl carbon and the oxygen of the ester), with a fragment at *m/z* 98 as base peak obtained, also in this case) after the cleavage between the second and the third methylene unit of the 2-oxazoline ring (**Figure 12d**).

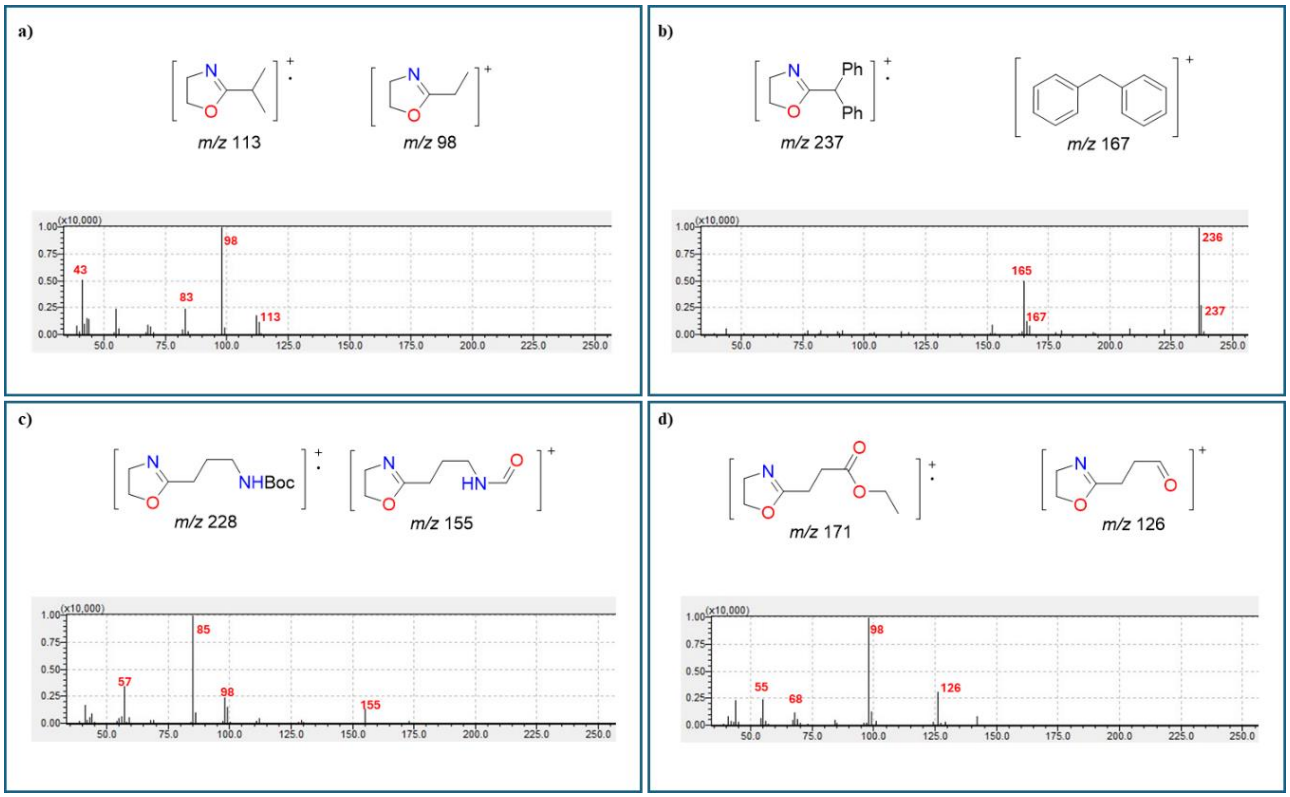

Figure 12 Mass Spectra analysis for 2-oxazoline monomers **11**, **13**, **18**, **21** (EI 70eV).

Following initial confirmation via mass spectrometry, ^{1}H-NMR experiments were performed to further corroborate the proposed structures of the synthesised monomers; the resulting proton spectra are presented in **Figure 13**. The observed signals were found to be entirely consistent with the expected protons within each molecule. Specifically, the two triplet signals (labelled "c" and "d") observed at approximately 3.00 and around 4.50 ppm are related to the 2-oxazoline ring protons and were common to all synthesised monomers, with each

signal integrating to two protons, consistent with their structural assignment. The remaining signals were found to align with the specific structural variations present within the lateral chains: (i) compound **11** exhibited the diagnostic doublet of the *iso*-propyl group at 1.18 ppm integrating for six proton, and a multiplet at 2.54 ppm attributable to the proton in β position relative to the nitrogen and the oxygen atoms (**Figure 13a**); (ii) compound **13** displayed a prominent multiplet at 7.33 ppm, assigned to the aromatic protons (integrating to ten protons), and an additional signals attributable to the proton in β position relative to nitrogen and the oxygen atoms at 5.11 ppm (**Figure 13b**); (iii) the spectrum of compound **18** featured two distinct triplets at 2.30 and 3.15 ppm, each counting for two protons, and a quintet at 1.81 ppm (integrating to two protons), all of them assigned to the methylene units within the later chain, and a sharp singlet at 1.42 ppm (counting for 9 protons) characteristic of the *tert*-butyl carbamate (**Figure 13c**); (iv) lastly, the spectrum of compound **21** displayed a multiplet at 2.61 ppm (counting for four protons) attributable to the methylene units within the lateral chain, the signal of the CH_2 moiety within the ethyl ester group at 4.21 ppm, partially overlapping with the 2-oxazoline ring protons (labelled "d"), and the triplet at 1.23 ppm (integrating to three protons) assigned to the CH_3 group of the ethyl ester. (**Figure 13d**).

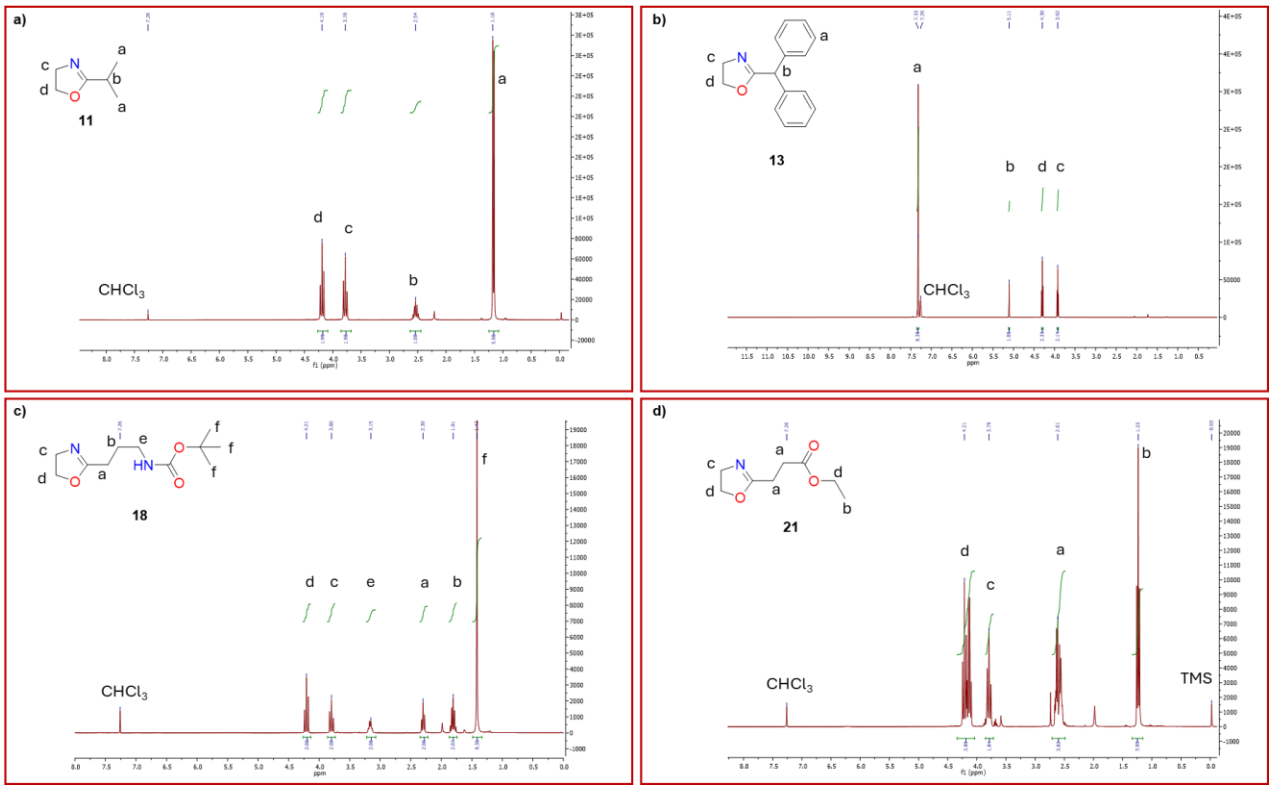

Figure 13 ^{1}H NMR (600MHz) spectra of the synthetised 2-oxazoline monomers **11**, **13**, **18**, **21** in $CDCl_3$.

The ^{1}H NMR analyses undoubtedly confirm the absence of any residual nucleophilic contaminants, the presence of which could prematurely terminate the controlled, chain-growth polymerisation processes. Therefore, the synthesised monomers were straightforwardly subjected to polymerisation reactions without any further purification.

3.2 Synthesis and characterization of poly(2-oxazoline)s

The polyoxazoline homopolymers derived from monomers **11**, **18**, and **21** were synthesised via living Cationic Ring-Opening Polymerisation (CROP) using methyl *p*-toluenesulfonate (**2**) as initiator, following a well-established procedure reported extensively in the literature,[90,93,123,124] and therefore no further optimization was necessary. All the polymerisations were performed under rigorously anhydrous atmosphere to avoid undesired premature chain termination, utilising freshly distilled (over CaH_2) acetonitrile (ACN) as reaction solvent and keeping continuous stirring of the reaction mixture for durations ranging from 8 to 48 hours at reflux temperature. Upon completion of the predetermined reaction time (**Table 2**), the living polymerisation was quenched through the addition of a nucleophile stronger than the monomer, employed in excess relative. Specifically, in the case of monomer **11**, multiple polymerisation experiments were undertaken to generate the corresponding homopolymer PiPOx (**8**) of varying chain lengths, with the optimal results summarised in **Table 2**. The preparation of such a set of homopolymers was motivated to evaluate the relationship between PiPOx (**8**) chain length and its LCST temperature in aqueous solution, a parameter which is extensively explored in **Section 3.2.1**. For polymerisations utilizing monomers **18** and **21** experimental efforts were focused on minimizing the resulting polydispersity index (Đ) whilst maintaining acceptable chain lengths when methyl tosylate (**2**) was employed as initiator and ACN as reaction solvent at reflux temperature. The resulting polymers were characterised via Gel Permeation Chromatography (GPC), against polystyrene standards, employing 50 mM LiBr in dimethylformamide (DMF) as eluent, enabling the determination of molecular weight and polydispersity index (Đ). The optimal results in terms of yield, polydispersity index, temperature, and reaction time are detailed in **Table 2**.

Table 2 Optimal polymerisation reaction conditions employing in the cases of monomers iPOx (**11**), AmOx (**18**), and EstOx (**21**).

Entry	Monomer	Initiator **2** (eq.)	Rt[a]	M_w[b,c]	Đ[c,d]	Y[e]
1	**11**	0.10	8 h	3.4	1.1	90%
2	**11**	0.02	18 h	5.6	1.1	95%
3	**11**	0.01	24 h	9.8	1.1	98%
4	**18**	0.02	48 h	5.8	1.1	92%
5	**21**	0.02	48 h	8.7	1.1	80%

[a)] MR indicates the Molar Ratio; [b)] Rt indicates reaction time; [c)] M_w indicates Molecular weight (kDa), [d)] Đ indicates Polydispersity Index; [e)] Y indicates the observed yields; [f)] M_w and Đ were obtained with GPC analyses using polystyrene reference materials and DMF 50 mM LiBr as eluent.

Bearing in mind the established mechanism of Cationic Ring-Opening Polymerisation (CROP) and the findings (**Table 2**), a range of reaction conditions (encompassing initiator type and concentration, as well as temperature) were systematically explored to optimise the polymerisation of the novel synthesised 2-oxazoline monomer **13**. The objective of this optimisation was to identify conditions that would promote both high polymer yield and a narrow polydispersity index (Đ). A summary of the most pertinent experimental conditions and their corresponding outcomes is presented in **Table 3**.

Table 3 optimization of the polymerisation reaction condition for monomer **13**.

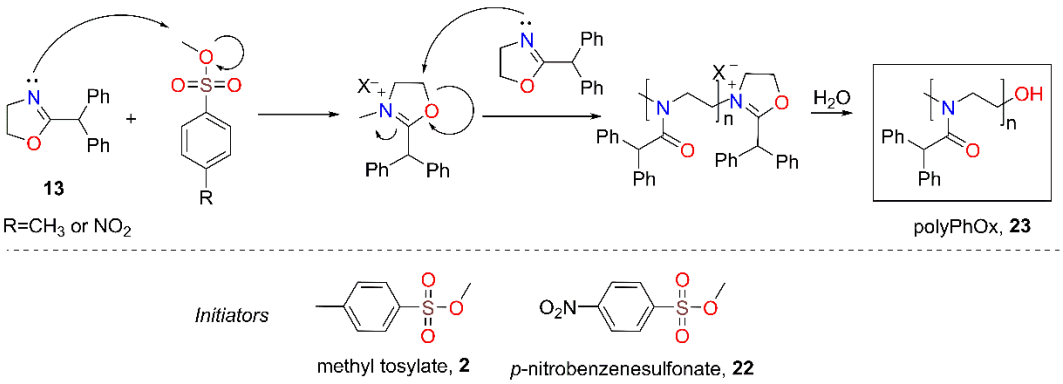

Entry	Initiator	MR[a](eq.)	Rt[b]	Temp (°C)	M_w[c,f]	Đ[d,f]	Y[e]
1	2	0.02	5 d	50	N.D.	\	\
2	2	0.01	11 d	25	1.4	\	4 %
3	2	0.02	24 h	90	24.6	2.8	95 %
4	2	0.01	24 h	90	34.7	1.9	72 %
5	2	0.02	8 h	90	19.7	1.5	85 %
6	22	0.02	8 h	90	6.5	1.1	88 %
7	22	0.01	8 h	90	6.8	1.1	75 %

[a)] MR indicates the Molar Ratio; [b)] Rt indicates reaction time; [c)] M_w indicates Molecular weight (kDa), [d)] Đ indicates Polydispersity Index; [e)] Y indicates the observed yields; [f)] M_w and Đ were obtained with GPC analyses using polystyrene reference materials and DMF 50 mM LiBr as eluent.

Given the capacity of the methyl tosylate (**2**) to typically furnish well-defined polymers with narrow molar mass distribution,[88,123] initial polymerisation trials were conducted using e freshly prepared 2-oxazoline **13** and varying stoichiometric equivalents of initiator **2**. While reactions performed at lower temperature failed to yield appreciable quantities of the desired poly(2-benzhydryl-4,5-dihydro-1,3-oxazole) (polyPhOx, **23**) except in traces and after an excessively long reaction time (entry 2), performing the polymerisation at 90 °C with 0.01 eq. of **2** for only 24 hours afforded the desired product in very good yield (72%, entry 4). Increasing the initiator loading to 0.02 eq. led to a further enhancement in yield (95%, entry 3). Decreasing the reaction time from 24 hours to 8 hours (entry 5) resulted in a slight reduction in yield from 95% to 85%, as well as a decrease in the observed molecular weight (from 24.6 to 19.7 kDa), however, this approach did yield an improvement in monodispersity (Đ =1.5). Moreover, in contrast to results reported for other alkyl 2-oxazolines,[123,125,126] the GPC analysis consistently revealed a pronounced heterogeneity of the samples (polydispersity index, Đ = 2.8) even when minimising both the initiator amount (Đ = 1.9, entry 4) and the reaction time at 8 hours (Đ = 1.5, entry 5). Therefore, alternative sulfonates as initiator were screened and, notably, the most promising results were observed with *p*-nitrobenzenesulfonate (**22**). Indeed, the use of such initiator led to the isolation of the desired polymer in good-to-high yield (75-88%, entries 6 and 7), in reasonable reaction time (8 h) and, most significantly, with a narrow polydispersity index (Đ = 1.1). This successful outcome is likely attributable to the superior leaving group ability of the *p*-nitrobenzenesulfonate (**22**) as an initiator, facilitating a rapid and quantitative initiation step that outpaces the subsequent propagation step. The resultant uniform growth of the

polymer chains led to a lower Đ value with **22** as initiator compared to **2**. In fact, the propagation rate of this reaction is supposed to be inherently high due to the presence of the aromatic substituent that could increase the electronic donation effect, stabilizing the intermediate cation (**Scheme 1**). The polymer obtained by employing 0.02 eq. of **22** and carrying out the reaction at 90 °C for 8 h (entry 6) represents, at this stage, the optimal compromise among length, number of monomers, and polydispersity for the synthesis of the corresponding polyPhOx (**23**). To confirm the molecular structures of all homopolymers synthesised (derived from monomers **11**, **13**, **18**, and **21** respectively) comprehensive ^{1}H NMR spectroscopic analyses were performed. Consistent with the existing literature,[127] the spectra (**Figure 14**) confirm the successful polymerisation.

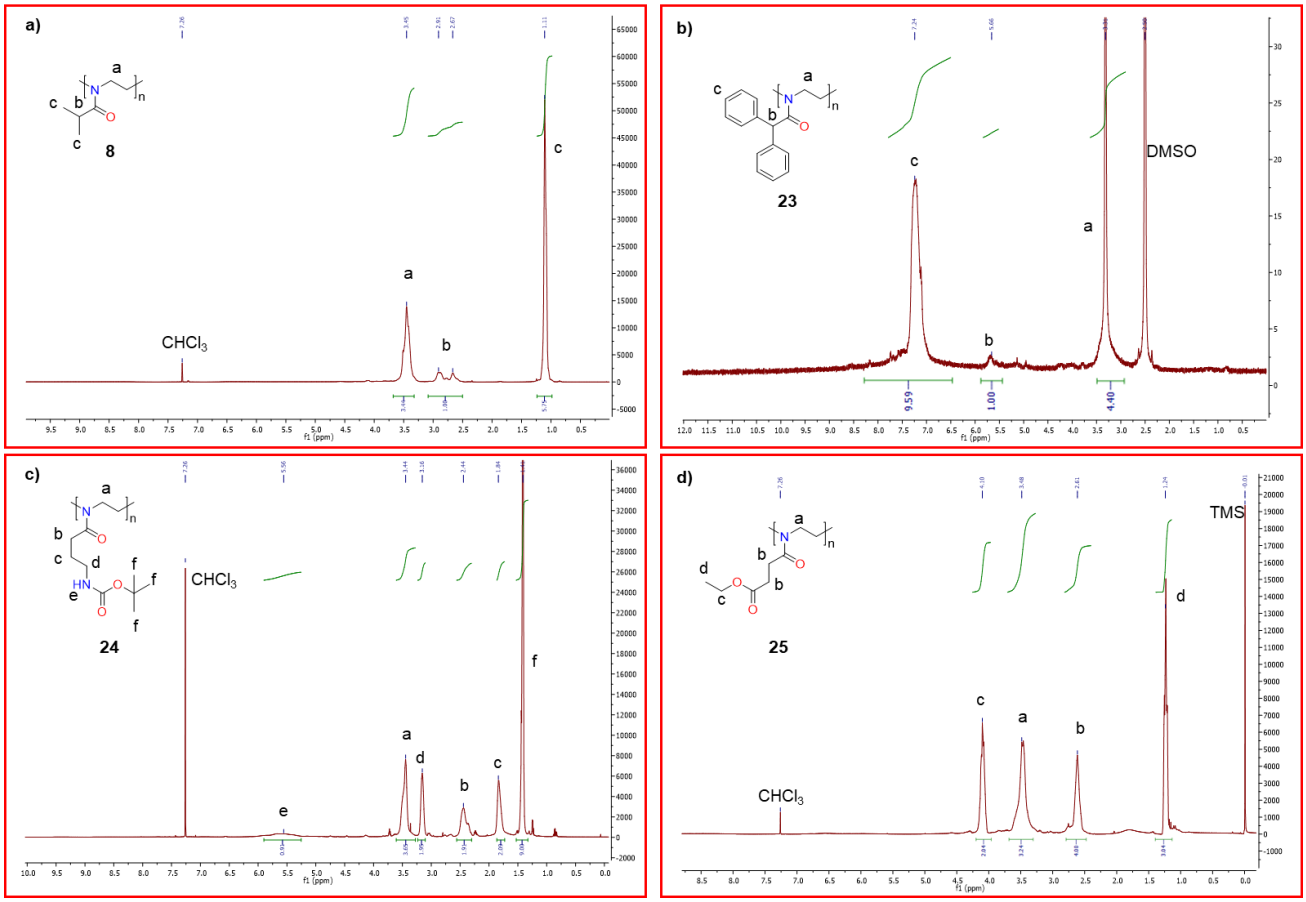

Figure 14 ^{1}H NMR (600MHz) spectra of the obtained poly(2-oxazoline)s in $CDCl_3$ for polymers **8**, **24**, and **25**; and in DMSO-d6 for polymer **23**.

All spectra show a signal at approximately 3.31-3.48 ppm attributable to methylene along the principal polymer backbone. Furthermore, PiPOx (**8**) spectrum displays the diagnostic signal for the *iso*-propyl group in the polymer chain at 1.11 ppm, and the two signals at 2.67 and 2.91 ppm attributable to the single proton in the α position of the carbonyl function (**Figure 14a**). The polyPhOx (**23**) spectrum features a multiplet at 7.24 ppm attributable to the aromatic protons and a signal at 5.66 ppm attributable to the proton in α position relative to the carbonyl function (**Figure 14b**). The poly(2-(3-(Boc-amino)propyl)-2-oxazoline) (pAmOx, **24**). spectrum displays three main signals at 1.84, 2.44, and 3.16 ppm relating to the later chain, as well as a signal at 1.41

ppm characteristic of the *tert*-butyl carbamate moiety (**Figure 14c**). Lastly, the poly(2-ethoxycarbonylethyl-2-oxazoline) (pEstOx, **25**) spectrum features signals at 2.61 ppm (lateral chain), at 4.10 ppm (CH_2 in the ethyl ester), and the signal at 1.24 (CH_3 protons in the ethyl ester) (**Figure 14d**).

Prior to their utilisation in downstream applications, the homopolymers pAmOx (**24**) and pEstOx (**25**) underwent deprotection to remove the Boc and the ethyl ester protecting groups, respectively. The efficacy of these deprotection procedures was rigorously assessed through ^{1}H NMR spectroscopic analyses. For the Boc protected polymer (pAmOx, **24**) deprotection reaction was achieved by stirring the polymer, dissolved in chloroform ($CHCl_3$), at room temperature in the presence of trifluoracetic acid (TFA). Conversely, the ethyl ester group of pEstOx (**25**) was removed by stirring the polymer in a 5 % (w/v) aqueous potassium hydroxide (KOH) solution at room temperature. As depicted in **Figure 15**, in both cases, the signals of the polymer chains remain consistent through the deprotection process, with the exception of the characteristic Boc and the ethyl ester protons, which were effectively eliminated. Specifically, in **Figure 15a** the spectrum of poly(2-(3-amino)propyl)-2-oxazoline) (deprotected pAmOx, **26**) demonstrates the complete disappearance of the Boc proton signals at 1.41 ppm, previously well visible in the spectrum of the Boc protected polymer (pAmOx, **24**). Similarly, in **Figure 15b** the proton signals of the ethyl group at 1.24 and at 4.10 ppm, previously present in the spectrum of protected pEstOx (**25**) in **Figure 14d**, are absent in the spectrum of poly(2-ethoxycarboxyl-2-oxazoline) (deprotected pEstOx, **27**).

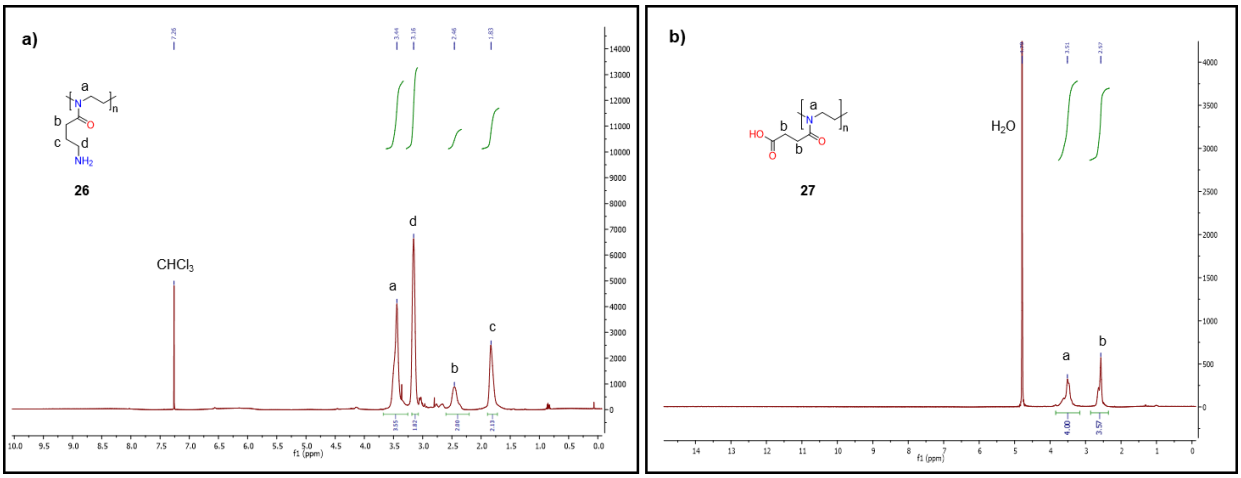

Figure 15 ^{1}H NMR (600MHz) spectra for a) deprotected pAmOx (**26**) in $CDCl_3$, and b) deprotected pEstOx (**27**) in D_2O.

The homopolymers **8**, **23**, **26**, and **27** were characterized using Thermogravimetric Analysis (TGA) and Fourier- Transform Infrared Spectroscopy (FT-IR). However, in this paragraph, only the analyses of the newly synthesized polyPhOx (**23**) are presented, as the TGA and FT-IR data for the other homopolymers (**8**, **26**, and **27**) are discussed in relation to their relative composite materials in **Chapters 3.4** and **3.5** avoiding redundant data. The FT-IR spectrum of polyPhOx (**23**) (**Figure 16a**) exhibits the following characteristic features: a broad O-H stretching vibration at 3440 cm^{-1}, attributable to the adsorbed water or atmospheric contamination; a series of C-H stretching vibration between 3070-2844 cm^{-1} arising from both sp^3 and sp^2 hybridised carbons; a sharp and strong amidic band at 1645 cm^{-1}; C-H scissoring and aromatic C=C stretching vibrations in the region

1495-1415 cm^{-1}; and C-O and C-N stretching vibrations in the region 1185-1147 cm^{-1}. The TGA curve (**Figure 16b**) reveals a single, pronounced thermal degradation event commencing approximatively at 300 °C and concluding at 430 °C, with the maximum rate of weight loss occurring at 400 °C. Following heating to 600 °C, no residual ash was observed.

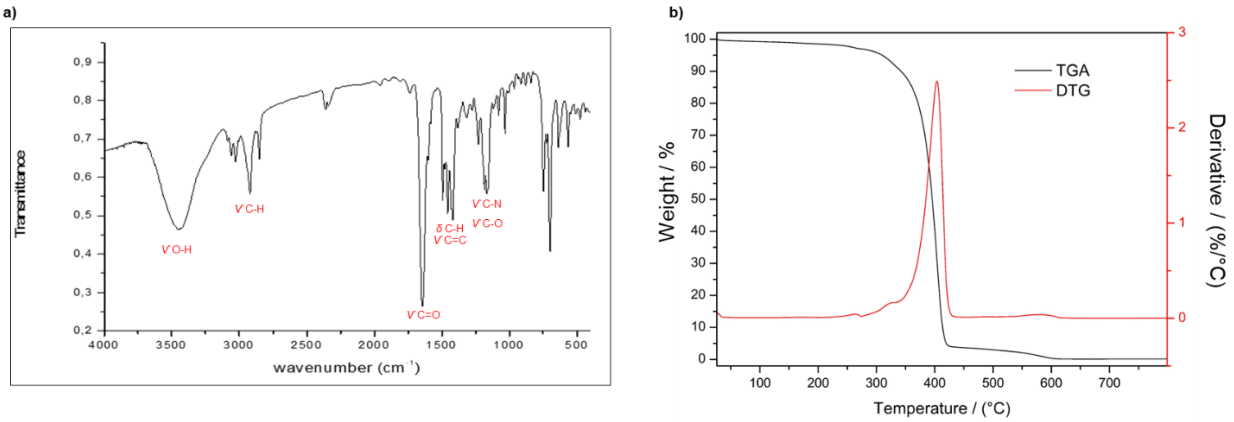

Figure 16 a) FT-IR Spectrum (KBr pellet), b) TGA and derivative TGA (DTG) (N_2 100 mL min^{-1}, heat rate 10 °C min^{-1}) for polyPhOx (**23**).

3.2.1 Thermoresponsivness of poly(2-isopropyl-2-oxazoline), PiPOx **8**

Poly(2-isopropyl-2-oxazoline) (PiPOx, **8**) is a polymeric amide belonging to the class of poly(2-oxazoline)s The hydrophilic tertiary amide of the polymeric backbone is substituted with an *iso*-propyl group which endows the polymer with a lower critical solution temperature (LCST) behaviour in water. Concerning PiPOx (**8**), the phase diagram for a range of polymer concentrations was reported for the first time in 2010;[128] it was shown that PiPOx, (**8**) follows a type I phase behaviour, i.e. the transition temperature (the cloud point temperature, T_{cp}) is affected by the molecular mass. ^{1}H NMR, Raman, and FT-IR spectroscopy measurements detected that, following de-mixing, the polymer chains dehydrate and undergo relevant conformational transitions. In these conditions, liquid-liquid phase separation (LLPS) occurs.[129–131] Moreover, upon continued heating above the cloud point temperature, the macromolecules crystallise with the formation of a macroscopic precipitate composed of nanofibers.[99,132–135] In particular, below the T_{cp} the conformations adopted by the polymer chains are almost disordered and well hydrated (with the macromolecules being dispersed in the solution). Above the cloud point, the polymer adopts an ordered and dehydrated conformation, and the regular conformation of the polymeric chains reached at high temperature, eventually, drives the formation and precipitation of the crystals.[99,131,132] However, what drives the conformational change with temperature is not yet clear. In collaboration with Prof. Barbara Capone's theoretical group, and specifically to support extensive atomistic Molecular Dynamics (MD) simulations led by Dr. Sara Del Galdo, a series of experiments were systematically conducted. These investigations focused on the aqueous PiPOx, examining diverse degrees of polymerisation (DPs) (that is, the number of monomer units per polymer chain) across various concentrations and evaluated both below and above the transition.[136] A summary of the research is reported in this paragraph. Aqueous solutions of PiPOx (**8**) at infinite dilution, for different degrees of polymerisation (DPs: 10, 20 and

30), were simulated above and below the T_{cp}. The aim was to unveil, at the single chain level, both hydration and preferential conformations achieved by the polymer in response to a change in temperature. The three solutes selected, namely, PiPOx10, PiPOx20 and PiPOx30 (that represent PiPOx (**8**) polymer made by 10, 20 or 30 monomers), are employed to model the behaviour of aqueous solutions of the PiPOx (**8**) of molar mass around 1, 2 and 3 kg mol^{-1}. In general, for aqueous PiPOx (**8**), the T_{cp} depends both on the polymer molar mass and on the concentration of the solution. Literature reports that PiPOx (**8**) LCST spans from 34 °C for the polymer with Mn of 3.3 kg mol^{-1} at weight fraction x_w = 0.3; to 26 °C for Mn of 13 kg mol^{-1} at x_w = 0.2.[128] Experimental data relative to the particular systems analysed in this work (for the combinations of molar mass and concentration studied) were not available, thus we had no preliminary information on the actual T_{cp}. Nevertheless, we expected our T_{cp}s to be consistent with the ones reported in literature (T_{cp}, ~ 27 °C). This motivates our choice of selecting two temperatures, one T_L well below and the other T_H well above T_{cp}, to assess the thermoresponsiveness of the system. Moreover, T_L and T_H were chosen to be distant from both the freezing and the boiling point of water. All considerations brought us to define T_L= 10 °C and T_H= 50 °C to model the thermodynamically stable solution and in de-mixing condition, respectively. To compare our results to experimental data, we added an analysis of the infinite dilution cases (single molecule in water) at room temperature condition (i.e. T_R= 30 °C). In particular, we compared the computational trend of the diffusion coefficient (D) as a function of DP, with the one measured on our samples by means of Dynamic Light Scattering (DLS) experiments at ambient temperature. The measured autocorrelation functions of the scattered light intensity were analysed using the NNLS algorithm[137] to obtain the distributions of the hydrodynamic radius, which was converted to a diffusion coefficient distribution. Computationally, the Einstein relation was applied to compute D from the mean square displacement of the centre of mass of the chains, as computed by Gromacs2020.[138] The comparison between the computed and measured data is reported in **Figure 17**. Exact matching of the results cannot be expected; the computational data, reproducing the order of magnitude of D, are in agreement with the experimental ones, thus contributing to the validation of our computational results.

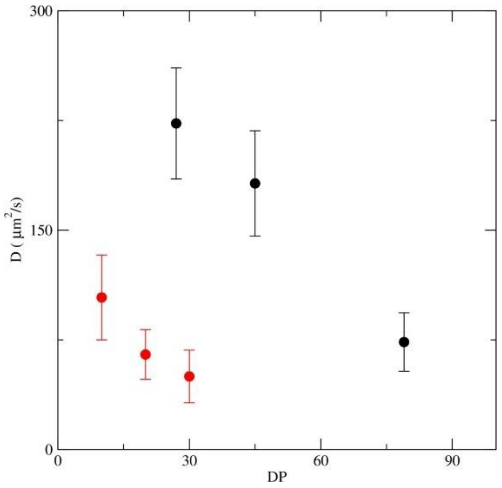

Figure 17: Diffusion coefficient (D) of PiPOx (**8**) as a function of the DP for the single molecule aqueous solutions at room temperature. Both computational (red dots) and experimental (black dots) results are reported. For the computational data we set the temperature T=T_R=303 K.

DLS experiments allow to evaluate the hydrodynamic radius of a macromolecule in solution as the radius of an effective sphere that moves as a Brownian particle. In the analysed systems this spherical assumption seems to be too strong to expect a favourable comparison with the computational data of the gyration radius. Moreover, the evaluation of hydrodynamic radius may be flawed due to the presence of a layer of solvent surrounding the polymer coil while it diffuses. For these reasons, it is well known that a direct comparison between a theoretical radius of gyration and an experimental hydrodynamic radius (R_h) is not straightforward. In addition, even if the macromolecule would have an average spherical conformation, the comparison between the gyration radius obtained computationally and the experimental hydrodynamic radius R_h is not straightforward. According to the specific nature of a system and the corresponding hydration features, we can thus expect either $R_g \geq R_h$ or $R_g \leq R_h$. For this reason, we selected the diffusion rather than the radius of gyration, as the observable for evaluating the agreement between experiment and simulation.

About the single chain conformation, the stretching of the polymer is governed by the conformation of the backbone, which depends on the rotations around the C-C and the C-N bonds. As shown in **Figure 18a**, two independent dihedral angles describe such rotations, namely the Φ and Ψ dihedral angles. We defined Φ and Ψ trough the quadruplets of atoms on the backbones N-C-C-N and C(O)-N-C-C, respectively (where C(O) represents the carbon of the amide moiety while C represents the aliphatic carbon atom in the main chain). From the simulations of PiPOx20 at infinite dilution at low and high temperature, we computed the instantaneous values of each Φ and Ψ dihedral angle along the trajectory thus obtaining the two-dimensional histograms reported in **Figure 18b,c.** For clarity, in the same figure, the corresponding histograms of Φ and Ψ, taken separately, are also reported. Both systems show a pronounced peak in the region (Φ,Ψ) ≈ (±180,−90) which corresponds to polymeric chains in stretched conformations with the *iso*propyl groups alternatively oriented upward and downward from the backbone plane. By comparing the two panels, it clearly emerges that small deviations from such behaviour are responsible for the different macroscopic average conformations that characterise the low and high temperature simulations. In fact, the few values of Φ in the interval [50, 90] obtained for the low temperature system, correspond to regions along the backbone where the series of trans dihedral conformation is interrupted, and the structure partially folds. Such results confirm that temperature at the level of the single chain in solution, has the effect of inducing a stretched and ellipsoidal-like conformation.

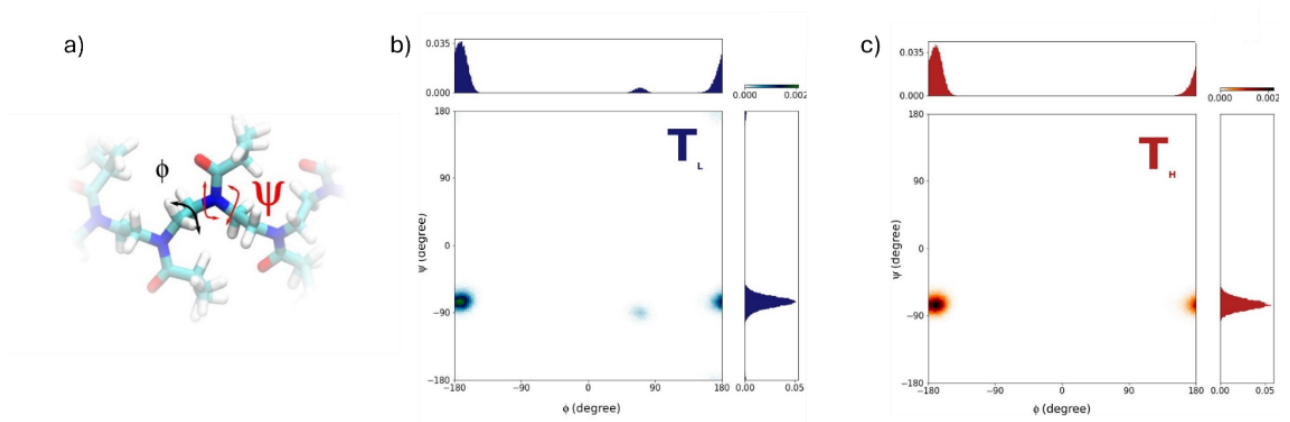

Figure 18: a) Non-redundant Φ and Ψ dihedral angles that determine the conformations of the PiPOx main chain; b) Mono and bi-dimensional histograms of the Φ and Ψ values characterising the conformations of PiPOx20 at infinite dilution at T= 10 °C; c) Mono and bi-dimensional histograms of the Φ and Ψ values characterising the conformations of PiPOx20 at infinite dilution at T= 50 °C.

To gain insight on the phase domain within the mixing gap and explore the interplay between the chains, we performed an in-depth investigation of a finite concentration of aqueous PiPOx10, at the two temperatures T_H and T_L. **Figure 19** clearly shows that for $T<T_{cp}$, even if some extent of aggregation can be observed, the PiPOx (**8**) chains are well hydrated, and sparse polymeric clusters can be observed; on the contrary, above the cloud point, only one cluster enclosing all the solute molecule is formed. Such a condition is consistent with the LLPS which is known to characterise the PiPOx (**8**) aqueous solution de-mixing. The Solvent Accessible Surface Area (SASA), computed by considering all the solute chains together,[139] confirms that, on average, at high temperature the polymeric chains form a compact cluster. In fact, SASA per chain is 8.3 ± 0.2 and 5.5 ± 0.6 nm^2 for the systems below and above the transition point, respectively: the smallest value clearly reports on the increased average compactness of the polymeric cluster at high temperature. However, the values of SASA corresponding to the infinite dilute simulations of PiPOx10 at T_L and T_H are 16.8 ± 0.3 and 17.2 ± 0.3 nm^2 respectively. We can thus conclude that even for the T_L case some clustering can be appreciated, as the corresponding SASA value is around half of that of the single chain in solution. Qualitatively, the fact that some degree of aggregation is detected even in the T_L case, is to be expected as, in general, experimental solutions of aqueous PiPOx (**8**) at the mass fraction of about 0.1 do not appear completely transparent, suggesting the presence of supramolecular structures of polymeric particles that act as visible light scattering centres. The computational analysis allowed us to directly observe that the stiff conformations reached at high temperature prompt the inter-chain interactions that lead to the formation of a polymer-rich region typical of the LLPS. The reduction in excluded volume therefore appears to be the main driving force for stabilising the de-mixed condition.

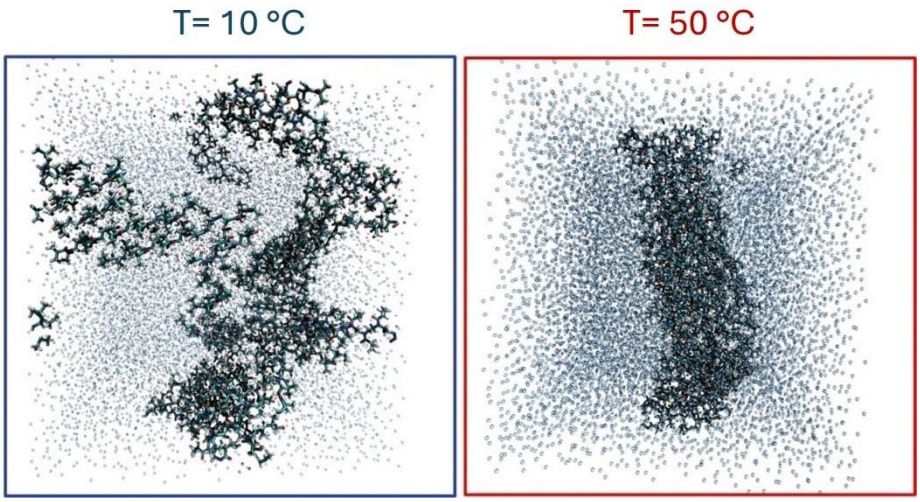

Figure 19: Representative snapshots extracted from the aqueous PiPOx10 simulations at x_w=0.1, for the T= 10 °C and T= 50 °C cases (length 8.1 nm). Polymers are highlighted through the licorice representation, while water is represented through lines. While at T<T_{cp} the polymer chains clusterize while remaining well hydrated, liquid-liquid phase separation occurs above the T_{cp}.

The results obtained should not be considered exhaustive; rather, they represent a more detailed investigation that enhances the understanding of the well-documented thermoresponsiveness of this class of polymers. Furthermore, these findings are poised to contribute to the future development of smart materials tailored for the selective adsorption of specific cargos or for use in drug delivery systems, including applications within biological matrices. This potential is largely due to the biocompatibility of these polymers and their LCST which is proximal to the human body temperature. In fact, PAOx (**5**) can be conjugated to protein and small-molecule drugs while maintaining their activity,[140] grafted onto liposomal bilayers,[88] or formulated into micellar carriers,[141] thereby underscoring their versatility in biomedical applications.

3.3 Application of PolyPhOx **23** as adsorbent for hydrophobic organic pollutants

Contemporary to the PiPOx (**8**) thermoresponsivness investigation, the novel synthesised homopolymer (PolyPhOx, **23**) was employed in specific investigation without a solid scaffold (differently as performed with PiPOx (**8**), deprotected pAmOx (**26**), and deprotected pEstOx, (**27**), for which GO and lignocellulosic substrates have been considered). Due to its high insolubility in water and the presence of aromatic moieties, the possibility of employing polyPhOx (**23**) in wastewater remediation was evaluated, in particular, targeting hydrophobic pharmaceutical products. Following the successful synthesis and comprehensive characterization of the polyPhOx (**23**) via ^{1}H NMR, FT-IR, and thermogravimetric analyses (TGA), this novel homopolymer was subjected to a series of rigorous tests designed to validate its efficiency in adsorbing pharmaceutical pollutant from aqueous media.[121] Aspirin (**28**), ibuprofen (**29**), metoclopramide (**30**), pyramidone (**31**), oestradiol (**32**), and indomethacin (**33**) were selected as model organic pollutants (**Figure 20**) based on their well-documented chemical and physical properties and their widespread detection in municipalized wastewater,[142–144] particularly originating from livestock farms, slaughterhouses, and densely populated urban agglomerations.[145]

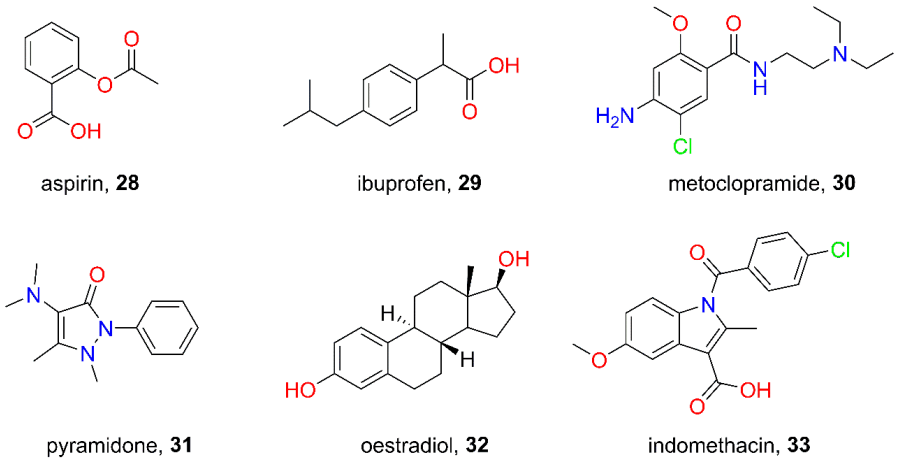

Figure 20 pharmaceutical compound chosen for adsorption experiments.

Initially, batch adsorption experiments were performed under controlled laboratory conditions utilising a water:methanol (70:30) solvent system to ensure homogeneous solutions and to achieve reliable and reproducible results, even at the highest tested concentration of the most non-polar compounds. Specifically, 2 mL of each pharmaceutical in hydroalcoholic solution at varying concentrations were added to 5 mg of polymer, and the resulting suspension was incubated for 24 hours at room temperature. For each pharmaceutical, the adsorption capacity [q_e (mg g^{-1})] and the percentage removal efficiency (R%) were evaluated by comparing the amount of adsorbed pollutant to either the amount of the employed adsorbent (**Equation 4**) or to the initial concentration of the drug (**Equation 5**):

$$q_e = \frac{(C_0 - C_e)V}{W} \qquad (4)$$

$$R\% = \frac{(C_0 - C_e)}{C_0} \times 100 \qquad (5)$$

where C_e (mg L^{-1}) is the experimentally determined liquid-phase concentration of pharmaceutical at equilibrium, C_0 (mg L^{-1}) represents the average concentration of pharmaceutical in the corresponding control, V is the volume of the solution (L), and W represents the amount (g) of the adsorbent used. The results presented in **Figure 21a-b** provided clear evidence of a quite linear trend in the adsorption coefficient (q_e) as a function of the initial concentration of the tested pharmaceuticals up to 200 mg L^{-1}, a concentration that significantly exceeds permissible environmental limits.

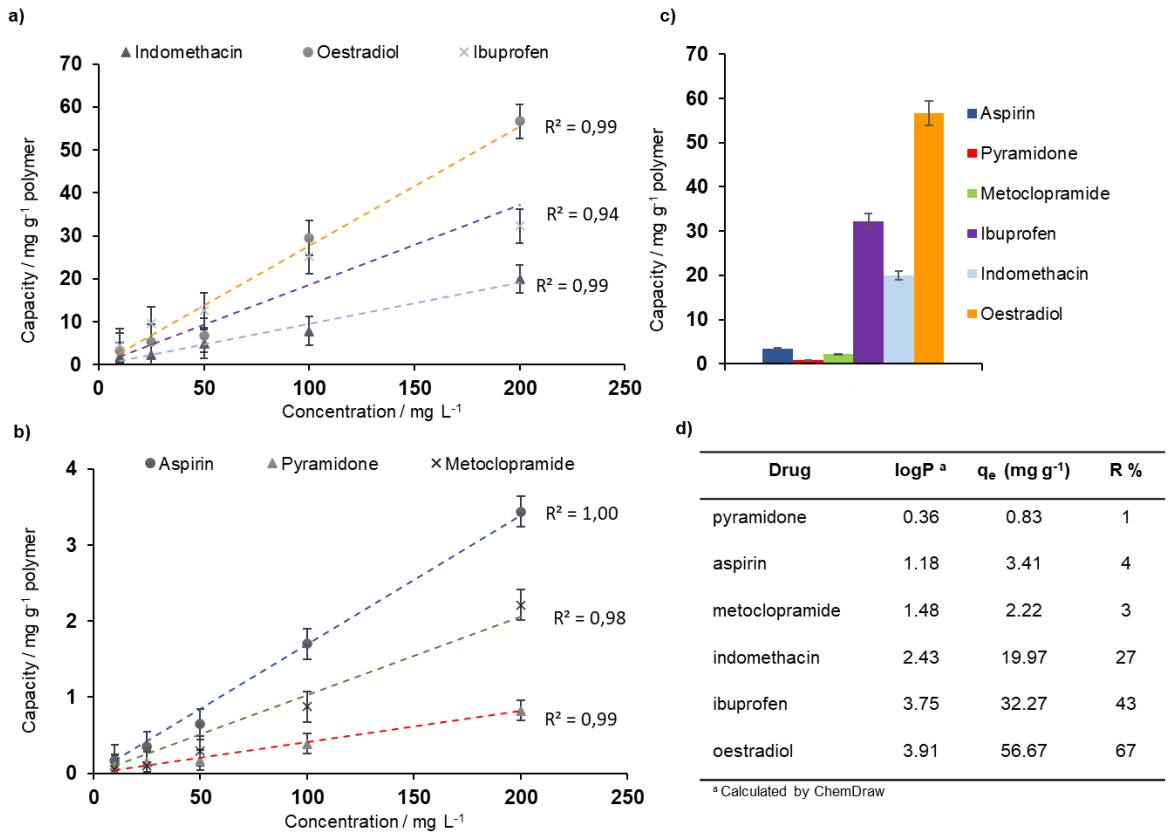

Drug	logP [a]	q_e (mg g^{-1})	R %
pyramidone	0.36	0.83	1
aspirin	1.18	3.41	4
metoclopramide	1.48	2.22	3
indomethacin	2.43	19.97	27
ibuprofen	3.75	32.27	43
oestradiol	3.91	56.67	67

[a] Calculated by ChemDraw

Figure 21 a) adsorption capacity (q_e) of polyPhOx (**23**) vs initial concentration for indomethacin (**33**), oestradiol (**32**), and ibuprofen (**29**). b) q_e of polyPhOx (**23**) vs initial concentration for aspirin (**28**), pyramidone (**31**), and metoclopramide (**30**). c) q_e of polyPhOx (**23**) for pharmaceuticals at 200 mg L^{-1} as initial concentration. d) Table of logP values and removal % (R%).

Notably, polyPhOx (**23**) demonstrated remarkable efficacy in the removal of ibuprofen (**29**) and indomethacin (**33**) for which we found adsorption capacities of 32.27 and 19.97 mg g^{-1} respectively. Furthermore, excellent performance was observed in the removal of oestradiol (**32**), with a q_e of 56.67 mg g^{-1} (**Figure 21c**). In fact, oestradiol (**32**), possessing the lowest water solubility and the greatest hydrophobicity among the tested compounds, demonstrated the most favourable interaction with the hydrophobic domains of the polymer. The findings presented above indicate that polyPhOx (**23**) treatment is markedly more effective in removing those ligands with lower water solubility, offering a promising avenue for future water treatment strategies. A comparison of the removal percentage (R%) with the octanol-water partition coefficient (logP), an indicator of hydrophobicity, reveals a direct correlation: the highest R% values (67, 43, and 27 respectively for **32**, **29**, and **33**) were observed for those ligands with higher logP values (3.91, 3.75, and 2.43 respectively for **32**, **29**, and **33**) (**Figure 21d).** This observation suggests that non-polar species have a reduced affinity for water and aqueous environments, thereby favouring absorption within the hydrophobic domains of the polymer structure. Such a behaviour is probably mediated by a combination of several π-π and electrostatic interactions between the hydrophobic moieties of the pollutants and the aromatic substituents present on the polymer chains. Consistent with these considerations, lower values of adsorption capacity were obtained for aspirin (**28**), metoclopramide (**30**) and pyramidone (**31**), i.e. 3.41, 2.22, and 0.83 mg g^{-1} respectively. Indeed, compounds **28**, **30**, and **31** appear to have a low ratio between hydrophobic and hydrophilic functionalities, leading to significantly lower logP values (i.e. 1.18, 1.48, and 0.36 respectively). In this regard, the increased stabilization

of the aqueous media has the effect of lowering the affinity for the hydrophobic phase, despite the presence of the aromatic rings and the possible favourable π-π stacking interactions. Furthermore, steric hindrance may contribute to preventing the formation of stable interactions between the aromatic groups of polyPhOx (**23**) and those present within the tested pharmaceuticals.

3.3.1 Evaluation of the adsorption properties of polyPhOx **23** in real samples

To assess the adsorption performance of the synthesized polyPhOx (**23**) within a more complex environmental matrix (i.e. considering parameters such as pH, ionic strength, and potential interference of various natural organic matter) subsequent evaluation was performed using a water sample obtained from Albano Lake, which was selected as representative model system. Selected pharmaceuticals were spiked into the lake water (native pH 8.20, serving as a free control sample) at a concentration of 10 mg L^{-1}. This concentration was empirically determined to represent the optimal compromise in terms of solubility for the most hydrophobic compound under investigation [oestradiol (**32**)] and the overall experimental reproducibility. Removal tests on these spiked water samples were conducted in triplicate following the protocol previously established. As depicted in **Figure 22a**, the results reveal that pyramidone (**31**) and metoclopramide exhibited negligible adsorption (approximately 1%).

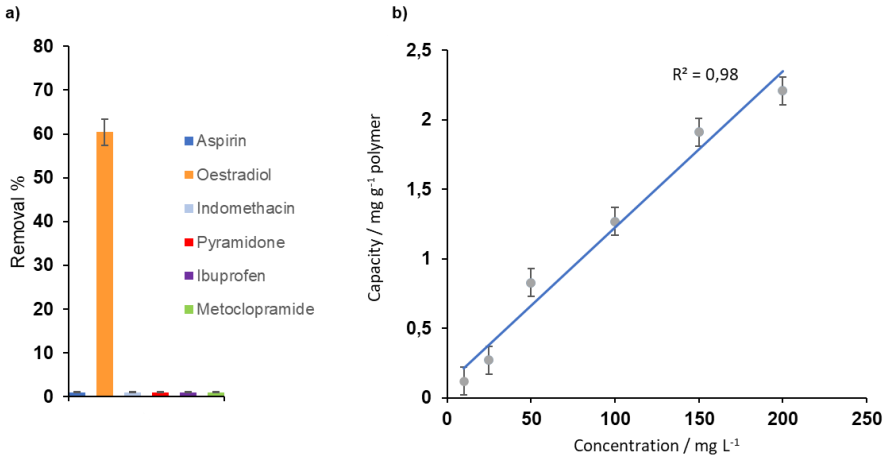

Figure 22 a) Removal percentage of selected drugs in Albano Lake water for pharmaceuticals at a concentration of 10 mg L^{-1}; b) adsorption capacity (q_e) vs initial concentration for aspirin (**28**) in spiked Albano Lake at various concentrations.

The removal percentages of aspirin (**28**), indomethacin (**33**), and ibuprofen (**29**) significantly decreased with respect to the hydroalcoholic solution, moving to 1% from 4%, 27%, and 43% respectively. This phenomenon is likely posited to arise from acid-base reactions occurring at the slightly alkaline pH of 8.20. Indeed, these compounds will predominantly exist in their more stable deprotonated form within this matrix, thereby preventing their effective adsorption by the polymer. Conversely, oestradiol (**32**), the most hydrophobic compound examined (logP = 3.91) was removed with the greatest efficiency (60%) by the synthesised polymer. This finding suggests that the polyPhOx system could be very attractive for the selective removal of non-polar pollutants, and, in particular, this specific pollutant, from complex environmental matrices. For aspirin (**28**) which has a good compromise in terms of solubility in water and removal percentage in the hydroalcoholic

experiments (logP=1.18 and R%=4), we also performed experiments in spiked Albano Lake water at various concentrations to ascertain any increase in q_e, despite the very low removal percentage (1%) observed in this matrix. The results, depicted in **Figure 22b**, illustrate a linear trend between the adsorption coefficient and the initial concentration of aspirin (**28**) (R^2= 0.98). It is postulated that this persistent underperformance may be primarily attributable to the deprotonation effect previously discussed.

3.3.2 Resusability of PolyPhOx (**23**)

The long-term applicability of novel materials is significantly impacted by the reusability of adsorbents, a crucial characteristic that should be considered when evaluating its potential for practical implementation, but it is often overlooked during the initial development stages. Effective reusability requires the adsorbent to successfully release the retained contaminant via a desorption or regeneration step, without compromising the chemical and physical stability of the underlying matrix.[146] To assess reusability in this study, following each adsorption experiment performed at the maximum initial drug concentration (200 mg L^{-1}), the polymer (5 mg) was subjected to a series of washes: thrice with tap water (15 mL), thrice with deionised water (15 mL) and finally with methanol (15 mL). The adsorption experiment was then repeated using the regenerated material, and the adsorption capacity (q_e) was calculated for each drug across ten such cycles. Only after the completion of ten loading and regeneration cycles was a slight decrease in adsorption capacity (q_e) observed, amounting to an approximate 1% reduction (**Figure 23**).

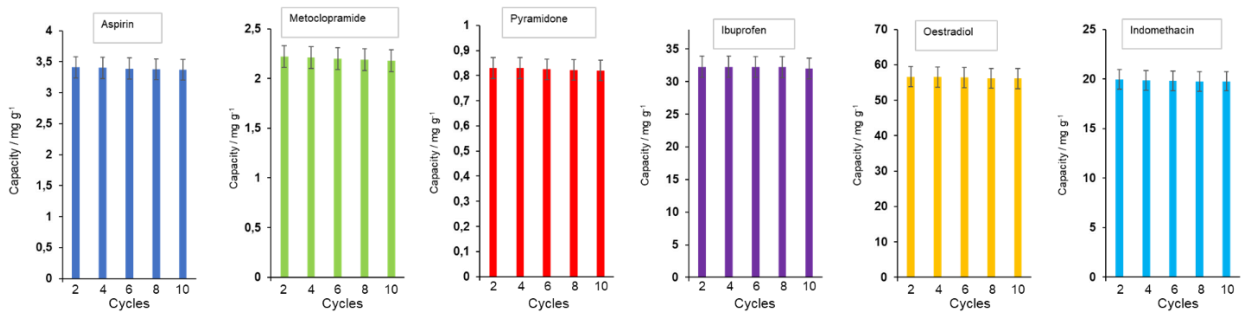

Figure 23 Adsorption capacity (q_e) calculated after ten loading cycles for the target pharmaceutical compounds after proper regeneration process, each bar represents two adsorption cycles.

To rigorously demonstrate the sustained stability of the polymer and its ability to be reused without further chemical modification following repeated adsorption and the regeneration cycles, comparative analyses were performed utilising ^{1}H-NMR and FT-IR spectroscopy to assess the material before and after ten loading and washing cycles. As shown in the FT-IR spectrum (**Figure 24a**), no new signals were found, demonstrating that the core polymer structure remain intact throughout the process. Similarly, the ^{1}H NMR analysis confirmed that the regenerated adsorbent material retained the original molecular structures of the parent polymer, thereby verifying its chemical stability. Indeed, the spectrum shows only a barely noticeable increase in signal integration (**Figure 24b**), particularly in the aromatic region, compared to the spectrum of the unemployed polymer **23** presented in **Figure 14b**. Such evidence suggests that a minor quantity of pharmaceutical

compounds may persist within the polymer after all the loading and regeneration cycles. However, this residual contamination does not significantly alter the adsorbent's overall characteristic or performance.

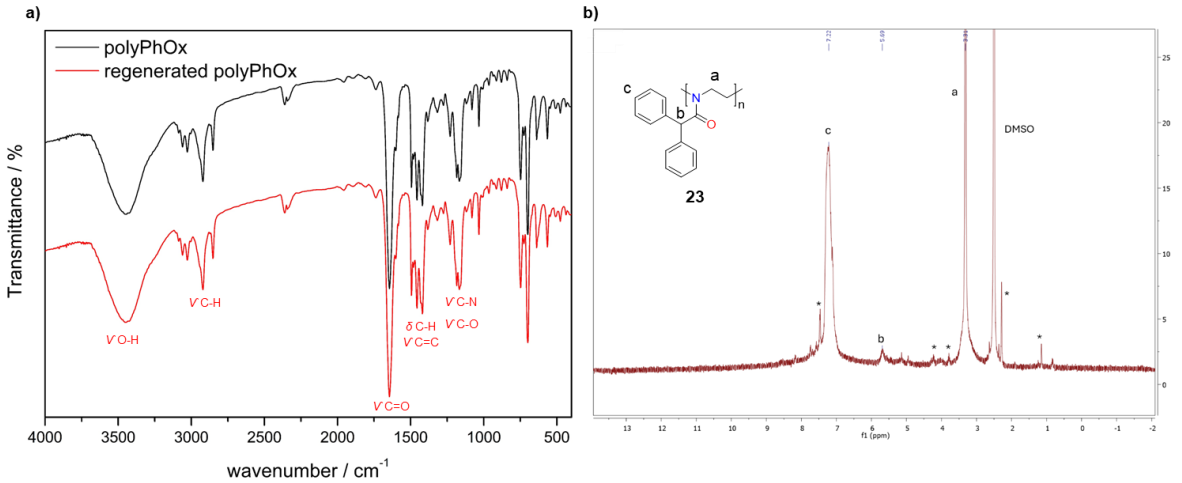

Figure 24 a) FT-IR spectrum of polyPhOx **23** before and after the adsorption cycles and washing, b) ^{1}H NMR spectrum of polyPhOx (**23**) in DMSO-d6 after the adsorption cycles and washing.

The observed positive outcomes highlighted the remarkable efficiency of the evaluated systems, especially in adsorbing the most apolar organic compounds [i.e. oestradiol (**32**), ibuprofen (**29**) and indomethacin (**33**)], which exhibited a greater affinity for the fixed polymeric phase.

Given the demonstrated efficacy in removing non-polar compounds, it was decided to target the more polar acidic organic compounds exploiting the peculiar action of pAmOx polymer (**26**), hypothesizing a potential acid-base reaction between the amine moieties on the polymer and the carboxylic acid groups present within the targeted pharmaceutical products. Due to its inherent water solubility, pAmOx (**26**) requires immobilization onto a solid support to facilitate its removal from the treated aqueous solution after the adsorption process. Among a diverse range of potential substrates, including nanoparticles, Graphene Oxide (GO) was chosen as a possible substrate based on its robust mechanical strength and low chemical degradability.[147] Additionally, the presence of oxygen-containing functional groups on GO, such as carboxyl, carbonyl, epoxy, and hydroxyl, enable facile surface modification, making it highly reactant-specific for various organic entities.[148] Knowing that, several efforts were thus directed towards designing and synthesizing a polymeric-based adsorbent capable of interacting with NSAIDs and covalently linking it onto GO. In addition, lignocellulosic materials, specifically native cellulose and commercially available lignin, were considered as alternative solid support materials for poly(2-oxazolines)s such as PiPOx (**8**), pAmOx (**26**), and pEstOx (**27**), due to their high availability in the environment and their inherently low cost.

3.4 Graphene Oxide (GO) composites with poly(2-oxazoline)s for organic pollutants adsorption

In pursuit of an efficacious adsorbent medium for organic pollutants, the possibility of grafting active polymers on Graphene Oxide (GO) has been investigated. Preliminary investigations indicated that a "*Grafting To*" approach, whereby a pre-synthesised polymer is conjugated to the substrate, should be superior to a "*Grafting From*" approach in which the monomer polymerization is initiated directly from the substrate surface. The latter approach necessitates additional complex activation steps for the substrate itself. This finding has informed the decision to prioritize the "*Grafting To*" strategy in subsequent phases of adsorbent material development.

3.4.1 Preparation and characterization of composite materials with GO and poly(2-oxazoline)s

In initial experiments, poly(2-isopropyl-2-oxazoline) (PiPOx, **8** was selected as a model polymer owing to the facile monomer synthesis and subsequent purification. The same "*Grafting To"* procedure was then extended to poly(2-(3-(Boc-amino)propyl)-2-oxazoline) (pAmOx, **24**). This approach necessitated the preliminary preparation, characterisation, and purification of graphene oxide (GO), the detailed methodology is delineated in the experimental section. Briefly, GO was obtained through graphite oxidation employing a modified Hummers' method.[149] This methodology involves a sequential, multi-step addition of H_2SO_4, $NaNO_3$, $KMnO_4$, and H_2O_2 to oxidize the carbon atoms in graphite lattice (**Figure 25a**), followed by filtration and rigorous washing to recover the pure oxidised product. In contrast to Brodies's method, the replacement of $KClO_3$ with $KMnO_4$ enhanced the safety profile of the reaction by obviating the formation of explosive chlorate (ClO_3^-), while the inclusion of $NaNO_3$ eliminated the evolution of noxious fume from HNO_3.[150] The UV-Vis spectrum of the resulting dark-brown powder, presented in **Figure 25b**, suggest the presence of sp^2-hybridised carbon domains. Specifically, GO (black curve) exhibits a maximum absorption peak at approximately 235 nm, attributable to π-π* transition of the atomic C-C bonds, and a shoulder peak at approximately 300 nm arising from n-π* transitions of aromatic C-C bonds,[149] as compared to the lack of significant absorbance from untreated graphite flakes (red curve).

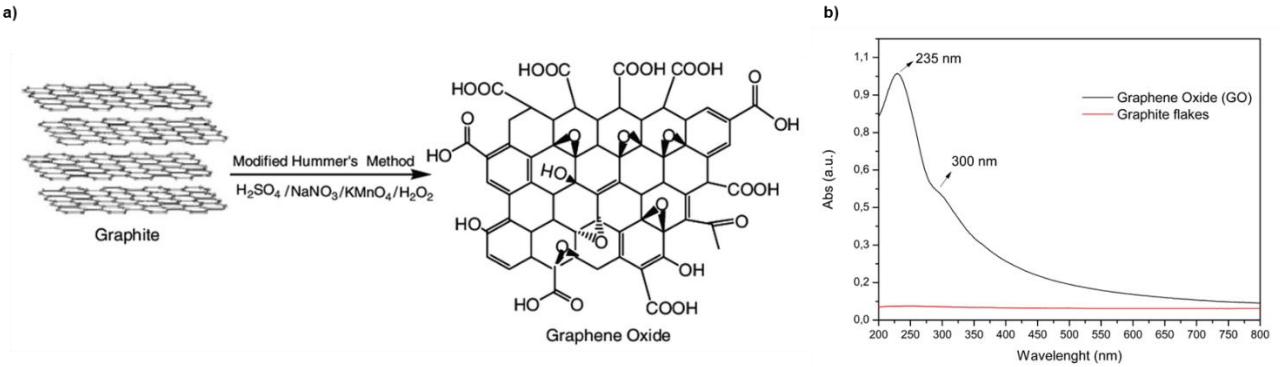

Figure 25 a) GO preparation with the Hummers' method starting with graphite flakes, b) Uv-Vis spectra comparison for GO (black curve) and graphite flakes (red curve), suspended in milli-Q-grade water at 100 μg mL^{-1}.

After the GO preparation and characterization, the designed poly(2-oxazoline) was newly synthesised according to the previously described protocol, with the critical modification pertaining to end-chain functionality. In fact, the living polymerisation process was quenched by the addition of 1,6-hexamethylenediamine (**34**) affording an amine-terminated polymer suitable for conjugation to GO, as illustrated in **Scheme 3**, This procedure yielded the composite materials named GO-PiPOx and GO-pAmOx, contingent upon the specific poly(2-oxazoline) involved. The linkage of poly(2-ethoxycarbonylethyl-2-oxazoline) (pEstOx, **25**) was not pursued due to its carboxylic moieties, which are already present on GO resulting in no introduction of a new functionality on the substrate. Moreover, the deprotection reaction of pEstOx (**25**) to obtain the free carboxylic moiety, necessitates the use of 5% KOH in water, which could, albeit partially, hydrolyse the amide bond mediating the polymer-GO linkage. PolyPhOx (**23**) was also deemed unsuitable to be linked onto GO because it bears aromatic moieties, which are already present in the substrate.

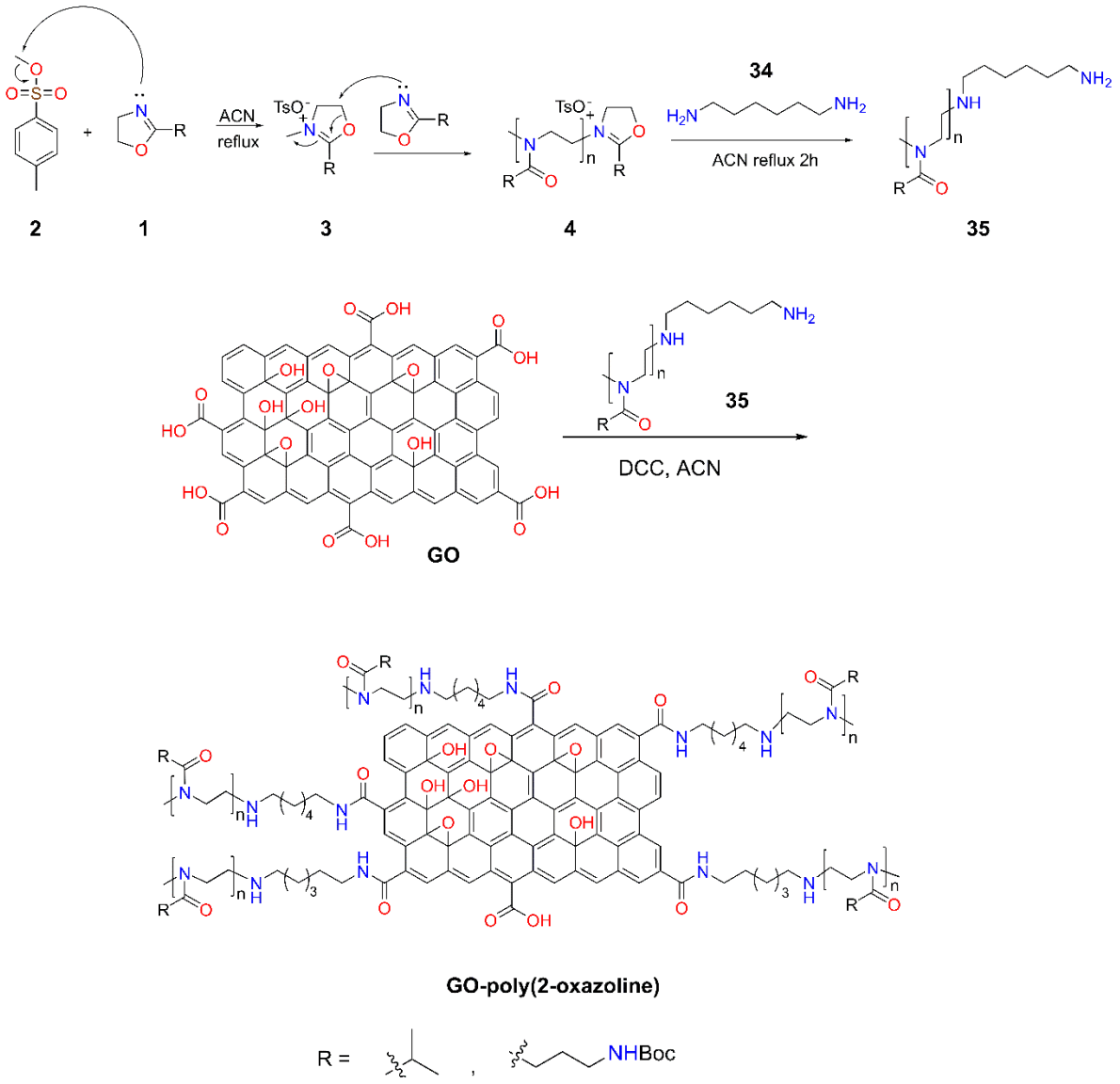

Scheme 3 General procedure for GO-poly(2-oxazoline) synthesis.

After the preparation, the composite materials GO-poly(2-oxazoline), recovered as a brown-to-black powders, underwent extensive washing with tetrahydrofuran (THF) to remove any unlinked polymer and secondary reaction byproducts. For GO-pAmOx the deprotection reaction was carried out according to the well-established protocol as detailed in the experimental part, involving overnight stirring of the composite material in chloroform ($CHCl_3$) dispersion, with the addition of trifluoroacetic acid (TFA) to remove the Boc protecting group and generate the free amine moieties of the polymer pAmOx (**26**). To initially evaluate successful deprotection, the Boc-protected homopolymer pAmOx (**24**) was subjected, at the same time, to analogous reaction conditions, and the resulting product was analysed via ^{1}H NMR analyses (as shown in **Figure 15a**). Afterward, to assess the covalent linkage of the poly(2-oxazolines) to the GO sheets, Thermogravimetric Analysis (TGA) was employed. This technique facilitates continuous monitoring of the sample weight loss as a function of temperature, enabling the comparative analysis of the thermal degradation profile of GO and the obtained GO-poly(2-oxazolines). In addition, Attenuated Total Reflectance Infrared Spectroscopy (ATR-FTIR) was considered to compare spectra of the starting GO and the synthesised composite materials, with the corresponding homopolymer spectra included as reference (**Figure 26**).

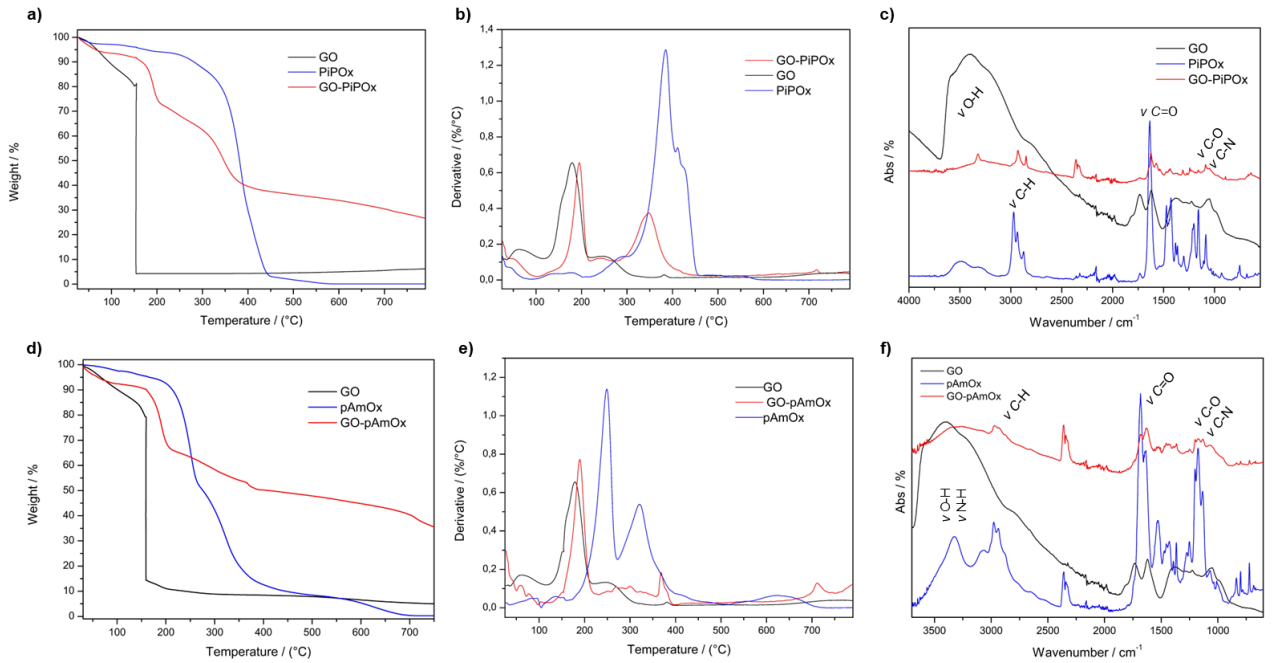

Figure 26 TGA, derivative TGA (DTG), and ATR-FTIR for GO, PiPOx (**8**) and GO-PiPOx (a-c) and for GO, pAmOx (**26**), and GO-pAmOx (d-f) heat rate 10 °C min^{-1}, N_2 100 mL min^{-1}.

TGA curve obtained for the prepared Graphene Oxide (GO) exhibits the following distinct features: (i) a 6% of weight loss up to 100 °C, attributed to the thermal desorption of water molecules, physically adsorbed onto the hydrophilic GO surface; (ii) a rapid and pronounced weight loss (80%) between 100 and 200 °C, resulting from the decomposition of oxygen-containing functional groups to CO, CO_2, and H_2O;[151] and (iii) a further 6% of weight loss up to 800 °C, associated with the removal of more thermally stable oxygen functionalities and the thermal decomposition of GO framework. The observed thermal degradation profile for GO alone is consistent with findings reported in publications by Kohji Ohno et. al.[152] and by Jiangbo Wang et. al.[153] where GO-based composite materials, incorporating organic polymers have been investigated using the same

analytical technique. The TGA curve obtained for GO-PiPOx composites (**Figure 26a,b**) exhibits two distinct decomposition peaks: the first with a maximum at 194 °C, consistent with the decomposition range of the GO, and a second one with a maximum at 347 °C consistent with the decomposition range of the homopolymer PiPOx (**8**), confirming the effective linkage of the polymer to the GO support. The shape of the thermal decomposition curve for the GO-pAmOx composite (**Figure 26d, e**) exhibits notable variations relative to the profiles obtained for GO and pAmOx (**26**) as single components. Indeed, the composite material exhibits a four-stage weight loss profile: approximately 7% below 100 °C, approximately 20% between 100 and 200 °C, and approximately 20% between 200 and 500 °C, resulting in a high ash residue up to 800 °C. The ATR-FTIR spectrum of GO-PiPOx (**Figure 26c**) features: the C-H sp^3 stretching vibrations at 2926 and 2849 cm^{-1}, and the C-N and C-O stretching vibrations at 1162 and 1084 cm^{-1}, indicating that the original GO infrared absorption profile has been modified by the successful polymer linkage. The spectrum of GO-pAmOx (**Figure 26f**) exhibits characteristics consistent with a superposition of the spectra of its individual components. Specifically, the following diagnostic features are discernible: (i) a broad band in the 3450-3250 cm^{-1} region, primarily attributable to O-H stretching vibrations from GO, overlapping with N-H stretching vibrations arising from the polymer contribution; (ii) the C-H sp^3 stretching vibrations from the polymer component at 2978 and 2938 cm^{-1}, (iii) the carbonyl absorption at 1679 cm^{-1} diagnostic of the amide bond formation, and exhibiting a distinct shift compared to the C=O stretching vibration at 1733 cm^{-1} observed in the spectrum of pristine GO; (iv) C-H bending vibrations from the polymer side chains, along with other skeletal vibrations, are present in the region between 1560-1355 cm^{-1}, features largely absent in the spectrum of the original GO; and (v) the C-N and C-O stretching vibrations at 1220, 1170, and 1136 cm^{-1} are present in the reference spectrum of the poly(2-oxazoline) homopolymer **26**, but absent in the GO spectrum, further confirming the linkage of the polymer to the support material. These observations, in total, support the successful formation of the GO-pAmOx composite. To further elucidate the structure and morphology of the GO-pAmOx composite, which is the composite employed in adsorption experiments targeting acidic drugs (**Chapter 3.4.2**), Atomic Force Microscopy (AFM) was also employed to compare the composite material with pristine GO. (**Figure 27**).

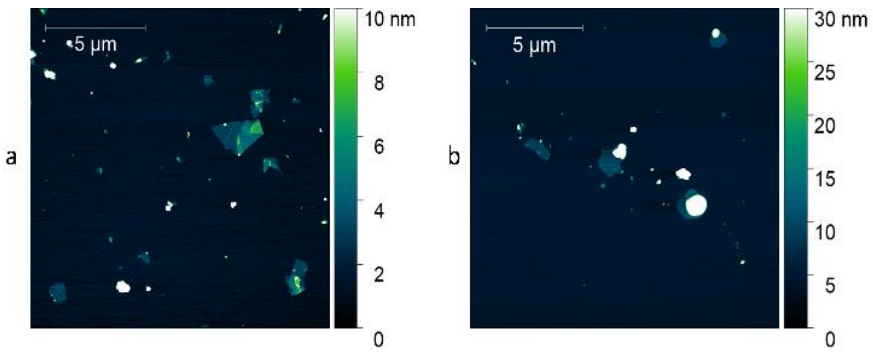

Figure 27 15x15 µm AFM images of GO (a) and GO-pAmOx (b). The height of the sample is given by the colour scale on the right.

AFM investigation of both GO and GO-pAmOx involved the acquisition of a large-field scans, ranging from 10x10 to 50x50 µm to ensure a statistically representative sampling of the materials. Both GO and GO-pAmOx

appear as randomly distributed flakes, with GO-pAmOx exhibiting notably more dispersed distribution than that observed for GO. The height for both samples varied from approximately 5 nm to 50 nm, verifying that the sonication process successfully exfoliated the GO sheets into structures of varying lateral dimensions and thickness. In terms of surface morphology, GO flakes are characterised by ridges with an average thickness of about 10 nm. In contrast, GO-pAmOx flakes displayed a flatter profile, with a ridges thickness of approximately 3 nm, as shown in **Figure 27b**. This disparity in surface thickness could be attributed to the presence/absence of the pAmOx (**26**) on the simple GO surface. Specifically, GO layers typically fracture and break during the exfoliation process, leading to an increase in surface thickness. In contrast, GO-pAmOx single layers appear to entirely exfoliate during the sonication, yielding a notably smoother, less corrugated surface profile.

To complement the AFM analysis, the GO and GO-pAmOx samples were deeply investigated by Transmission Electron Microscopy (TEM) with sub-angstrom resolution coupled with Electron Energy Loss Spectroscopy (EELS) analyses to provide detailed morphological and chemical characterization, facilitating a comprehensive understanding of the interaction and grafting of the pAmOx polymer (**26**) onto the GO substrate (**Figure 28**). Initial morphological analyses, provided in **Figures 28a,b**, do not reveal any discernible differences between the GO and GO-pAmOx samples. It is imperative to note that all analyses were performed under stringent vacuum conditions, in the absence of any solvent that could potentially induce morphological alteration in the GO sheets. The chemical composition of GO and GO-pAmOx materials were further investigated by EELS technique. **Figure 28c,d** present the EELS spectra acquired for GO and GO-pAmOx respectively. In the case of GO alone, only two prominent peaks are detected at 281 eV and 528 eV, corresponding to the presence of carbon and oxygen of the GO sheets. Magnification of the region between 300 and 700eV (inset, **Figure 28c**) clearly confirms the absence of any signals related to nitrogen (typically observed around 400eV. In contrast, the EELS spectrum of GO-pAmOx, (**Figure 28d**) exhibited a third prominent peak at 396 eV, confirming the presence of nitrogen atoms originating from the pAmOx polymer (**26**). Furthermore, magnification of this region (inset **Figure 28d**) revealed a distinct nitrogen signal with an intensity comparable to that of the oxygen one. To visualise the spatial distribution of the pAmOx polymer (**26**) across the GO sheets, a TEM image and its related nitrogen signal intensity map (acquired by EELS analyses) are presented in **Figure 28e,f.** As can be seen, the nitrogen signal is uniform all over the GO-sheets providing compelling evidence that the polymer is grafted uniformly and ubiquitously onto the GO sheets and attesting to the robust interaction between the polymer anchoring groups and the GO surface moieties.

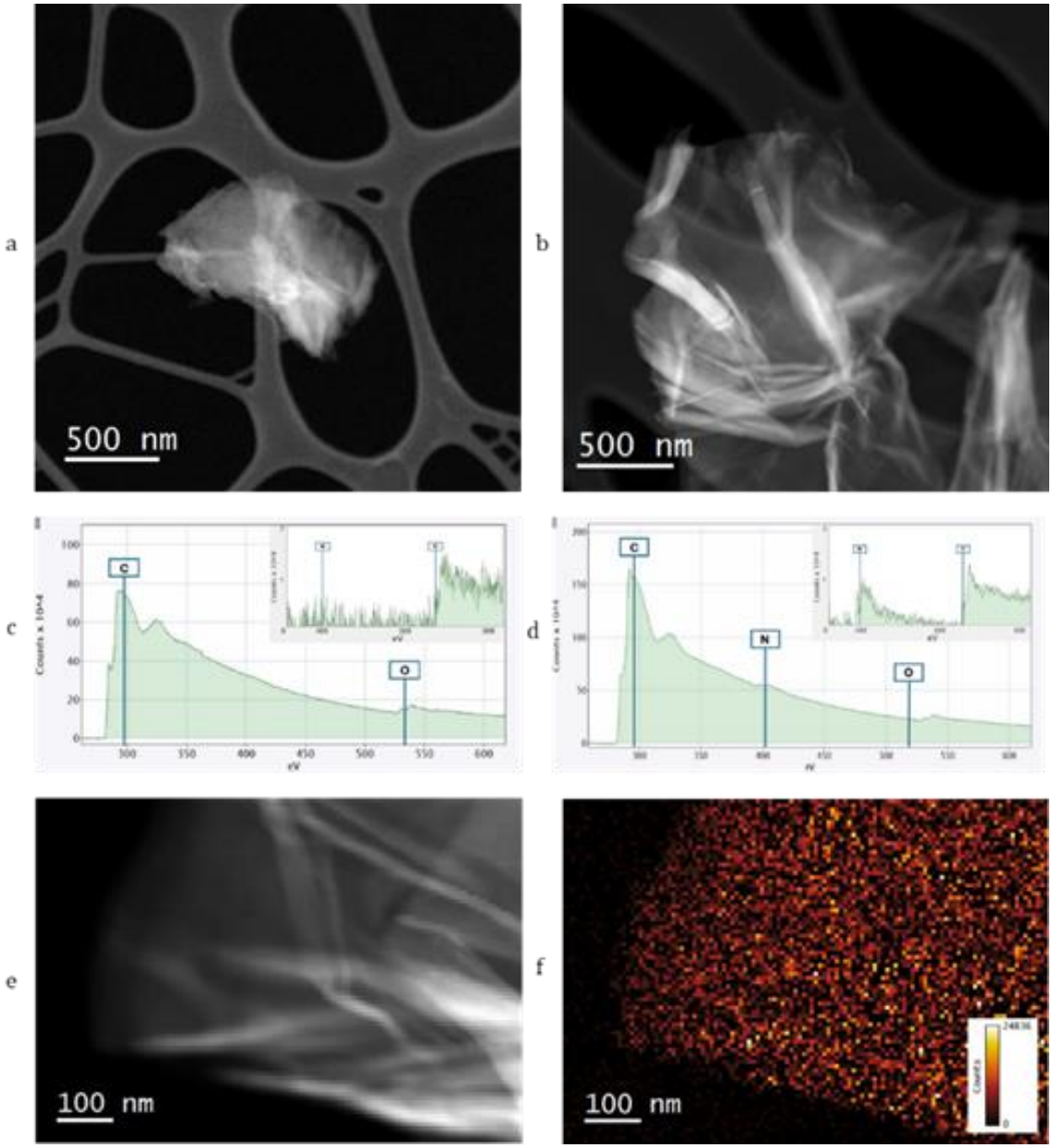

Figure 28 TEM images of GO (a) and GO-pAmOx (b). EELS spectra of GO (c) and GO-pAmOx (d) with the magnified region between 300-600eV (insets). TEM images related to the EELS analysed area of GO-pAmOx (e), EELS nitrogen distribution map (f).

Following the thorough characterization of GO-pAmOx composite material, a series of adsorption experiments were undertaken to evaluate its efficacy in removing acidic organic compounds detected in wastewater as thoroughly described in the following sections.

3.4.2 Evaluation of the adsorption properties of GO-pAmOx

To comprehensively assess the adsorptive behaviour of the developed novel material, this study investigates the adsorption of carefully selected pharmaceutical compounds onto the GO-pAmOx. Our hypothesis posits the existence of significant interactions between these amine functionalities and the carboxyl groups present in small acidic drugs, namely ibuprofen (**29**), aspirin (**28**), and ketoprofen (**36**). Moreover, benzoic acid (**37**) was selected as further representative pollutant due to its well-documented carcinogenic and toxic properties at specific concentrations as well as its widespread industrial use primarily in food, cosmetic, and

pharmaceutical related products.[154] Crucially to rigorously test and validate our underlying hypothesis regarding acid-base interaction, this investigation was designed to also include non-acidic compounds, specifically metoclopramide (**30**), pyramidone (**31**), and etoperidone (**38**), expecting for them very low adsorption. The structures of all compounds employed in these initial adsorption experiments are shown in **Figure 29**.

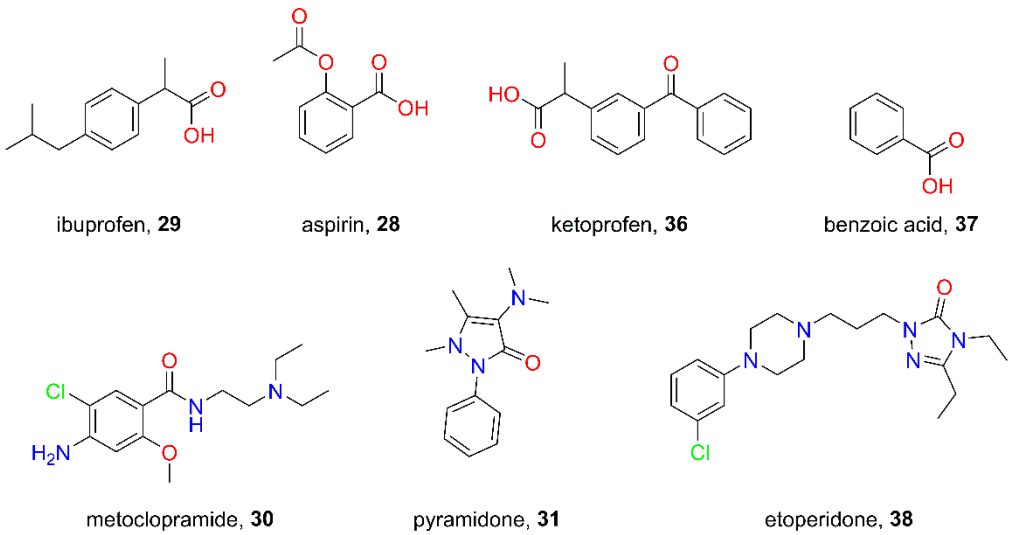

Figure 29 Pollutant pharmaceutical compounds commonly detected in wastewater.

To investigate the adsorption performances of the GO-pAmOx composite material, a series of batch adsorption experiments were initially conducted utilising a water:methanol (70:30) solvent system. Briefly, 10 mg of adsorbent materials (either GO or GO-pAmOx) were added to 5 mL aliquots of each drug solution (with concentrations ranging from 25 to 250 mg L^{-1}) and, following 12 h incubation period, the residual concentrations of pharmaceutical products were quantified with HPLC analysis. All experiments were conducted in triplicate for each pharmaceutical compound, using GO, GO-pAmOx, and control samples (no adsorbent added) to facilitate direct comparative assessment of the material's adsorption properties and efficiencies. Adsorption capacity [q_e (mg g^{-1})] was determined using **Eq.4**, which directly correlates the amount of adsorbed pollutant to the amount of the employed adsorbent. **Figure 30** presents the adsorption coefficient q_e as a function of the initial concentration for each pharmaceutical species, along with a table detailing the logP values of the tested compounds to aid in the analysis of the observed structure-activity relationship. The data reveal a clear and compelling contrast in the adsorption of ibuprofen (**29**), aspirin (**28**), ketoprofen (**36**) and benzoic acid (**37**), which was significantly favoured by GO-pAmOx over GO, in contrast to the opposite behaviour observed for metoclopramide (**30**), pyramidone (**31**) and etoperidone (**38**). A preliminary examination of **Figure 29** suggests that the presence of aromatic rings strongly promotes the interaction with GO layers via π-π stacking, which facilitates the removal of all the tested pharmaceuticals, however, other factors may be involved and are discussed in subsequent paragraphs.

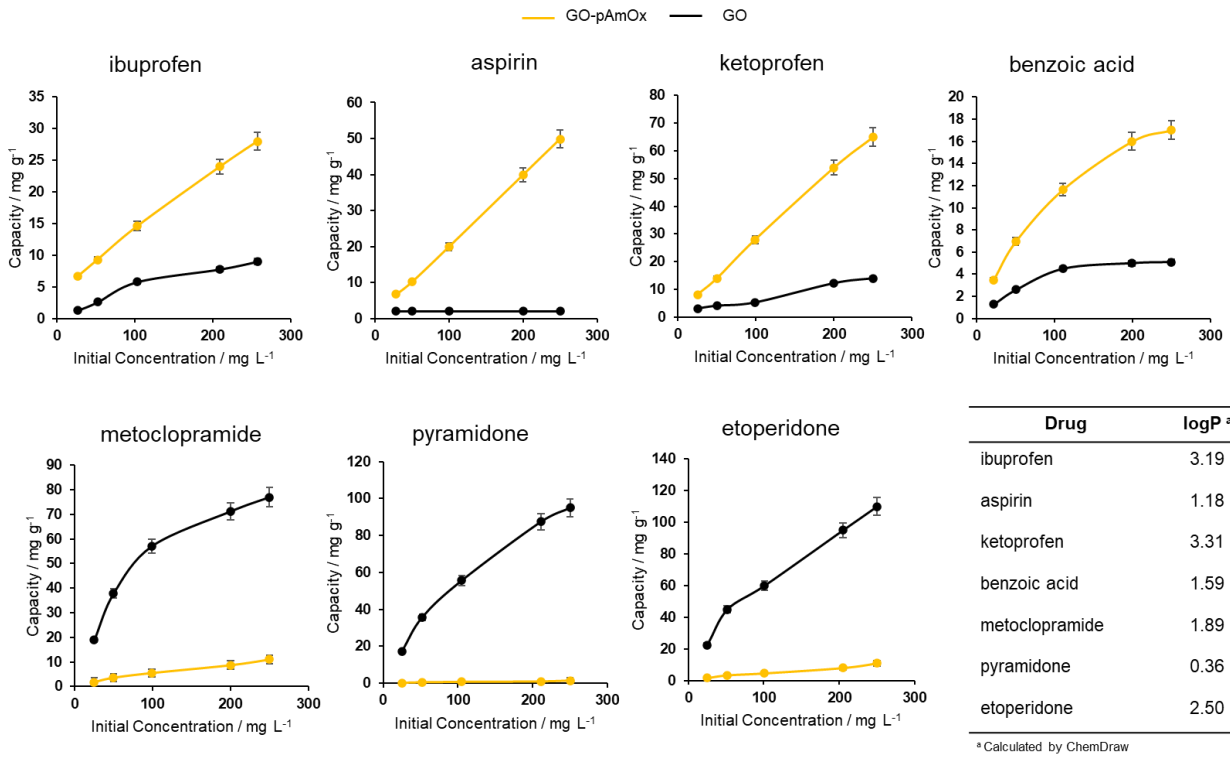

Drug	logP [a]
ibuprofen	3.19
aspirin	1.18
ketoprofen	3.31
benzoic acid	1.59
metoclopramide	1.89
pyramidone	0.36
etoperidone	2.50

[a] Calculated by ChemDraw

Figure 30 q_e vs initial concentration for each drug in adsorption experiments conducted in hydroalcoholic medium, and logP values table.

Notably, the marked differences in adsorption capacities observed between the GO-pAmOx composite and pristine GO should be primarily attributed to the interplay between carboxyl moieties, a common feature in compounds **28**, **29**, **36**, and **37**, and amine functionalities, which are ubiquitous in compounds **30**, **31**, and **38**. Specifically, at the maximum initial concentration explored (250 mg L^{-1}), GO-pAmOx exhibited impressive q_e values of 28.0, 49.8, 65.0, and 17.0 mg g^{-1} for ibuprofen (**29**), aspirin (**28**), ketoprofen (**36**) and benzoic acid (**37**) respectively. Conversely, the corresponding q_e values for these compounds when using pure GO were substantially lower, measuring 9.0, 2.0, 14.0, and 5.1 mg g^{-1}. This disparity highlights the critical role of acid-base interactions between the amino groups of pAmOx (**26**) and the acidic groups of compounds **29**, **28**, **36**, and **37**, which substantially enhance the adsorption affinity of the GO-pAmOx composite, thereby strengthening the overall adsorption process. Meanwhile, the repulsion due to the carboxylic acid functionalities that decorate the pure GO surface negates any alternative positive interactions that could potentially occur between compounds **29**, **28**, **36**, **37**, and the GO. In the case of metoclopramide (**30**), pyramidone (**31**), and etoperidone (**38**), the absence of carboxylic moieties significantly diminished their affinity for the GO-pAmOx composite, resulting in notably lower q_e values of 11.0, 1.4, and 11.0 mg g^{-1}. However, when tested with pure GO, the presence of various amine functionalities strongly fosters complementary acid-base interactions, which, coupled with potential halogen bonding involving the sp^2 hybridised carbon atoms of GO, yield striking q_e values of 77.0, 95.0, and 110.0 mg g^{-1}. By leveraging these synergistic interactions, these findings not only reinforce the inherent utility of GO as an adsorbent but also highlight the enhanced selective removal capabilities of the GO-pAmOx composite for a targeted subset of organic pollutants in aqueous environments. This selectivity underscores its remarkable potential for advanced

applications in water remediation strategies. Given our overarching aim to develop a material specifically tailored for water remediation, the adsorption performance of GO-pAmOx was subsequently investigated in aqueous solutions, limiting our experiments to the compounds **29**, **28**, **36**, and **37**, selected based on their preferential adsorption onto GO-pAmOx in hydroalcoholic media. **Figure 31a** depicts the adsorption capacity (q_e) as a function of the initial concentration, ranging from 25 to 90 mg L^{-1} for each drug. The concentrations explored fall within the linear range of the adsorption trend, as evidenced by the high R^2 values (>0.99) obtained from the linear fitting of the data for all compounds. At the maximum initial concentration tested (90 mg L^{-1}), the adsorption coefficient values were 37.4, 27.5, 43.5, and 26.0 mg g^{-1} for ibuprofen (**29**), aspirin (**28**), ketoprofen (**36**) and benzoic acid (**37**), respectively. For comparison, equivalent experiments were conducted with GO alone at 50 mg L^{-1}, and the results are compared with the experiments performed with GO-pAmOx at the same initial concentration in **Figure 31b**.

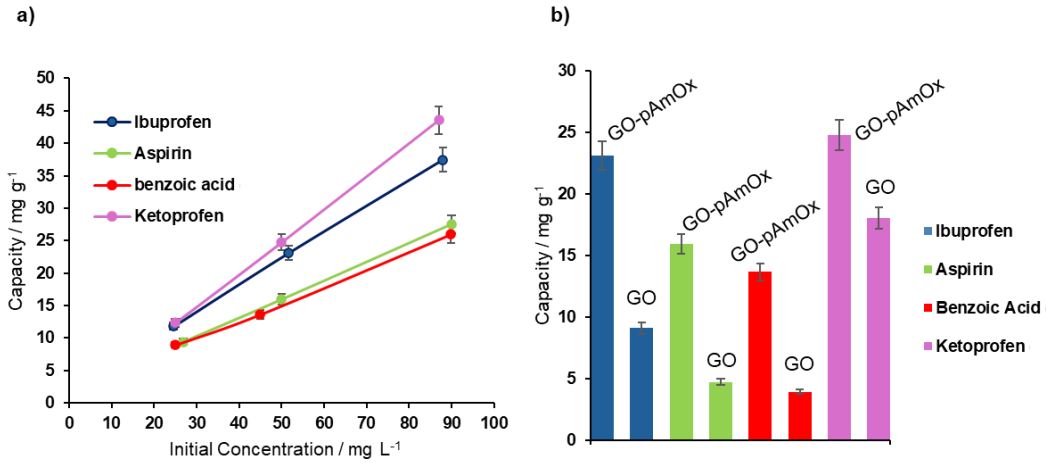

Figure 31 a) q_e vs initial concentration for each drug in adsorption experiments conducted in water. b) q_e comparison between GO-pAmOx and GO for each drug in water adsorption experiments at 50 mg L^{-1} as initial concentration.

Comparing the adsorption experiments conducted at an initial pharmaceutical concentration of 50 mg L^{-1} in water confirms the superior adsorption capacity of the GO-pAmOx composite compared to GO for the removal of compounds **29**, **28**, **36**, and **37**. Specifically, the q_e values for GO-pAmOx were 23.1, 15.9, 24.8, and 13.6 mg g^{-1} for ibuprofen (**29**), aspirin (**28**), ketoprofen (**36**), and benzoic acid (**37**) respectively, significantly exceeding the values obtained with GO (9.1, 4.7, 18, and 3.9 mg g^{-1}). Analogous to observations made in the hydroalcoholic solvent system, the enhanced adsorption performance could be attributed to the synergistic effect of π-π stacking (between the aromatic rings of the pollutants and GO sheets) and acid-base interactions (between the carboxylic acid groups of the pollutant and the amine moieties of pAmOx (**26**) component). Therefore, while π-π stacking interaction alone contributes to some degree of the adsorption with GO, the derivatization with pAmOx (**26**) dramatically improves the overall adsorption process by providing a second, energetically favourable interaction pathway. Importantly, the q_e values measured in pure water (at the same initial concentration) were consistently higher than those obtained in water:methanol (70:30) solution (**Table 4**). Such behaviour is consistent with the known decreased aqueous solubility of these pharmaceutical

compounds in pure water, thus rendering them more susceptible to adsorption at the solid-liquid interfase (a phenomenon also evident in the case of the GO alone adsorbent).

Table 4 adsorption coefficient (q_e) in mg g^{-1} in different solvents at 50 mg L^{-1} as initial concentration.

	H_2O:CH_3OH (70:30)		H_2O	
Drug	GO-pAmOx	GO	GO-pAmOx	GO
ibuprofen	9.3	2.6	23.1	9.1
aspirin	10.2	2.0	15.9	4.7
ketoprofen	14.0	4.0	24.8	18.0
benzoic acid	7.0	2.6	13.6	3.9

Furthermore, it is noteworthy that the adsorption of ibuprofen (**29**) is enhanced in water, such that it is more readily adsorbed than aspirin (**28**), whereas in the hydroalcoholic environment the trend is reversed. This observation likely reflects the higher hydrophobicity of ibuprofen (**29**) relative to aspirin (**28**) (as indicated by the log P table detailed in **Figure 30**). Taken together, these findings suggest that, while experiments in hydroalcoholic mixtures enable the exploration of higher drug concentrations due to the enhanced solubility of the target compounds, experiments performed in pure water are also essential to better understand the adsorption processes in more environmentally relevant matrices.

Adsorption isotherms of GO-pAmOx

To study how ibuprofen (**29**), aspirin (**28**), ketoprofen (**36**), and benzoic acid (**37**), distribute between the liquid and the adsorbent phases, the data of equilibrium adsorption capacity for GO-pAmOx were analysed according to Langmuir and Freundlich models of adsorption isotherms. The type 2 Langmuir isotherm model can be expressed in a linearised form as follows, (**Eq.6**):

$$\frac{1}{q_e} = \frac{1}{K_L\, q_{max}} \; \frac{1}{C_e} + \frac{1}{q_{max}} \qquad (6)$$

where K_L is the Langmuir constant, which provides a measure of the binding affinity and q_{max} is the maximum adsorption capacity.[155]

The Freundlich isotherm model can be expressed as follows (**Eq.7**):

$$lnq_e = lnK_F + \frac{1}{n}\, lnC_e \qquad (7)$$

where K_F is the Freundlich constant that, similarly to K_L, provides a measure of the binding affinity, n is a parameter that quantifies the heterogeneity of adsorption.[156] The Langmuir model assumes monolayer adsorption (that is, layers of only one adsorbed molecule can form), where all the adsorption sites are equivalent and have the same affinity for the adsorbed molecule, i.e. adsorption is homogeneous. Instead, the Freundlich model can be applied to multilayer adsorption and heterogeneity is considered (heterogeneous surface and/or adsorption sites and/or affinity for the ligand). According to **Eq.6** and **Eq.7**, the parameters of

the two models can be obtained from the linear regression of $1/q_e$ vs 1/Ce and $\ln q_e$ vs $\ln C_e$, as reported in **Table 5**. In the same table also the value of R^2 is reported as a measure of goodness of each linear fit. Analysis of the adsorption isotherms (**Table 5**) using both Langmuir and Freundlich models yielded excellent fits (R^2>0.9) for all four compounds.

Table 5 GO-pAmOx Langmuir and Freundlich parameters for hydroalcoholic medium experiments.

Langmuir Isotherm Model			
Drug	q_{max} (mg g^{-1})	K_L (L mg^{-1})	R^2
ibuprofen	27 ±7	0.023 ±0.009	0.921
aspirin	78 ±30	0.006 ±0.002	0.965
ketoprofen	68 ±16	0.033 ±0.007	0.989
benzoic acid	27 ±2	0.009 ±0.001	1.000

Freundlich Isotherm Model			
Drug	n	K_F (L mg^{-1})	R^2
ibuprofen	1.7 ±0.2	1.4 ±0.3	0.975
aspirin	1.3 ±0.2	0.6 ±0.1	0.988
ketoprofen	1.7 ±0.1	3.8 ±0.5	0.988
benzoic acid	1.6 ±0.2	0.7 ±0.2	0.971

In detail, the Freundlich model provided a superior fit, i.e. the best correlation coefficients with respect to the Langmuir one, for both ibuprofen (**29)** and aspirin (**28**), while both models performed similarly for ketoprofen (**36**), differently for benzoic acid (**37**) the Langmuir model showed a marginally better fit. The Langmuir q_{max} values (mg g^{-1}) corresponds to 27, 78, 27, and 68 respectively for ibuprofen (**29**), aspirin (**28**), benzoic acid (**37**) and ketoprofen (**36**). These values are consistent with the experimental adsorption capacities calculated at the highest concentration explored. Freundlich n values between 1 and 10 suggest remarkably favourable adsorption for each compound.[157] Similarly, the K_F and K_L values, confirm that GO-pAmOx has the strongest affinity for ketoprofen (**36**). However, due to both the very high R^2 values obtained for both fitting procedures preclude a definitive determination of both the precise adsorption mechanism (monolayer versus multilayer) and the assessment of the heterogenicity or homogeneity of the adsorption sites.

Evaluation of pH effects on the adsorption process

Given the presence of carboxylic acid group within the target pharmaceuticals and basic amine groups within the pAmOx (**26**) component of the composite, the influence of pH on the adsorption process in aqueous solution was systematically investigated. Adsorption experiments were conducted at fixed pharmaceutical concentration of 90 mg L^{-1} (corresponding to the maximum concentration used in previous aqueous adsorption experiments at the natural pH equilibrium; **Figure 32**).

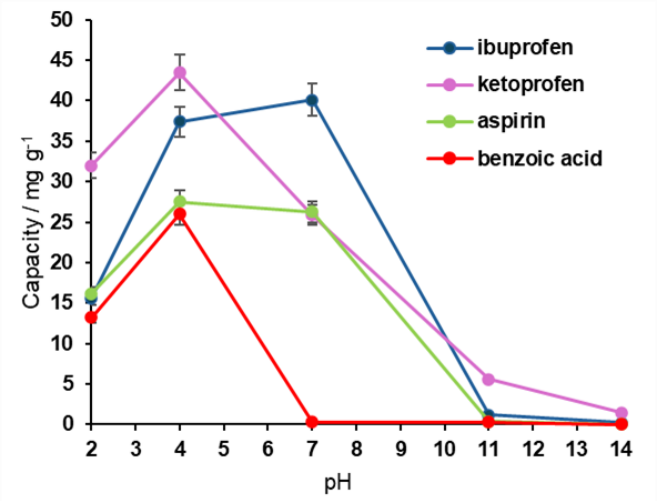

Figure 32 q_e vs pH in water experiments at 90 mg L^{-1} as initial concentration.

The pH of the prepared solutions was adjusted precisely to the desired value through the addition of either 0.1 M NaOH or 0.1 M HCl. Maximal adsorption (q_e) was achieved at the natural pH equilibrium (approximately pH 4) for both ketoprofen (**36**) and benzoic acid (**37**) In contrast, for ibuprofen (**29**) and aspirin (**28**), maximal adsorption was observed not only at pH~4 but also remained comparatively high even at pH 7. Specifically, as the pH increased from 2 to 4, the deprotonation of carboxylic groups intensified, enhancing their suitability for an electrostatic interaction with the protonated amine moieties. However, when the pH dropped below 4, the protonation of the amine groups within the GO-pAmOx composite increases, but it is induced by the external addition of HCl, competed with the acid-base interactions involving the carboxyl groups of the target pharmaceuticals. A notable decrease in q_e was observed also at pH values exceeding 7. This reduction is likely attributable to the deprotonation of the acidic groups of the pharmaceutical compounds, that is caused by the external addition of NaOH, which subsequently rendered them less capable of effective interaction with the active amine moieties of the polymer.

3.4.3 Reusability of GO-pAmOx

As underscored previously, the reusability of an adsorbent material is a key parameter to consider and evaluate when assessing its potential for practical application but is often overlooked during the development of novel materials. For effective reuse, the adsorbent must successfully release the adsorbed contaminant via a desorption or regeneration step without compromising the chemical and physical stability of the underlying matrix.[146] To evaluate the reusability of the prepared GO-pAmOx composite as an adsorbent, ten consecutive adsorption-desorption cycles were performed, employing polluted aqueous solutions of compounds **29**, **28**, **36**, and **37** at an initial concentration of 90 mg L^{-1}. Following each adsorption step, GO-pAmOx (10 mg) was washed successively with tap water (3 x 10 mL), distilled water (3 x 20 mL), and finally with methanol. The adsorbent material was recovered after each washing step through centrifugation (5000 rpm, 10 min) and subsequent vacuum drying. Following this regeneration procedure, the adsorbent material was reloaded with 5 mL of the drug's water solution. The adsorption capacity (q_e) was recalculated after each regeneration cycle.

As demonstrated in **Figure 33**, a negligible reduction in q_e of less than 1% was observed after ten such cycles, highlighting the exceptional reusability and stability of the GO-pAmOx composite material.

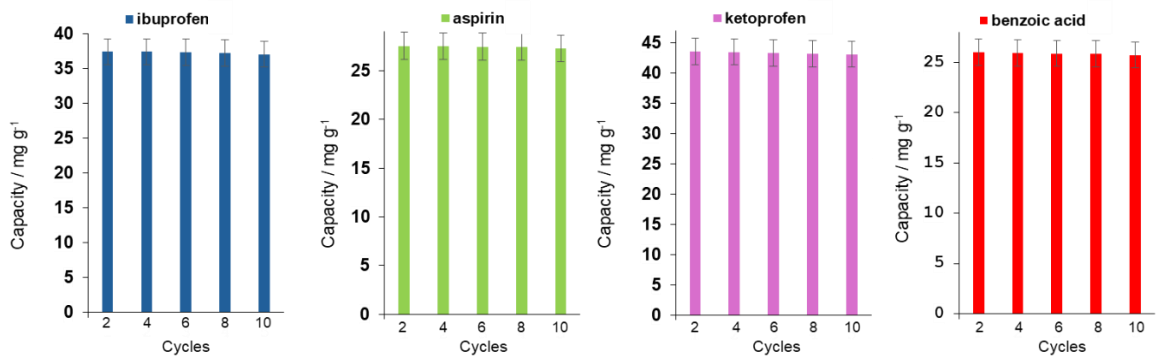

Figure 33 q_e calculated for the loading cycles (each bar represents two adsorption cycles) employing the highest initial concentration.

The structural integrity of the regenerated GO-pAmOx was further validated through post-regeneration TGA and ATR-FTIR analyses. As depicted in **Figure 34** no significant changes in the TGA and FT-IR profiles were observed, confirming the sustained stability and non-degradation of the adsorbent material.

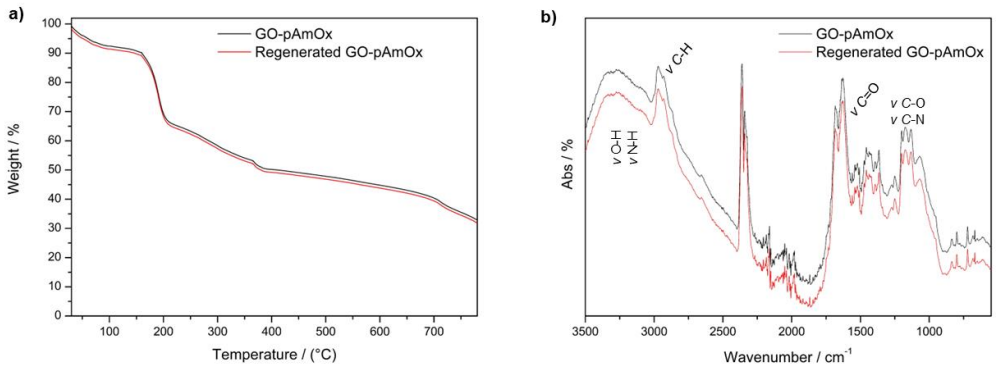

Figure 34 Comparison of TGA curve for GO-pAmOx and regenerated GO-pAmOx, and b) Comparison of ATR-FTIR spectrum for GO-pAmOx and regenerated GO-pAmOx.

3.5 Lignocellulosic composites with poly(2-oxazoline)s for heavy metal ions adsorption

To produce a composite material consisting of cellulose and poly(2-oxazoline) copolymer, it is first imperative to activate the cellulose by introducing a suitable and effective leaving group capable of initiating the polymerization process. Following this activation, the polymerization is commenced by adding the chosen monomer and refluxing the mixture dissolved in acetonitrile (ACN) under controlled heating. This "*Grafting From"* approach has been demonstrated to be superior and more effective to the "Grafting To" approach. Preliminary experimental data supports this assertion: attempts to synthesize the desired composite material via a *Grafting To* analogous procedure—involving the linkage of an amine-terminated polymer **35** to activated cellulose—were unsuccessful. This result contrasts sharply with the more extensive functionalization achieved in the synthesis of graphene oxide (GO)-poly(2-oxazoline) composites, highlighting the distinct advantages of the grafting-from methodology for cellulose-based composite materials.

3.5.1 Synthesis and characterization of activated cellulose.

The functionalisation of cellulose to facilitate subsequent grafting processes involves the introduction of specific leaving groups, including chlorine (Cl^-), bromine (Br^-), and tosyl (Ts). These groups are typically introduced via selective substitution of the primary hydroxyl (OH) group of commercially available cellulose Avicel PH 101, as illustrated in **Scheme 4** and detailed within the experimental section.

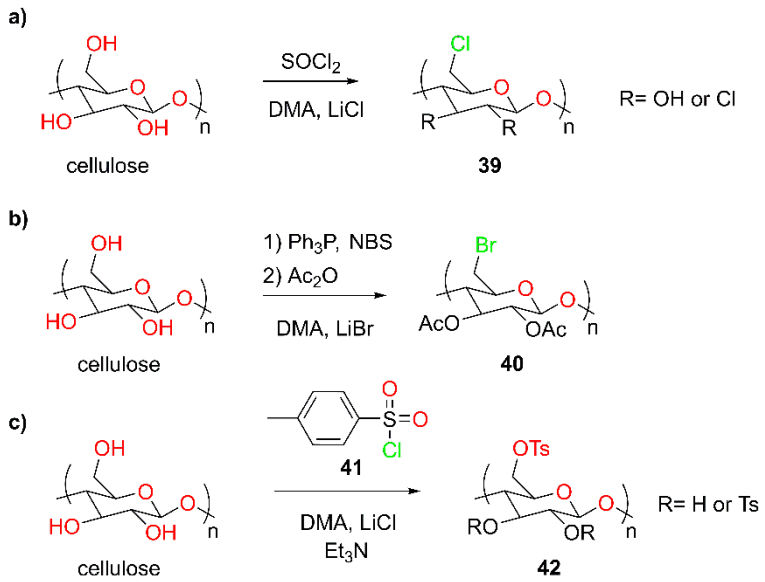

Scheme 4 Activated celluloses synthesis, with: (a) chlorination, (b) bromination and (c) tosylation reaction, yielding chlorinated cellulose (**39**), brominated cellulose (**40**), and tosyl cellulose (**42**).

Briefly, following and modifying established procedures[158–161], the general approach is as follows: (i) chlorinated cellulose (**39**) was obtained by treating the starting material, dissolved in *N,N*-dimethylformamide (DMF) with lithium chloride (LiCl), with 1 eq. of thionyl chloride ($SOCl_2$); (ii) brominated cellulose (**40**) was prepared by treating the starting material, solubilized in *N,N*-dimethylacetamide (DMA) with lithium bromide

(LiBr), initially in the presence of 4 eq. of triphenylphosphine (Ph_3P) and 4 eq. of *N*-bromosuccinimide (NBS), followed by derivatisation of the secondary hydroxyl groups with 10 eq. of acetic anhydride (Ac_2O) to give more chemical stability to the substrate; (iii) tosyl cellulose (**42**) was obtained by reacting the starting cellulose, dissolved in DMA with LiCl, with 5.5 eq. of triethylamine (Et_3N) and 5 eq. of tosyl chloride (TsCl, **41**) at 4 °C. All the reaction products were subsequently precipitated and washed thoroughly with water and/or ethanol, yielding pure powder characterised by a white to pale yellow hue, obtained in excellent yields ranging from 88 % to 99%. The activated celluloses were characterized with thermogravimetric analysis (TGA) as presented in **Figure 35**, with the aim of assessing the thermal stability and elucidating the changes in decomposition temperatures consequent to the chemical modifications by evaluating the different thermal behaviour of starting cellulose and reaction products.

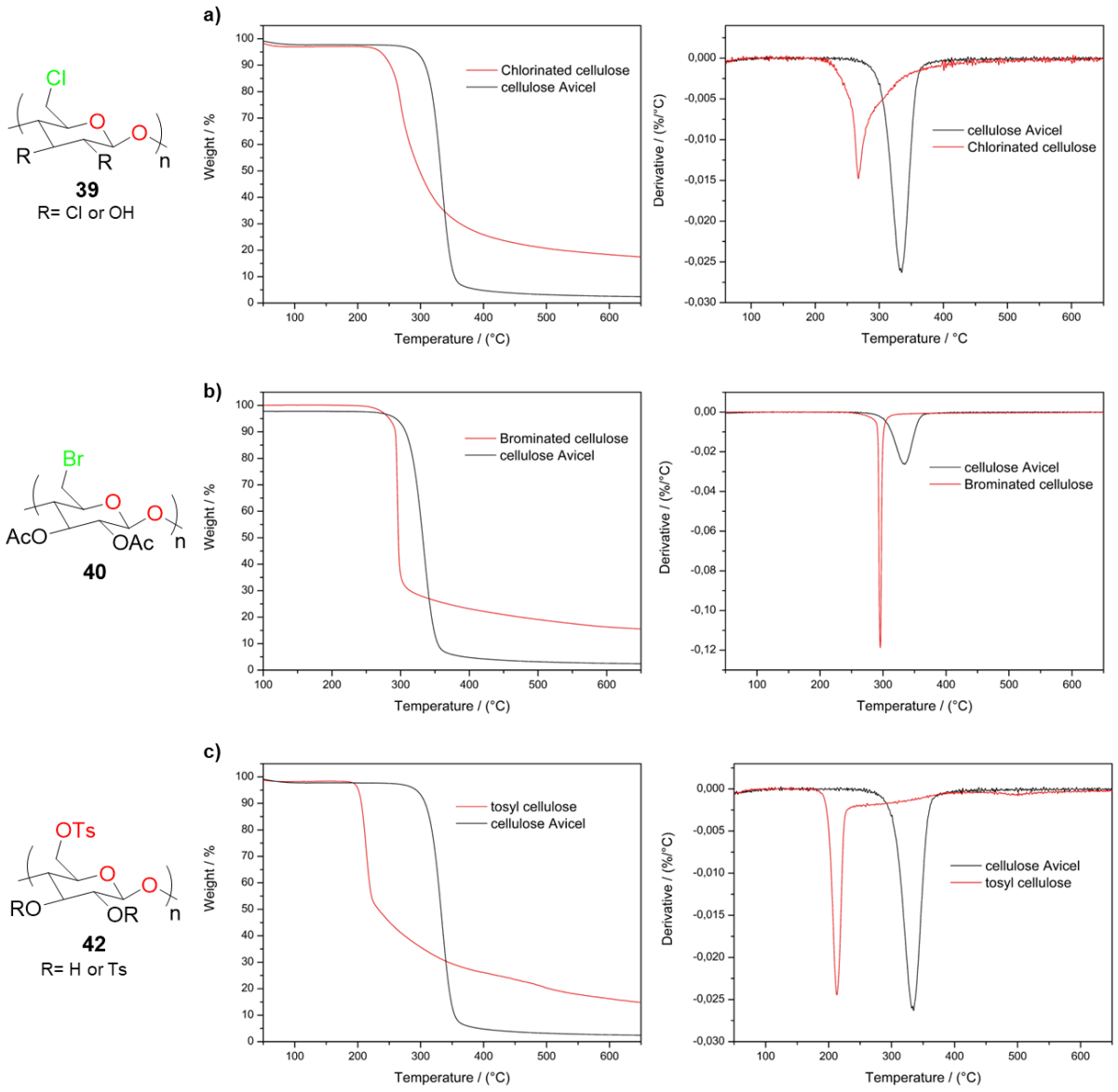

Figure 35 TGA and derivative TGA (DTG) for the three activated celluloses: a) chlorinated cellulose (**39**), b) brominated cellulose (**40**), and c) tosyl cellulose (**42**) with the starting material as reference. Heat rate 10 °C min^{-1}, N_2 80 mL min^{-1}.

All functionalised celluloses exhibit a reduction in decomposition onset and peak temperatures compared to the unmodified starting material. Specifically, the maximum decomposition temperatures correspond to 265 °C, 295 °C, and 213 °C for chlorinated (**39**), brominated (**40**), and tosyl cellulose (**42**), respectively, whereas pristine cellulose Avicel PH 101 decomposes around 333 °C. Furthermore, the modified cellulose displays a residual ash content of approximately 15-25% in weight even heating up to 650 °C, whereas for the original cellulose the ashes residuum is completely absent after 400 °C. These findings indicate that the chemical modification induces structural alteration within the cellulose matrix, resulting in a measurable decrease in thermal stability relative to the unmodified commercial cellulose used as the starting material. Another analytical technique employed was the Attenuated Total Reflection Fourier-Transform Infrared Spectroscopy (ATR-FTIR). As illustrated in **Figure 36**, the spectra of each different chemically activated cellulose derivative are compared to that of the unmodified, commercial starting material. In the case of chlorinated cellulose (**39**, **Figure 36a**), the undeniable appearance of a new absorption band around 602 cm^{-1} is evident, attributable to the stretching vibration of C-Cl bond indicating successful substitution.

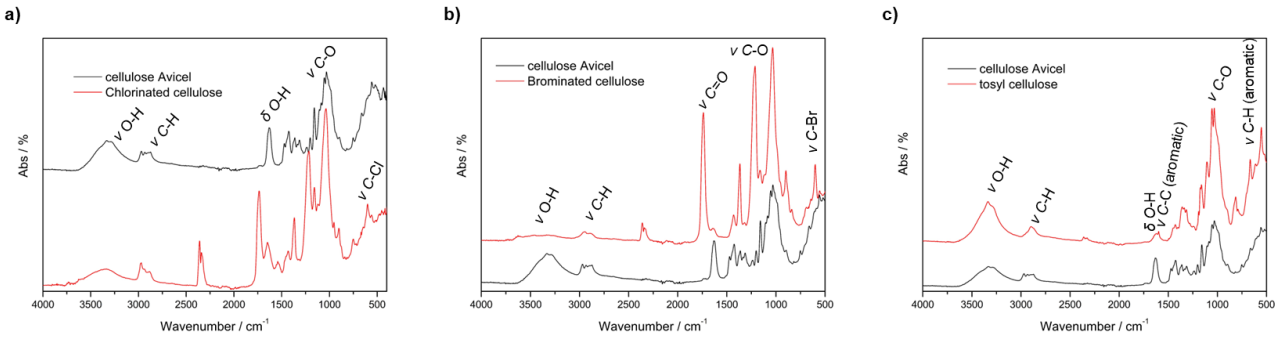

Figure 36 ATR-FTIR of: a) chlorinated cellulose (**39**), b) brominated cellulose (**40**), and c) tosyl cellulose (**42**) in comparison with starting material.

A similar spectra feature is also observed for brominated cellulose (**40**, **Figure 36b**), where a distinct signal at approximately 592 cm^{-1} corresponds to C-Br stretching vibrations. Additionally, for both halogenated celluloses, a notable shift in the O-H bending vibration is observed within the 1600-1750 cm^{-1} region compared to the unmodified material, reflecting alterations in hydrogen bonding interactions consequent to the substitution. In the case of tosyl cellulose (**42**, **Figure 36c**), characteristic diagnostic signals for the introduced tosyl group are evident:[161] a distinctive aromatic C-H stretching band around 815 cm^{-1} and an aromatic C-C stretching vibration near 1595 cm^{-1}, both completely absent in the reference sample. Concerning the broad O-H stretching region (3200-3500 cm^{-1}), this signal is only absent in the brominated cellulose (**40**), attributable to the subsequent acetylation reaction. Other diagnostic peaks, documented extensively in literature, overlap with signals in the reference spectrum and therefore could not be reliably employed to unequivocally confirm the successful functionalisation process.

3.5.2 Synthesis and characterization of cellulose and poly(2-oxazoline)s composite materials

Following the activation of the cellulose substrate, the monomer iPOx (**11**) was selected as primary candidate for the initial polymerization reactions onto the three activated substrates. This choice was driven not only by its notably rapid polymerization kinetic, but also by its cost-effective, straightforward synthesis and facile purification process. The polymerization reactions (**Scheme 5**) were performed in ACN as reaction solvent with reflux conditions maintained for a duration of 48 to 72 h. After the proper reaction time, the crude products were precipitated in petroleum ether: diethyl ether 1:1, and finally purified by several methanol washes, aimed to remove byproducts or unlinked polymers, recovering the pure products after centrifugation (for detailed experimental conditions, refer to the experimental part).

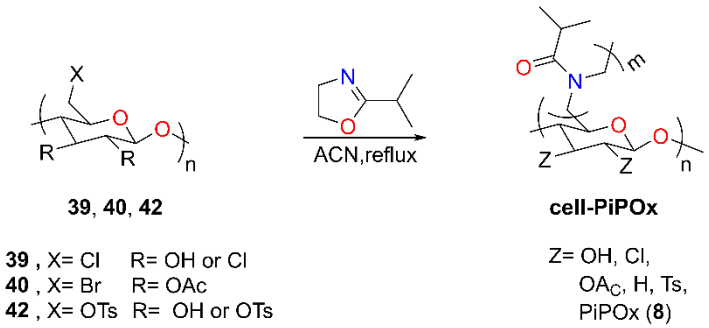

Scheme 5 Reaction scheme for cellulose-PiPOx composite materials (cell-PiPOx) preparation through Grafting From approach starting with chlorinated cellulose (**39**), brominated cellulose (**40**), and tosyl cellulose (**42**)

ATR-FTIR technique was employed to verify the effective formation of covalent linkages as illustrated in **Figure 37**. Across all substrates, notable variations in the intensity ratios of characteristic signals were observed, suggesting that the starting material had undergone chemical modification. Specifically in **Figure 37a**, the absorption band at approximately 602 cm^{-1}, corresponding to the C-Cl stretching vibration, decreases in intensity, indicative of the dissociation of the chlorine leaving group during the polymerization. In the case of brominated cellulose (**40**), reported in **Figure 37b**, the C-Br stretching band around 592 cm^{-1} remains relatively unchanged in intensity, suggesting incomplete elimination of the bromine leaving group under the initially employed reaction conditions.

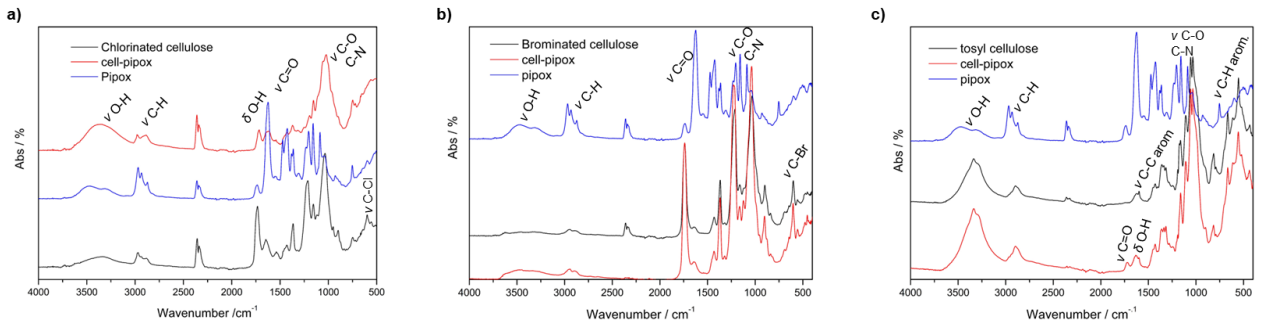

Figure 37 ATR-FTIR spectra for cell-PiPOx made with the three different activated celluloses: chlorinated (a), brominated (b), and tosyl cellulose (c).

Repeating the reaction at higher temperature using DMA as reaction solvent yielded no significant alteration to these spectral features, therefore chlorination and bromination reactions were considered the less suitable to introduce the 2-oxazoline-based polymers onto cellulose substrate. Upon utilising tosyl cellulose (**42**) as the initial substrate (**Figure 37c**) the spectrum of the composite material exhibited the most pronounced modification, notably relative to the chlorinated and brominated counterparts. Particularly, the distinct signal at 1735 cm^{-1}, attributable to the amide stretching vibration characteristic of the polymer PiPOx (**8**) (serving as reference) appears in the spectrum of the composite material but is entirely absent in the tosyl cellulose (**42**) prior to reaction. This absence confirms successful covalent conjugation of the polymer. Additionally, the residual tosyl signal at 1595 cm^{-1} showed a marked decrease in intensity, further corroborating the successful polymerization. The facile synthesis and purification of cell-PiPOx composite material from tosyl cellulose (**42**), along with its higher yield under mild reaction conditions, prompted the selection of substrate **42** for polymerizations with monomers AmOx (**18**) and EstOx (**21**). These two monomers, as previously mentioned, upon appropriate deprotection, feature, respectively, amine and carboxyl moieties capable of interacting with heavy metal ions in aqueous environments. Reaction conditions are mirrored those utilised for iPOx (**8**), with detailed methodological specifics provided in the experimental section. Also in this case, ATR-FTIR analyses were performed to verify polymer linkage onto the cellulose, spectra were performed before and after the deprotection reactions necessary to give the amine and carboxyl moieties. The obtained cell-pAmOx and cell-pEstOx were stirred either respectively with trifluoroacetic acid (TFA) in $CHCl_3$ to remove Boc moiety, and with KOH 5% in water to hydrolyse the ethyl ester groups. These reactions were evaluated by performing contemporarily the same procedure on the corresponding protected homopolymers pAmOx (**24**) and pEstOx (**25**). The ^1H NMR confirms the removal of the protecting groups (**Figure 15**) as previously mentioned, which was further validated by the adsorption experiments reported below. In **Figure 38a** ATR-FTIR spectrum of cell-pAmOx evidences the presence of the amide stretching signal around 1679 cm^{-1}, characteristic of the homopolymer pAmOx (**26**), plotted as reference, and indicative of the successful polymerization and therefore of the covalent attachment within the cell-pAmOx composite. This signal shifts to 1730 cm^{-1} for the cell-pEstOx composite (**Figure 38b**), aligning with the reference signal of the homopolymer pEstOx (**27**). Notably, in both spectral instances, no corresponding signals are evident in the unmodified starting material.

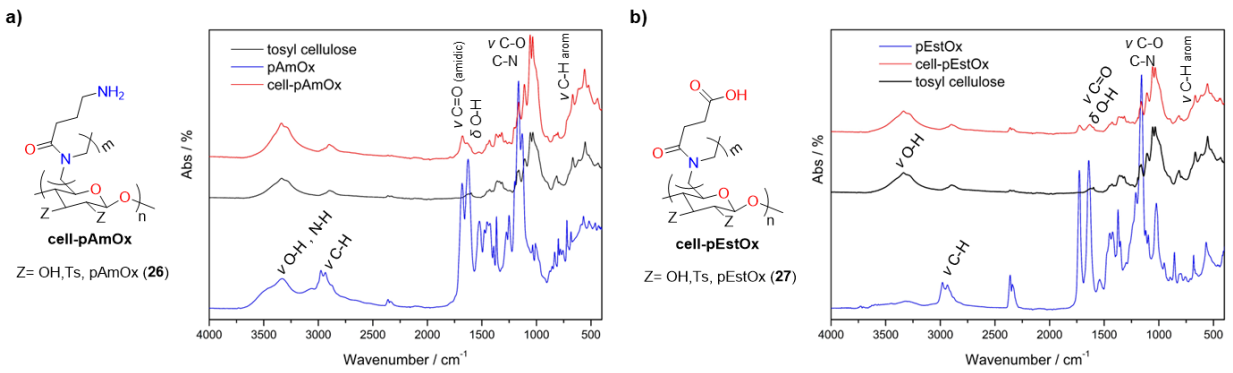

Figure 38 ATR -FTIR spectra for cell-pAmOx (a) and cell-pEstOx (b).

These three cellulose-poly(2-oxazoline) (cell-PiPOx, cell-pAmOx, and cell-pEstOx) underwent to TGA analyses that highlighted several differences from the starting tosyl cellulose (**42**) confirming the effective linkage of the polymer. As seen in **Figure 39**, the tosyl cellulose (**42**) exhibits a 45% in weight loss at its decomposition peak (with a maximum at 213 °C) and a gradual secondary decomposition from 400 °C to 650 °C, leaving a 15% of ashes residuum. In contrast, the cell-PiPOx displays a different thermal profile (**Figure 39a,d**), with an initial 60% weight loss at a decomposition peak (with a maximum at 235 °C) and a slower secondary decomposition to 650 °C, resulting in a reduced 10% of ashes residuum. For reference, the TGA curve of homopolymer PiPOx (**8**) was also plotted and exhibits a single sharp decomposition peak (from 335 °C to 425 °C (maximum at 408 °C), resulting in a 90% weight loss. Cell-pAmOx (**Figure 39b,e**) shows a single, pronounced decomposition temperature between 275 °C and 375 °C with an 85% weight loss, consistent with the second decomposition peak of the homopolymer pAmOx (**26**), plotted as reference, within the same temperature range.

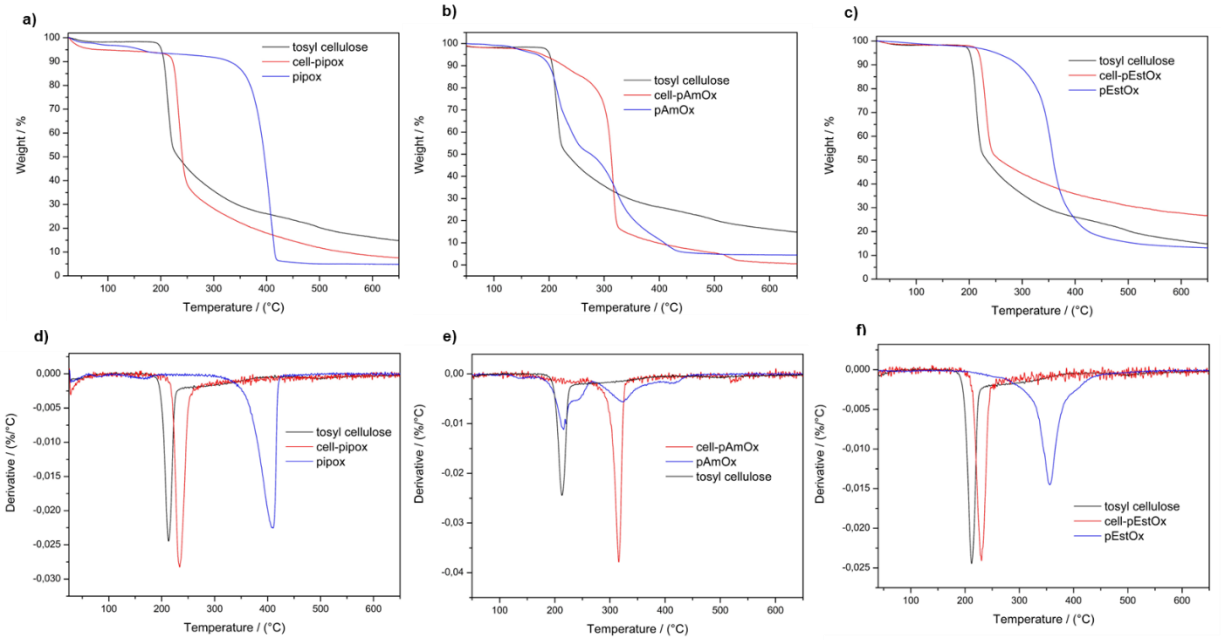

Figure 39 TGA and DTG analyses for cellulose-poly(2-oxazolines) composite materials starting from tosyl cellulose (**42**) as initiator. Heat rate 10 °C min^{-1}, N_2 80 mL min^{-1}.

Regarding cell-pEstOx (**Figure 39c,f**) the composite material exhibits minor modifications in the thermal behaviour compared to tosyl cellulose (**42**), evidenced by a 55% weight loss between 200 °C and 260 °C and an increased ash residue (30% in weight with respect to 15%).

3.5.3 Synthesis and characterization of lignin and poly(2-oxazoline)s composite materials

The tosylation reaction was also performed on lignin, which was considered as a prospective and alternative substrate for polymerization initiation. The reaction was facilely executed by stirring the substrate overnight at room temperature in presence of 2 eq. of *p*-toluensulfonilchloride (**41**), and 3 eq. of triethylamine (Et_3N) in aqueous solution, following a procedure established in the literature (**Scheme 6**).[162]

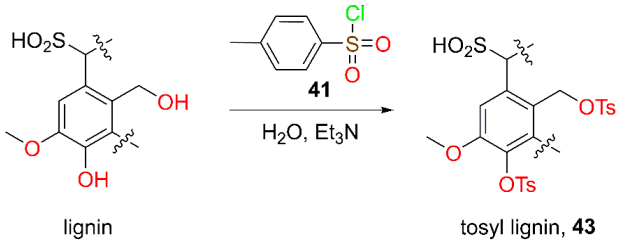

Scheme 6 tosyl lignin preparation from commercially available lignin.

The reaction mixture was subsequently cooled down to 4 °C to facilitate precipitation, then filtered and washed several times with water and ethanol to yield tosyl lignin (**43**). TGA and ATR-FTIR analyses were employed to assess the reaction outcome. As illustrated in **Figure 40a-b**, the maximum decomposition temperature shifted from 357 °C to 291 °C in tosyl lignin (**43**) with a 45% weight loss). From the ATR-FT-IR spectra (**Figure 40c**) displayed a reduction in intensity of the O-H stretching band around 3200-3500 cm^{-1}, indicative of tosyl group substitution, and the emergence of diagnostic peaks[162] at approximately 1365 cm^{-1} and 1173 cm^{-1} attributed to the SO_2 of the tosyl moiety, completely absent in the starting material.

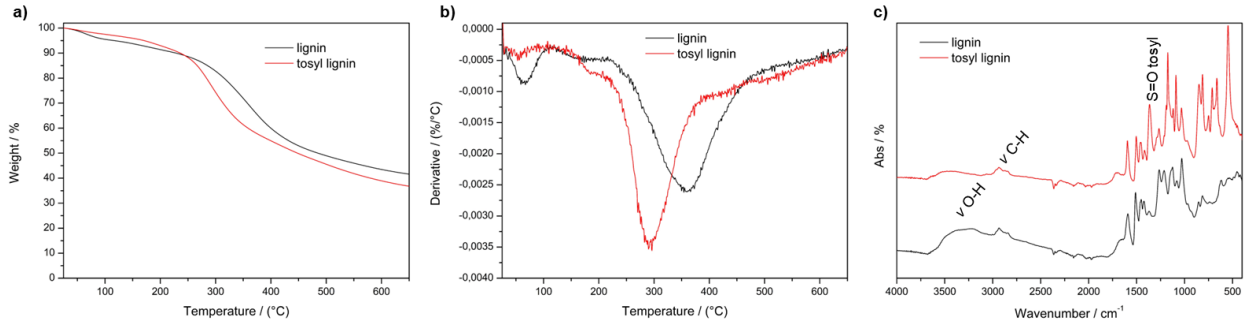

Figure 40 TGA (a), DTG (b), and ATR-FTIR (c) analyses for lignin and tosyl lignin (**43**), heat flow 10 °C min^{-1}, N_2 80 mL min^{-1}.

Following substrate activation, the tosyl lignin (**43**) was employed to initiate the polymerization initially using iPOx (**11**) as monomer. The reaction was performed by refluxing the monomer, dissolved in ACN, in presence of tosyl lignin (**43**) for 48 h, as detailed in the experimental section. After the workup and the proper washing, the resulting lignin-PiPOx product was subjected to TGA and ATR-FTIR analyses to confirm the successful polymerisation and, consequently, to evaluate the conjugation of the polymer on the substrate. As shown in **Figure 41a-b**, lignin-PiPOx exhibit two decomposition steps (approximately at 400 °C and 424 °C), comparable to the reference homopolymer PiPOx (**8**) that decomposes having a maximum at 390 °C, distinctly separate from starting material decomposition at approximately 291 °C. Furthermore, a notable difference in the ash residue was observed: the tosyl lignin (**43**) exhibited a substantial ash residue (around 45%) up to 850 °C. The ATR-FTIR spectrum (**Figure 41c**) confirmed successful achievement of desired lignin-PiPOx composite, displaying characteristic homopolymer PiPOx (**8**), such as the C-H sp^3 stretching (three peaks) around 2970-2865 cm^{-1} and carbonyl stretching near 1726 cm^{-1}. These signals are less intense or completely absent in the tosyl lignin (**43**) spectra.

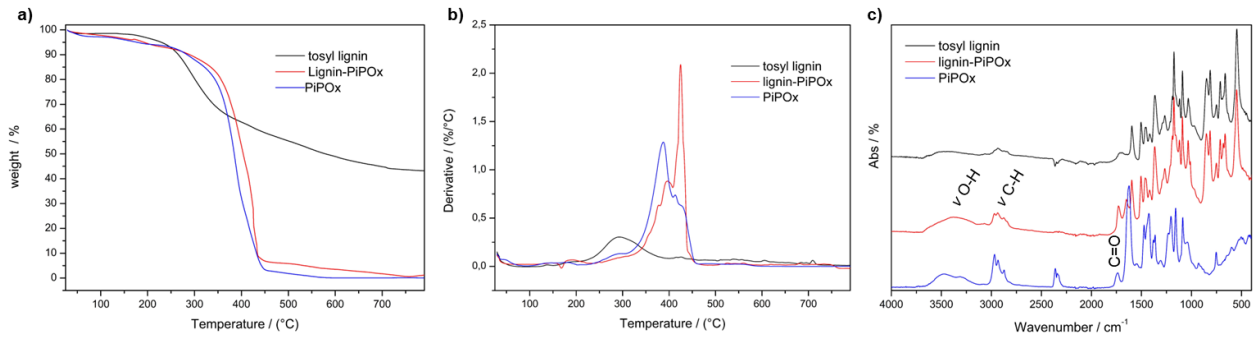

Figure 41 TGA (a), DTG (b), and ATR-FT-IR (c) for lignin-PiPOx, tosyl lignin, and PiPOx (**8**)

Although the synthesis of lignin-PiPOx yielded the desired composite material of reasonable quality and a quite good yield, its partial solubility in water at room temperature limited its use. Consequently, adsorption properties targeting heavy metal ions were exclusively tested on cellulose-poly(2-oxazoline) composites.

3.5.4 Evaluation of the adsorption properties of cell-PiPOx, cell-pAmOx, and cell-pEstOx targeting heavy metal ions

Because of the pEstOx (**27**) has carboxyl moieties, the possibility of chelating cations present in water was studied, testing in addition the composites with PiPOx (**8**) and pAmOx (**26**) to asses differences. For doing this, the synthesised cellulose-poly(2-oxazoline) composites were employed in adsorption experiments aimed at sequestering harmful heavy metal ions, including Pb^{2+}, Cd^{2+}, Cr^{3+}, Co^{2+}, Ni^{2+}, and Hg^{2+}. The heavy metal ions solutions were prepared by dissolving the respective chloride salts in HCl 0.01M, achieving the concentration of the corresponding cation of 50 ppm. This acid medium ensures the predominance of the cations, avoiding precipitation as hydroxides. For each adsorption experiment, 10 mL of solution was combined with 4 mg of cellulose, cell-PiPOx, cell-pAmOx, and cell-pEstOx in separate setups. After 18 h of incubation at controlled temperature of 25 °C, the supernatant was filtered, acidified, and injected into Inductively Coupled Plasma Optical Emission Spectroscopy (ICP-OES) instrument to exactly quantify the residual concentration. These experiments were conducted in triplicate for each cation and for each adsorbent, with results reported as averages. Adsorption capacities, calculated for each adsorbent using **Eq.4**, are presented in **Figure 42** and in **Table 6**, comparing the adsorption performances for the composite materials with the commercial cellulose AVICEL PH 101.

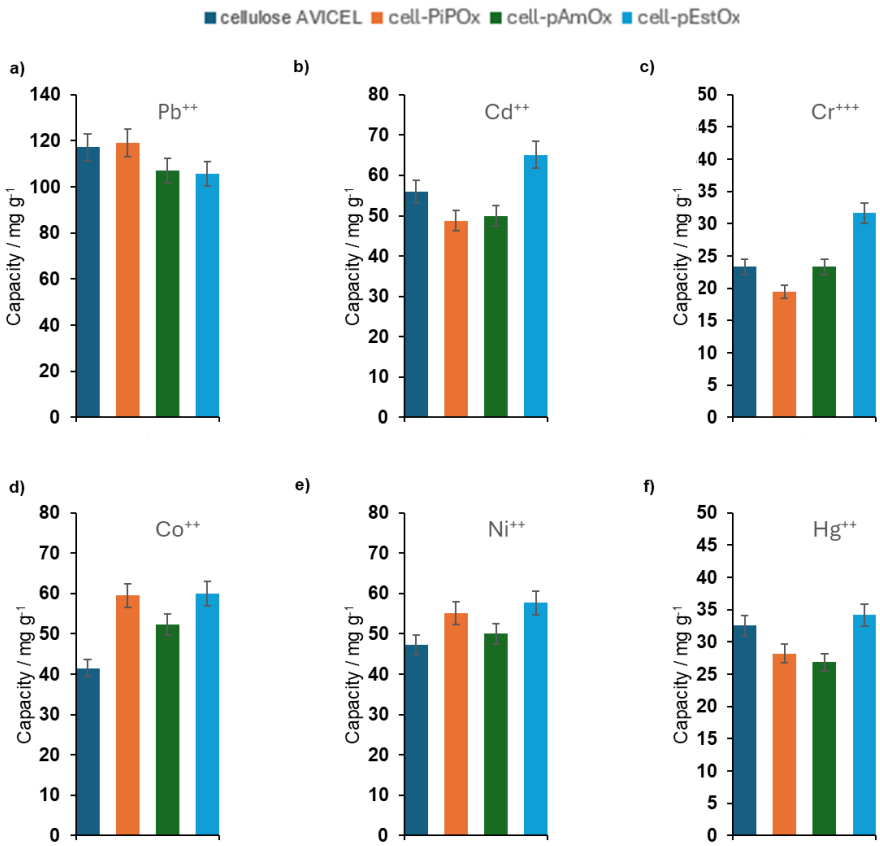

Figure 42 (a-f) adsorption capacity (q_e) for cellulose AVICEL and cellulose-poly(2-oxazoline) composites in heavy metal ions adsorption experiments at 50 ppm as initial concentration of cation in HCl 0.01M.

In the case of Pb no enhancement in adsorption performance was observed, as the q_e values for the cell-pAmOx (entry 3) and cell-pEstOx (entry 4) were lower, and the q_e value for cell-PiPOx (entry 2) was within the margin of error (119.0 vs 117.0 mg g^{-1}). Similarly, for mercury (**Figure 42f**), the composite materials exhibited negligible improvement over cellulose, expert for a slight increase in q_e value for cell-pEstOx (q_e 34.1 vs 32.5 mg g^{-1}, entry 4).

Table 6 Adsorption capacity (q_e) for cellulose AVICEL and cellulose-poly(2-oxazoline) composites in heavy metal ions adsorption at 50 ppm as initial concentration of cation in HCl 0.01M.

Entry	Adsorbent	Pb^{++}	Cd^{++}	Cr^{+++}	Co^{++}	Ni^{++}	Hg^{++}
1	Cellulose	117.0	56.0	23.0	41.5	47.2	32.5
2	Cell-PiPOx	119,9	48.8	19.5	59.5	55.1	28.2
3	Cell-pAmOx	107.0	50.0	23.0	52.3	50.0	26.8
4	Cell-pEstOx	105.9	65.1	31.6	60.0	57.7	34.1

q_e values are expressed as mg g^{-1}

Conversely, for the other heavy metals, i.e. Cd^{2+}, Cr^{3+}, Co^{2+}, and Ni^{2+}, cell-pEstOx demonstrated superior adsorption capacities compared to reference cellulose, with q_e values of 65.1, 31.6, 60.0, and 57.7 mg g^{-1}(entry 4), respectively, compared to 56.0, 23.0, 41.5, and 47.2 mg g^{-1} (entry 1). The adsorbents cell-pAmOx (entry 3),

and cell-PiPOx (entry 2), showed enhanced performance over cellulose only for cobalt and nickel, exhibiting q_e values of 52.3 and 59.5 mg g^{-1} respectively for cobalt and 50.0 and 55.1 mg g^{-1} in case of nickel. The superior performances of cell-pEstOx with respect to the other adsorbents (except for Pb^{2+} and Hg^{2+}) could be related to the molecular structures of these polymers. Indeed, the carboxylic groups in pEstOx (**27**) enabling a more efficient chelation of the free cations; in contrast, the amine group of pAmOx (**26**) in cell-pAmOx may engage in acid-base interaction with the hydrochloric acid, limiting their availability for cation binding at operating pH (c.a. 2). Finally, the carbonyl group in PiPOx (**8**) are the less nucleophilic making hard the interaction with cations. However, chelation of heavy metal ions concerns many factors, such as: (i) chelation/complexation that means a covalent or an ion-covalent coordination between the metal ion and donor atoms on the adsorbent's surface (this is often the dominant and strongest mechanism), and (ii) ion exchange involves the substitution of ions initially present on the adsorbent with metal ions from the solution. In addition, hydrogen bonding plays a role in several ways, often as a secondary but significant mechanism: (i) *Interaction with Solvating Water Molecules*: metal ions in aqueous solution are surrounded by a hydration shell of water molecules. OH or NH_2 groups on the adsorbent can form hydrogen bonds with these water molecules, thereby indirectly "anchoring" the metal ion to the surface, and (ii) *Stabilization of Binding Sites*: the hydrogen bond network within an adsorbent material can influence its porous structure and the arrangement of functional groups, making binding sites more accessible or more stable for metal ion complexation. A comparative analysis of the results obtained with cell-pEstOx, identified as the most effective adsorbent against the majority of the tested heavy metal ions, under analogous experimental conditions (i.e., cation type, initial concentration, pH, and adsorbent quantity) against established adsorbents—including graphene derivatives, nanoparticles, and biosorbents—indicates that the adsorption capacities are generally of a comparable order of magnitude.[163] Specifically, while these values are generally lower than those observed for zeolites, cell-pEstOx demonstrates an higher adsorption capacity, against Ni^{++}, Cd^{++}, Pb^{++}, respect to functionalized mesoporous silica,[164] against Co^{++} in comparison with various activated carbon and coal,[165] and against Cr^{+++} and Hg^{++} relative to chitosan derivatives.[166,167]

4. Conclusions

In summary, this Doctoral Thesis has detailed a comprehensive investigation into the design, synthesis, and characterization of novel adsorbents tailored for the selective and efficient removal of prevalent and harmful pollutants commonly detected in wastewater. Successful synthetic routes were established for three previously known monomers, 2-isopropyl-2-oxazoline, iPOx (**11**), *tert*-Butyl(3-(4,5-Dihydrooxazol-2-yl)propyl)carbamate, AmOx (**18**), and ethyl 3-(4,5-dihydrooxazol-2-yl)propanoate EstOx (**21**), alongside the development and full characterization (GC-MS and NMR) of a novel monomer 2-benzhydryl-4,5-dihydro-1,3-oxazole (**13**). This new monomer was subsequently subjected to a comprehensive optimization study of the cationic ring opening polymerization, varying key parameters such as reaction time, solvent, temperature, and initiator. The resulting homopolymer polyPhOx (**23**) was employed in a series of adsorption experiments targeting hydrophobic organic contaminants, notably pharmaceutical products. Outstandingly, polyPhOx (**23**) exhibited a high adsorption capacity for oestradiol (**32**), the most hydrophobic analyte tested. These promising findings were further validated through the investigation of performance in a real-world matrix, by spiking authentic lake water samples with selected pollutants and quantifying the adsorption capacities measuring residual concentration via HPLC-DAD analyses. Results confirm the effectiveness of polyPhOx (**23**) in adsorbing oestradiol (**32**) in such environmentally relevant medium, warranting further investigation.

Regarding the other monomers (**11**, **18**, **21**), the corresponding homopolymers were also successfully synthesised and characterised. However, as a result of their inherent solubility properties, it proved necessary to employ solid supports, such as graphene oxide (GO) or cellulose, to ensure the effective isolation of the adsorbent from the treated water. In the case of the graphene oxide support, a "*Grafting To*" approach was identified as the most effective method, facilitating the conjugation of the preformed homopolymer (suitably end chain functionalised) through an amide bond with 1,6-hexamethylenediamine as linking agent, yielding the GO-PiPOx and GO-pAmOx composite materials. Following full material characterization via TGA, ATR-FTIR, AFM, and TEM analyses, the performance of GO-pAmOx was carefully assessed through HPLC-DAD analyses, allowing for the precise quantification of the residual drugs concentrations after adsorption experiments targeting acidic pharmaceuticals in hydroalcoholic solution. These results undoubtedly confirmed that compounds capable of engaging in acid-base interactions with the polymer's amine moieties, namely ibuprofen (**29**), aspirin (**28**), ketoprofen (**36**), and benzoic acid (**37**), were preferentially adsorbed by GO-pAmOx composite. In contrast, neutral or basic compounds were only minimally removed from the solution, indicating selectivity in the adsorption process. Subsequent experiments demonstrate the high performances also in water medium.

For the cellulose as support material, the "*Grafting From*" approach proved more effective, allowing us to employ different monomer in separated polymerisation reactions with cellulose substrate as support. After determining the optimal leaving group to introduce onto the cellulose, the monomers **11**, **18**, and **21** were employed in separate polymerisation reactions. The resulting cellulose-poly(2-oxazoline) composites,

including cell-PiPOx, cell-pAmOx, and cell-pEstOx, were characterised using TGA and ATR-FTIR analyses. These materials were then utilised in adsorption experiments targeting harmful heavy metal ions such as Pb^{2+}, Cd^{2+}, Cr^{3+}, Co^{2+}, Ni^{2+}, and Hg^{2+}. ICP-OES analyses revealed that these materials, particularly cell-pEstOx, exhibited higher adsorption efficiencies compared to cellulose for Cd^{2+}, Cr^{3+}, Co^{2+}, and Ni^{2+} Additionally, cell-pAmOx and cell-PiPOx demonstrated superior adsorption capacities for cobalt and nickel compared to cellulose.

Building upon the significant findings detailed in this thesis, several exciting avenues for future research and development present themselves. Firstly, further exploration of alternative chemistries for the conjugation of poly(2-oxazolines) to graphene oxide is warranted, with a particular emphasis on developing facile and robust 'click' chemistry-based strategies to enhance the loading capacity and stability of the resulting materials. Secondly, the demonstrated selectivity of the GO-pAmOx composite for acidic pharmaceuticals motivates the synthesis of either novel 2-oxazoline monomers or variously decorated pAmOx, pEstOx, and polyPhOx incorporating recognition motifs tailored to specifically target other high-priority pollutant classes. Thirdly, the long-term performance and economic viability of the developed adsorbents will be enhanced through detailed investigations into large-scale production methods, optimization of regeneration protocols, and assessment of performance within complex, real-world wastewater samples. Finally, the biocompatibility, tuneable thermoresponsiveness, and low cytotoxicity of PAOx provide new opportunities for integration within advanced biomedical applications.

Through these investigations, we will continue to advance sustainable and effective solutions for addressing the pressing challenges of water contamination and protecting both human health and environmental integrity.

5. Experimental Part

5.1 General

All reactions were monitored by thin layer chromatography (TLC) carried out on Merck F-254 silica glass plates and visualised with UV light. Flash chromatography was performed on SigmaAldrich silica gel (60, particle size: 0.040-0.063 mm). ^{1}H NMR and ^{13}C NMR were recorded in $CDCl_3$ unless otherwise specified, (99.8 % in deuterium) using a Bruker DRX-600 spectrometer (600 MHz). All chemical shifts are expressed in parts per million (δ scale) and are referenced to the residual protons of the NMR solvent ($CDCl_3$, δ 7.26 ppm). The following abbreviation were used to explain the multiplicities: (s) = singlet, (d) = doublet, (t) = triplet, (m)= multiplet. Infrared Spectra (FT-IR) were obtained using a Nicolet 6700 FT-IR Spectrometer from Thermo Fisher in KBr pellets, 64 scan, resolution 4 cm^{-1} data are presented as the frequency of absorption (cm^{-1}). Attenuated total Reflectance Infrared Spectra ATR-FT-IR were carried out using aThermo Scientific IS50 FT-IR optical bench equipped with Attenuated Total Refclactance (ATR) compartment. Absorbance Spectra were collected in the range of 4000-500 cm^{-1}, with 4 cm^{-1} spectral resolution, and 64 scans. The background spectrum was obtained through acquisition in air, and data were acquired and processed using the Thermo Scientific OMNIC Atlus software. Reversed phase High Performance Liquid Chromatography (HPLC) were performed with an Agilent infinity 1260 II instrument equipped with a C18 column (5 µm, 100 Å, 150 × 4.6 mm) with DAD as detector, with 1 mM $HClO_4$ H_2O and methanol or acetonitrile with various ratios as mobile phase, with a flow of 0.5 or 1 mL min^{-1}. Calibration curves were performed with analytical standards (purity 99%) from 25 to 250 mg L^{-1}. Thermogravimetric analyses (TGA/DTG) were performed using a SDT Q600 thermoanalyzer (TA Instruments). Aliquots of 5.0-20.0 mg of each sample at dry state, were inserted into a platinum crucible and heated from room temperature (25 ± 1 °C) to 650-850 °C with a heating ramp of 10 °C min^{-1} under nitrogen flow (80-100 mL min^{-1}). Dynamic light scattering (DLS) measurements were carried out by a Malvern Zetasizer Nano-ZS in backscattering configuration i.e. the scattered light is collected at an angle of 173° Samples were dissolved in Milli-Q water at a concentration of 1 mg mL^{-1} and filtered with regenerated cellulose (RC) filter (0.45 µm), temperature was fixed at 298 K. Gel Permeation Chromatography (GPC) setup consists of three columns in series (a precolumn followed by two columns (300 x 4.6 mm) 5 µm 10 E5 Å (10-1.000 K) and 5 µm 10 E3 Å (1-75 K) respectively). Samples were injected with a concentration of 1.0 mg mL^{-1} and measured at 25 °C using DMF 50 mM LiBr as eluent, 0.27 mL min^{-1} flow and DAD as detector. The calibration was conducted with standard polystyrene reference materials (MW ranged from 1.3 K to 900 K). GC-MS analyses were performed with a SHIMADZU Nexis GC-2030 with a capillary column of SLBTM-5ms (30 m x 0.25 mm x 0.25 µm) coupled with a Mass Spectrometer SHIMADZU QP 2020NX; the mass values are reported as mass/charge ratios (m/z). All spectra were measured with a column temperature program from 50 °C to 250 °C and the injection temperature was set to 250 °C. AFM measurements were performed using a Dimension ICON (Bruker, Santa Barbara, CA). The AFM images were captured in tapping mode using a silicon probe RTESPA-150, which has a nominal spring constant of 6 N/m and a resonant frequency of 150

kHz. AFM samples were prepared by spin-coating SI (001) wafer at 2000 rpm after 1 min. standing, with WS-650mz-23nppb instrument, dropping the sample's suspension in ethanol (0.1 wt %). The AFM images were analysed and processed with Gwyddion software (https://gwyddion.net/). In detail, the images were flattened using the align rows tool, and 3 images per sample were analysed by masking flakes to record their mean roughness with the statistic quantities tool. TEM-EELS analyses were carried out with a Cs-corrected JEOL ARM200C operating at 200 keV. STEM images were acquired in scanning mode using the medium angle annular dark-field (MAADF) detector. SEELS spectra are acquired with a Gatan Quantum-ER spectrometer, using a pixel size of 5 nm and pixel time of 0.01 s. The spectra shown in figures are extracted summing spectra from an area of 150x150 nm with a total integration time of 20 s. All the data analysis, elemental quantification and background subtracted spectra and maps were carried out with Gatan Microscopy suite v3.4. The samples were prepared by drying one drop of methanol dispersion on a lacey carbon TEM grid in ambient temperature. Inductively Coupled Plasma Optical Emission Spectroscopy (ICP-OES) were performed with aVARIAN 710-ES instrument equipped with a concentric nebuliser and a glass cyclonic spray chamber. The operating conditions of the ICP-OES analysis were as follows: plasma power 1.2 KW, plasma and auxiliary gas flow-rates were 15 L min^{-1} and 1.5 L min^{-1} respectively, Argon has been employed as internal standard.

5.2 Chemicals

All chemicals were purchased from Sigma-Aldrich unless otherwise noted. Analytical grade solvents and commercially available reagent were used as purchased from Sigma-Aldrich without further purification. ACN (HPLC purity grade) was dried over calcium hydride, distilled over calcium hydride and stored under argon atmosphere, DMA was dried over calcium hydride, distilled over calcium hydride and stored under argon atmosphere. Methyl tosylate **2** (MeTos, 98%) was purified by vacuum distillation and stored under argon atmosphere.

5.3 Preparation of 2-oxazolines monomers

5.3.1 Synthesis of 2-isopropyl-2-oxazoline, iPOx, **11**

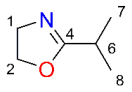

11

The monomer iPOx **11** was synthesised via a modified Witte−Seeliger cyclocondensation of *iso*butyronitrile, **9** (500 mmol, 1 eq) with 2-aminoethanol, **10** (600 mmol,1.2 eq.) and zinc acetate hydrate (10 mmol, 0.02 eq.) as catalyst at 130 °C for 48 h with a flow of nitrogen passed through the reaction vessel. The crude product was dissolved in dichloromethane (DCM) and extracted several times with water. The organic phases were dried over anhydrous magnesium sulphate ($MgSO_4$), filtered and then the solvent was removed with a rotatory evaporator. The pure product was obtained by vacuum distillation (58−60 °C at 50 mbar) first over NaOH and then over calcium hydride. The pure product was stored under argon atmosphere. Yield: 70% of a colourless liquid.

Characterization data

^{1}H NMR (600 MHz, $CDCl_3$): δ = 1.18 (d, *J* = 6.5 Hz, 6H, C(CH_3)$_2$, 2.40-2.58 (m, 1H, C*CH*(CH_3)$_2$), 3.78 (t, *J* = 9.4 Hz, 2H, OCH_2*CH*$_2$N), 4.19 (t, *J* = 9.4 Hz, 2H, O*CH*$_2$$CH_2$N) ppm.

^{13}C NMR (150 MHz, $CDCl_3$): δ = 167.1 (C-4), 67.4 (C-2), 54.1 (C-1), 31.1 (C-6), 19.3 (C-7, C-8) ppm.

5.3.2 Synthesis of 2-benzhydryl-4,5-dihydro-1,3-oxazole, **13**

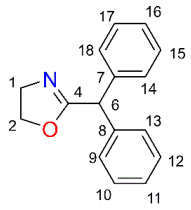

13

Compound **13** was synthesised by a modified Witte-Seeliger cyclocondensation of 2,2-diphenylacetonitrile, **12** (50 mmol, 1 eq.) with 2-aminoethanol, **10** (75 mmol, 1.3 eq.), and zinc acetate hydrate (2 mmol, 0.04 eq.) as catalyst. The reaction mixture was kept under stirring at 130 °C for 48 h with a nitrogen flow passing through the reaction vessel. The crude product was dissolved in dichloromethane (DCM) and extracted several times with water. The combined organic layers were washed with brine, dried with anhydrous magnesium sulphate ($MgSO_4$), and concentrated under vacuum. The residue was purified by flash chromatography on silica gel using petroleum ether:ethyl acetate (8:2) as eluent. The desired monomer was obtained as a white powder in 51% yield.

Characterization data

^{1}H NMR (600 MHz, $CDCl_3$): δ = 3.92 (t, *J*= 9.5 Hz, 2H, OCH_2CH_2N), 4.30 (t, *J*= 9.5 Hz, 2H, OCH_2CH_2N), 5.11 (s, 1H, $CCHPh_2$), 7.30-7.35 (m,10H, CH_{arom}) ppm.

^{13}C NMR (150 MHz, $CDCl_3$): δ = 168.4 (C-4), 139.6 (C-7, C-8), 129.1 (C-9, C-10, C-12, C-13, C-14, C-15, C-17, C18), 127.3 (C-11, C-16), 67.9 (C-2), 54.7 (C-6), 51.3(C-1) ppm.

5.3.3 Synthesis of 4-((*tert*-Butoxycarbonyl)amino)butanoic acid, **15**

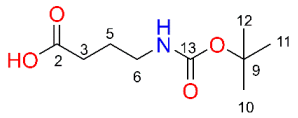

15

70 mL NaOH aqueous solution (5.5 M) and γ-aminobutyric acid, **14** (100 mmol, 1 eq.) were placed in a 250 mL flask, followed by *tert*butoxycarbonyl anhydride (Boc_2O) (110 mmol, 1.1 eq.), and the resulting mixture was stirred overnight at ambient temperature. The reaction mixture was acidified with 2 N HCl to pH ~3 and then extracted with ethyl acetate (70 mL x 3). The collected organic phase was washed with brine (30 mL x 2), dried over anhydrous $MgSO_4$, filtered, and concentrated under vacuum to give the product as white solid in 97% yield.

Characterization data

^{1}H NMR (600 MHz, $CDCl_3$)[1]: δ =1.44 (s, 9H, C(CH_3)$_3$), 1.82 (p, J = 9.3 Hz, 2H, $CH_2CH_2CO_2H$), 2.39 (t, J = 9.3 Hz, 2H, $CH_2CH_2CO_2H$), 3.17 (t, J = 9.3 Hz, 2H, CH_2CH_2NH) ppm.

^{13}C NMR (150 MHz, $CDCl_3$): δ = 182.7 (C-2), 154.9 (C-13), 79.5 (C-9), 38.7 (C-6), 35.5 (C-3), 27.4 (C-10, C-11, C-12), 23.3 (C-5) ppm.

[1] The ^{1}H-NMR spectrum was recorded after addition of a drop of D_2O

5.3.4 Synthesis of *tert*-Butyl (4-((2-Chloroethyl)amino)-4-oxobutyl)carbamate, **17**

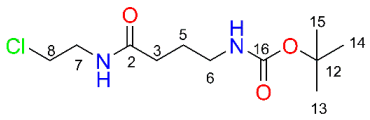

17

The first intermediate, **15** (97 mmol, 1 eq.), chloroethylamine hydrochloride, **16** (97,3 mmol, 1 eq.), and TBTU (97,3 mmol, 1 eq.) were dissolved in dry DCM (150 mL) at 0°C sequentially. Triethylamine (117 mmol, 1.2 eq.) was added dropwise to the solution over a period of 1 h, keeping the temperature at 0 °C. The reaction mixture was allowed to warm up to room temperature and was stirred overnight before 100 mL of saturated aqueous $NaHCO_3$ were added. The organic phase was washed twice with water and dried over anhydrous $MgSO_4$ and then filtered. After removal of the solvent, the residue was redissolved in $CHCl_3$ and purified by column chromatography on silica gel using ethyl acetate as eluent, obtaining a white solid, yield 86%.

Characterization data

^{1}H NMR (600 MHz, $CDCl_3$): δ =1.41 (s, 9H, C(CH_3)$_3$), 1.79 (p, J = 9.3 Hz, 2H, CH_2CH$_2$CONH), 2.23 (t, J = 9.3 Hz, 2H, CH$_2$$CH_2$CONH), 3.14 (t, J = 9.3 Hz, 2H, CH$_2$$CH_2$NH), 3.49-3.63 (m, 4H, Cl$CH_2$$CH_2$NH) ppm.

^{13}C NMR (150 MHz, $CDCl_3$): δ = 172.6 (C-2), 155.9 (C-16), 79.6 (C-12), 43.1 (C-8), 39.8 (C-7), 39.4 (C-6), 33.6 (C-3), 28.4 (C-13, C-14, C-15), 26.1 (C-5) ppm.

5.3.5 Synthesis of *tert*-Butyl (3-(4,5-Dihydrooxazol-2-yl)propyl)carbamate, AmOx **18**

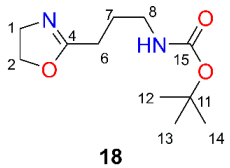

18

The ring closure of *tert*-butyl (4-((2-chloroethyl)amino)-4-oxobutyl)carbamate, **17** (83.7 mmol, 1 eq.) was carried out in a 70 mL saturated solution of NaOH in methanol. After stirring for 12 h at room temperature, the solvent was removed under reduced pressure. The residue was dissolved in DCM (50 mL), washed twice with water and dried over anhydrous $MgSO_4$ then filtered. The desired product was obtained after solvent removal, as a white solid in 79% yield and employed without any further purification.

Characterization data

^{1}H NMR (600 MHz, $CDCl_3$): δ = 1.42 (s, 9H, C(CH_3)$_3$), 1.81 (p, J = 9.3 Hz, 2H, $CH_2CH_2CH_2$), 2.30 (t, J = 9.3 Hz, 2H, CCH_2CH_2), 3.15 (t, J = 9.3 Hz, 2H, CH_2CH_2NH), 3.80 (t, J = 9.5 Hz, 2H, OCH_2CH_2N), 4.21 (t, J = 9.5 Hz, 2H, OCH_2CH_2N) ppm.

^{13}C NMR (150 MHz, $CDCl_3$): δ = 173.1 (C-4), 155.9 (C-15), 79.6 (C-11), 68.4 (C-2), 53.8 (C-1), 39.8 (C-8), 29.4 (C-12, C-13, C-14), 28.4 (C-7), 21.1(C-6) ppm.

5.3.6 Synthesis of Ethyl 4-((2-chloroethyl)amino)-4-oxobutanoate, **20**

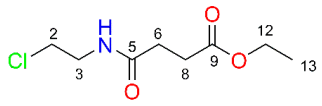

20

Ethyl succinyl chloride, **19** (100 mmol, 1eq.) and chloroethylamine hydrochloride, **16** (100 mmol, 1 eq.) were suspended in dry dichloromethane (150 mL). At 0 °C, triethylamine (220 mmol 2.2 eq.) was added dropwise over a period of 2 h. The reaction mixture was allowed to warm up to room temperature and was stirred for 4 days before water (40 mL) was added. The organic phase was subsequently washed twice with water, with brine, and finally dried over anhydrous $MgSO_4$. After filtration, the solvent was removed with a rotatory evaporator, and the residue was purified by column chromatography on silica gel using hexane:ethyl acetate 5:95 as eluent. The product appeared as a pale-yellow oil. Yield 83%.

Characterization data

^{1}H NMR (600 MHz, $CDCl_3$): δ = 1.23 (t, *J* = 7.1 Hz, 3H, $OCH_2\mathit{CH_3}$), 2.48 (t, *J* = 6.7 Hz, 2H, $OC\mathit{CH_2}CH_2CO$), 2.69 (t, *J* = 6.7 Hz, 2H, $OCCH_2\mathit{CH_2}CO$), 3.52-3.65 (m, 4H, $CH_2\mathit{CH_2}NH$ and $Cl\mathit{CH_2}CH_2$), 4.14 (q, *J* = 7.1 Hz, 2H, $O\mathit{CH_2}CH_3$) ppm.

^{13}C NMR (150 MHz, $CDCl_3$): δ = 173.2 (C-5, C-9), 61.2 (C-12), 43.1(C-2), 39.8 (C-3), 32.3 (C-6), 29.6 (C-8), 14.1 (C-13) ppm

5.3.7 Synthesis of Ethyl 3-(4,5-dihydrooxazol-2-yl)propanoate, EstOx **21**

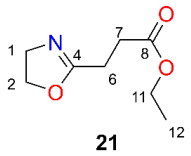

21

Ethyl 4-((2-chloroethyl)amino)-4-oxobutanoate, **20** (70 mmol, 1 eq.) and anhydrous sodium carbonate (70 mmol, 1 eq.) were reacted (neat) under stirring at a pressure of 0.1 mbar and at 60 °C on rotatory evaporator, distilling continuously the product formed. Yield 69% of a colourless liquid after a second distillation.

Characterization data

^{1}H NMR (600 MHz, $CDCl_3$): δ = 1.22 (t, *J* = 7.2 Hz, 3H, $OCH_2\mathit{CH_3}$), 2.61 (m, 4H, $C\mathit{CH_2CH_2}CO$), 3.79 (t, *J* = 9.4 Hz, 2H, $N\mathit{CH_2}CH_2O$), 4.17-4.24 (m, 4H, $NCH_2\mathit{CH_2}O$, $O\mathit{CH_2}CH_3$) ppm.

^{13}C NMR (150 MHz, $CDCl_3$): δ = 173.7 (C-8), 173.1 (C-4), 68.2 (C-2), 61.1 (C-11), 53.8 (C-1), 29.6 (C-7), 24.1 (C-6), 14.5 (C-12) ppm.

5.4 General procedure for polymerisations

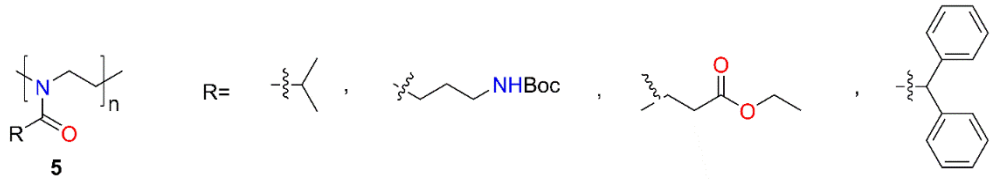

A two-neck round bottom flask equipped with an efficient reflux condenser and a magnetic stir bar was charged with monomer (**11** or **18** or **21**) (20 mmol) and anhydrous ACN (10 mL). The system was kept under Argon atmosphere, a proper amount of a solution 1:10 methyl tosylate: ACN was added to start the polymerisation, and the reaction mixture was stirred at 90 °C from 8 to 48 h. After, the reaction was quenched by addition of 10 eq. to initiator of 1M NaOH and the resulting mixture was stirred at the same temperature for 2 h. Finally, the solvent was reduced with a rotatory evaporator and the residue was added to a solution of petroleum ether: diethyl ether (1:1). The polymer was recovered as a white precipitate, the supernatant was removed, and the product was washed twice with the petroleum ether: diethyl ether solution and dried in vacuo. Finally, the polymer was dialysed (cut off 1 to 3.5 kDa) against methanol for 5 days changing the solvent 10 times. Homopolymerisation for monomer **13** has been extensively discussed in results and discussion section, best results were obtained refluxing the monomer for 8 h with 0.02 eq. of *p*-nitrobenzenesulfonate (**22**) as initiator.

Characterization data of 8 (yield 98%)

GPC: DMF with LiBr (0.05 M): 5.7 kDa, Đ = 1.1

^{1}H NMR (600 MHz, $CDCl_3$): δ = 3.45 (NCH_2CH_2), 2.91 and 2.67 $(CH_3)_2CHCO$), 1.11((CH_3)$_2$CH) ppm.

Characterization data of 24 (yield 92%)

GPC: DMF with LiBr (0.05 M): 5.8 kDa, Đ = 1.1

^{1}H NMR (600 MHz, $CDCl_3$): δ = 5.56 (OCN$H$$CH_2$), 3.44 (N$CH_2CH_2$), 3.16 (HN$CH_2CH_2$), 2.44 ($CH_2CH_2CO$), 1.84 ($CH_2CH_2CH_2$), 1.41 (($CH_3$)$_3$OCO) ppm.

Characterization data of 25 (yield 80%)

GPC: DMF with LiBr (0.05 M): 8.7 kDa, Đ = 1.1

^{1}H NMR (600 MHz, $CDCl_3$): δ = 4.10 (CH_3CH_2O), 3.48 (NCH_2CH_2), 2.61 (COCH_2CH_2CO), 1.24 (CH_3CH_2) ppm.

Characterization data of 23 (yield 88%)

GPC: DMF with LiBr (0.05 M): 6.5 kDa, Đ = 1.1

^{1}H NMR (600 MHz, DMSO-d6): δ = 7.24 (H arom.), 5.66 (Ph_2CHCO), 3.31 (NCH_2CH_2) ppm.

5.4.1 Cleavage of the amine protecting group

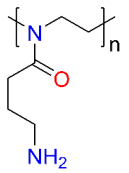

26

Poly(2-(3-(Boc-amino)propyl)-2-oxazoline), **24** (0.09 mmol) was dissolved in dry $CHCl_3$ (5 mL) and then trifluoroacetic acid (TFA) (1 mL) was added. The solution was stirred at room temperature overnight, and subsequently, the product was dry at reduced pressure. The crude product deprotected pAmOx (**26**) was redissolved in DCM and the polymer was precipitated by dropping the reaction solution into petroleum ether: diethyl ether (1:1), collected by centrifugation, and dried in vacuo. Yield: 98%.

Characterization data

^{1}H NMR (600 MHz, $CDCl_3$): δ = 3.44 (NCH_2CH_2), 3.16 ($HNCH_2CH_2$), 2.46 (CH_2CH_2CO), 1.83 ($CH_2CH_2CH_2$) ppm.

5.4.2 Cleavage of the carboxyl protecting group

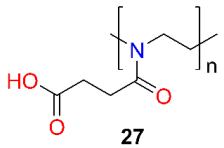

27

Poly((2-(3-ethyl propanoate)-2-oxazoline), **25** (0.09 mmol) was dissolved in 10 mL of a 5% KOH solution and stirred overnight at room temperature. Then, ~ 850 µL of glacial acetic acid was added to neutralize residual KOH, and the product (deprotected pEstOx, **27**) was dialysed (cut off 3.5 kDa) against milli-Q-grade water for 7 days changing the solvent 14 times. After lyophilization the product was obtained in 96% yield.

Characterization data

^{1}H NMR (600 MHz, D_2O): δ = 3.51 (NCH_2CH_2), 2.57 (COCH_2CH_2CO) ppm.

5.5 Organic compounds adsorption with PolyPhOx, **23**

High-Performance Liquid Chromatography (HPLC) Calibration Curves

Ibuprofen (**29**), aspirin (**28**), metoclopramide (**30**), pyramidone (**31**) oestradiol (**32**) and indomethacin (**33**) were dissolved in CH_3OH or ACN and after proper dilution the calibration curve was performed with different elution programs using as mobile phase various ratios of 1mM $HClO_4$ H_2O, CH_3OH, and ACN at either 0.5 or 1mL min^{-1} as flow rates.

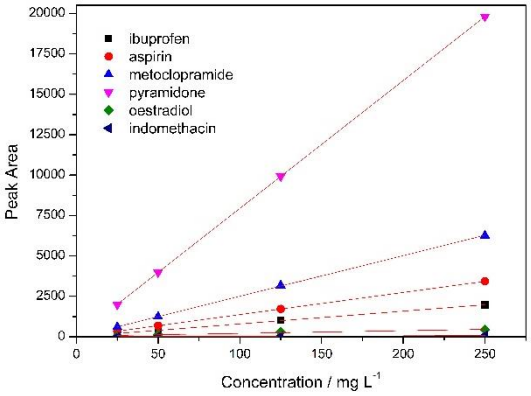

Compound	Retention time	λ (nm)	Slope Value	Standard Error	R^2
ibuprofen (**29**)	6.7	235	7.9	0.12	0.999
aspirin (**28**)	13.5	275	13.7	0.02	1
metoclopramide (**30**)	4.0	254	25.2	0.20	1
pyramidone (**31**)	4.1	254	79.1	0.06	1
oestradiol (**32**)	9.9	235	1.9	0.20	0.999
indomethacin (**33**)	13.5	275	0.3	0.01	0.999

Preparation of pharmaceuticals solutions

The proper amount of pharmaceutical compound (**28**, **29**, **30**, **31**, **32**,and **33**) was separately weighted and transferred in a conical flask equipped with a magnetic stir bar, then the solvent (hydroalcoholic mixture) was added, and the system was hardly stirred under heating at 35 °C through an oil bath. After complete dissolution of drugs, the solution was cooled down to 25 °C and employed in adsorption experiments.

Adsorption experiments

Adsorption experiments were done in triplicate under batch operation conditions targeting pharmaceutical compounds. First, an amount of 5 mg of polyPhOx (**23**) was added into 2 mL reaction tubes. Then, 2 mL of pharmaceuticals standard solutions with concentrations ranging from 10 to 200 mg L^{-1} were loaded into the cartridge. To allow homogenous adsorption on the polymer surface, the tubes were incubated in a thermostatic shaker (50 rpm for 24 h) Triplicate controls, which consisted of solutions of the corresponding pharmaceutical in the absence of any adsorbent and in the same conditions, were run in parallel. Finally, the supernatants were filtered using PTFE filters, transferred into glass vials, and analysed by HPLC-DAD.

5.6 Composite materials with Graphene Oxide (GO) and poly(2-oxazoline)s

5.6.1 Graphene Oxide preparation

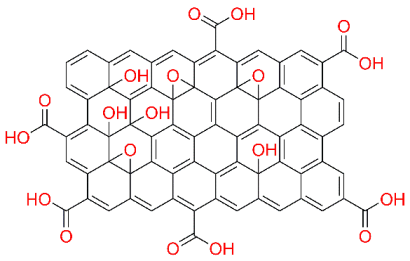

GO

Graphite (5 g) and 3.8 g of $NaNO_3$ are introduced in a 2 L flask equipped with a magnetic stir bar. Then, H_2SO_4 (375 mL) was added at 0 °C (ice bath), and the solution was stirred until homogeneous (1 h). $KMnO_4$ (25 g) was slowly added over 1 h, keeping the temperature below 10 °C. After 2 h, the solution was allowed to warm up at room temperature and stirred. After 5 days (colour change from dark green to brown) 700 mL of H_2SO_4 (5%) were added dropwise, keeping the temperature below 40 °C and the mixture was stirred for 2 h. Then 20 mL of H_2O_2 (30%) were added dropwise. After 2 h, the solution was diluted to 2 L with 5% H_2SO_4 and after one day of sedimentation, 1 L of the supernatant was removed and replaced with water (1 L), and 10 mL of H_2O_2 (30%) were added. After 18 h of sedimentation, the supernatant was removed and the solid was washed with 5% H_2SO_4 and 0.3% H_2O_2 solution (12 times), then with HCl 4% (3 times) and finally with deionised water (10 times). The solid was filtered and washed with deionised water, suspended in acetone, and recovered after centrifugation. The product (7g) was dried in vacuo before use.

Characterization data of Graphene Oxide (GO)

ATR-FT-IR: $\tilde{\nu}$ = 3400, 1733, 1622, 1053 cm^{-1}

UV-vis: λ= 235, 300 nm

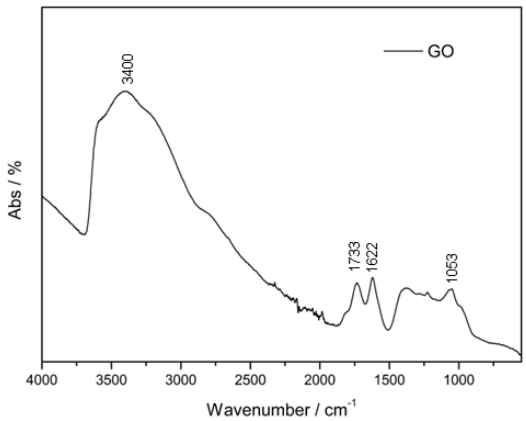

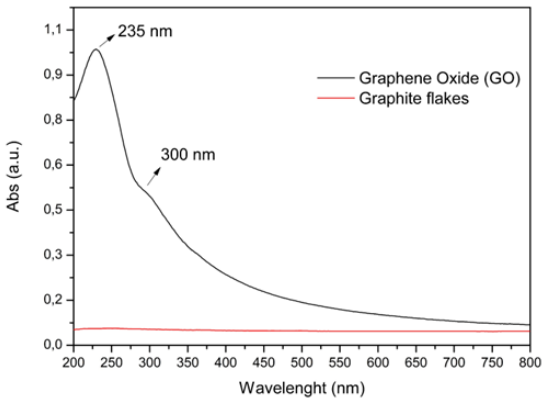

5.6.2 Preparation of amine terminated poly(2-oxazoline)s, **35**

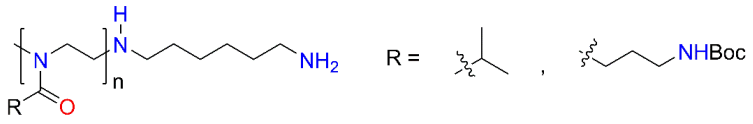

35

A two-neck round bottom flask equipped with an efficient reflux condenser and a magnetic stir bar was charged with the monomer (iPOx, **11** or AmOx, **18**) (20 mmol) and anhydrous ACN (12 mL). The system was kept under argon atmosphere, 600 µL of a solution 1:10 methyl tosylate (**2**): ACN was added to start the polymerisation, and the reaction mixtures was stirred 24 h for PiPOx (**8**) or 48 h for pAmOx (**24**) at 90 °C. After, the reaction was quenched by addition of 10 eq. to initiator of 1,6-hexamethylenediamine (**34**) solution in anhydrous ACN (4 mL), and the resulting mixture was stirred at the same temperature for 2 h. Finally, the solvent was reduced under vacuum and the residue was added to a solution of petroleum ether: diethyl ether (1:1). The polymer was recovered as a white precipitate, the supernatant was removed, and the product was washed twice with the petroleum ether: diethyl ether solution and dried in vacuo. Finally, the polymer was dialysed (cut off 3.5 kDa) against methanol for 5 days changing the solvent 10 times. Yield 85-90%.

Characterization data of 35 with R= iPr

^{1}H NMR (600 MHz, $CDCl_3$): δ = 3.45 (NCH_2CH_2), 2.92, 2.67-2.69 $(CH_3)_2CH$CO, NHCH_2CH_2, $CH_2CH_2NH_2$), 1.87 ($CH_2CH_2NH_2$) 1.41 (HNCH$_2CH_2CH_2CH_2$ CH_2), 1.11((CH_3)$_2$CH) ppm.

Characterization data of 35 with R= Pr-NHBoc

^{1}H NMR (600 MHz, $CDCl_3$): δ = 3.44 (NCH_2CH_2), 3.15 (HNCH_2CH_2), 2.69 (NHCH_2CH_2, $CH_2CH_2NH_2$) 2.46 (CH_2CH_2CO), 1.82 ($CH_2CH_2CH_2$NH), 1.67 ($CH_2CH_2NH_2$) 1.41 ((CH_3)$_3$OCO, HNCH$_2CH_2CH_2CH_2$ CH_2) ppm.

5.6.3 Linkage of amine terminated poly(2-oxazoline)s (**35**) onto GO

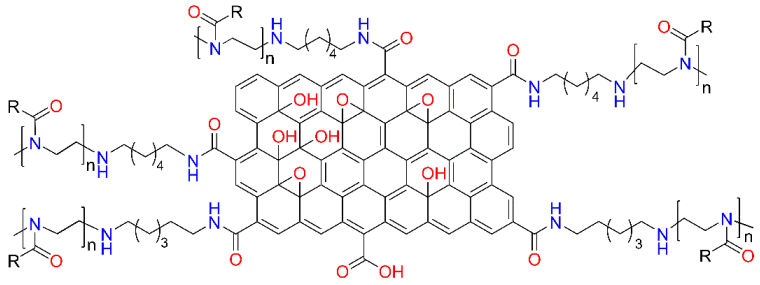

GO-poly(2-oxazoline)

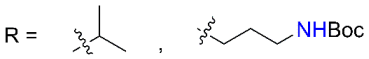

A two-neck round bottom flask equipped with an efficient reflux condenser and a magnetic stir bar was charged with amine terminated polymer (**35**) (1.4 g), 400 mg of dicicloesylcarbodiimmide DCC, 450 mg of GO, and anhydrous ACN (30 mL). The system was sonicated for 1 h, then placed in an oil bath at 90 °C and stirred overnight. After, the solvent was removed with a rotatory evaporator and the precipitate was washed three times with Tetrahydrofuran (THF) and recovered after centrifugation (GO-PiPOx 955 mg or GO-pAmOx 920 mg).

Characterization data of GO-PiPOx

ATR-FT-IR: $\tilde{\nu}$ = 3323, 2926, 2849, 1162, 1084 cm^{-1}

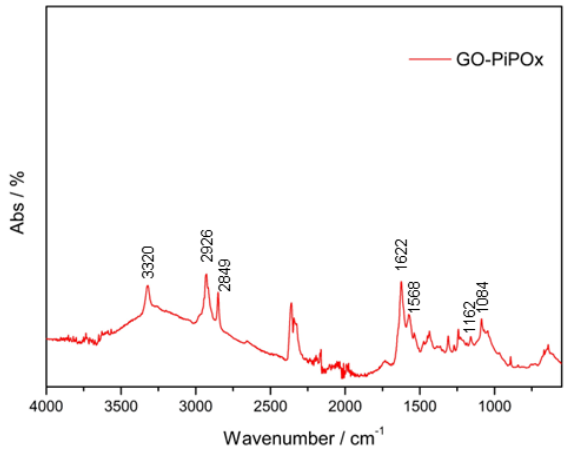

Cleavage of the amine protecting group

The GO-pAmOx was deprotected by stirring the substate, dispersed in anhydrous $CHCl_3$, overnight after the addition of 400 µL of TFA. The solvent was removed under vacuum and the final product was washed three times with THF, recovered after centrifugation and dried in vacuo (yield 910 mg).

Characterization data of GO-pAmOx

ATR-FTIR: $\tilde{\nu}$ = 3327, 2978, 2938, 1679, 1629, 1220, 1170, 1136 cm^{-1}

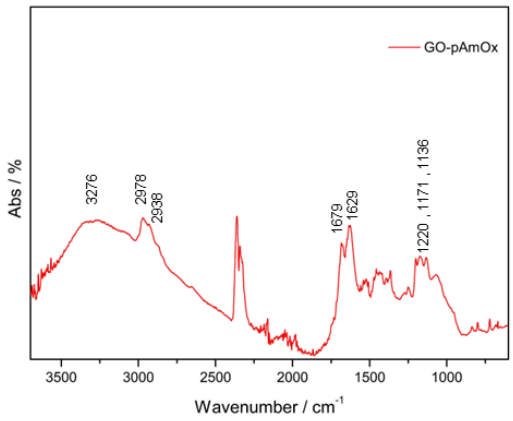

5.6.4 Organic compounds adsorption with GO-pAmOx

High-Performance Liquid Chromatography (HPLC) Calibration Curves

Ibuprofen (**29**), aspirin (**28**), metoclopramide (**30**), pyramidone (**31**), ketoprofen (**36**), etoperidone (**38**). and benzoic acid (**37**) were dissolved in CH_3OH or ACN and after proper dilution the calibration curve was performed with different elution programs using as mobile phase various ratios of 1mM $HClO_4$ H_2O, CH_3OH, and ACN at either 0.5 or 1 mL min^{-1} as flow rates.

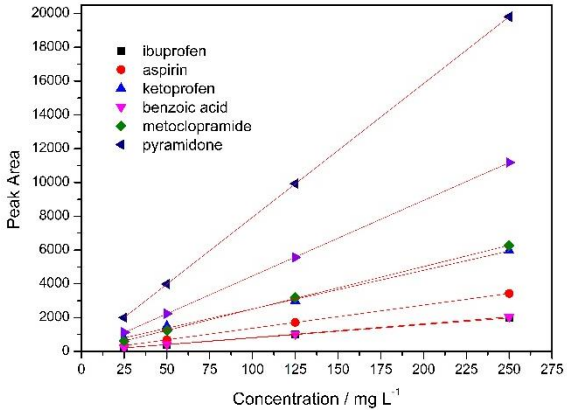

Compound	Retention time	λ (nm)	Slope Value	Standard Error	R^2
ibuprofen (**29**)	6.7	235	7.9	0.12	0.999
aspirin (**28**)	13.5	275	13.7	0.02	1
ketoprofen (**36**)	4.5	275	22.8	0.6	0.997
benzoic acid (**37**)	18.2	285	8.1	0.01	1
metoclopramide (**30**)	4.0	254	25.2	0.20	1
pyramidone (**31**)	4.1	254	79.1	0.06	1
etoperidone (**38**)	12.3	254	44.7	0.10	1

Preparation of pharmaceuticals solutions

The proper amount of pharmaceutical compound (**28**, **29**, **31**, **30**, **36**, **37**, and **38**) was separately weighted and transferred in a conical flask equipped with a magnetic stir bar, then the solvent (hydroalcoholic mixture or water) was added, and the system was hardly stirred under heating at 35 °C through an oil bath. After complete dissolution of drugs, the solution was cooled down to 25 °C and employed in adsorption experiments.

Adsorption experiments

Adsorption experiments were done in triplicate under batch operation conditions targeting pharmaceutical compounds. First, an amount of 10 mg of the GO-pAmOx (or GO) was added into 6 mL reaction tubes. Then, 5 mL of pharmaceuticals standard solutions with concentrations ranging from 25 to 250 mg L^{-1} were loaded into the cartridge. To allow homogenous adsorption on the polymer surface, the tubes were incubated in a thermostatic shaker (50 rpm for 12 h) Triplicate controls, which consisted of solutions of the corresponding pharmaceutical in the absence of any adsorbent and in the same conditions, were run in parallel. Finally, the supernatants were filtered using PTFE filters, transferred into glass vials, and analysed by HPLC-DAD.

5.7 Composite materials with cellulose and poly(2-oxazoline)s

5.7.1 Synthesis of chlorinated cellulose, **39**

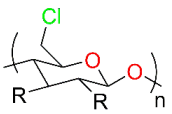

R= OH or Cl

39

1.0 g of microcrystalline cellulose (AVICEL PH 101) (6 mmol of anhydroglucose unit) was dried overnight in oven at 60 °C prior to use. Then 20 mL of anhydrous DMF were added in a two neck round bottom flask equipped with a magnetic stir bar and a reflux condenser, and the mixture was heated at 130 °C for 2 h. Then, reaction mixture was allowed to cool down at room temperature and 2 mL of thionyl chloride (1 eq.) were added dropwise and the reaction mixtures was stirred overnight at room temperature. The resulting mixture was added dropwise to into 1 L of water. The precipitate was filtered, washed with 1 L of water, then washed with 500 mL of 3.3% NH_3 solution, and finally with milli-Q-grade water. The product was recovered after drying in 99% yield.

Characterization data

ATR-FTIR: $\tilde{\nu}$ = 3343, 2969, 1738, 1645, 1366, 1218, 1159, 602 cm^{-1}

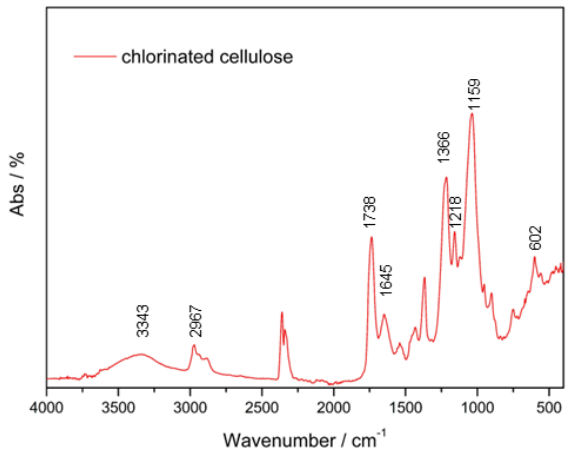

5.7.2 Synthesis of brominated cellulose, **40**

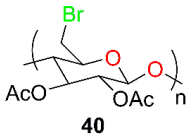

40

1.0 g of microcrystalline cellulose (AVICEL PH 101) (6 mmol of anhydroglucose unit) was dried overnight in oven at 60 °C prior to use. Then 50 mL of anhydrous DMA were added in a two neck round bottom flask equipped with a magnetic stir bar and a reflux condenser, and the mixture was heated at 160 °C for 1 h. Then, 9.0 g of LiBr was added and the mixture was slowly allowed to cool down at room temperature and stirred for another 2 h. Then, 6.45 g of triphenylphosphine (4 eq.) and 4.4 g of *N*-bromosuccinimmide (4 eq.) dissolved in anhydrous DMA were added, and the reaction temperature was adjusted to 70 °C. After 2 h, 6 mL of acetic anhydride (10 eq.) were added, and the reaction mixture was stirred at 70 °C overnight. The solutions was precipitated in 2 L of water:methanol 1:1, the precipitate was washed with water, then with ethanol. Then was resuspended in $CHCl_3$ and precipitated again in ethanol. The product was recovered after filtration and ethanol wash, in 88% yield after drying.

Characterization data

ATR-FT-IR: $\tilde{\nu}$ = 2947, 1739, 1631, 1366, 1218, 1033, 902, 592 cm^{-1}

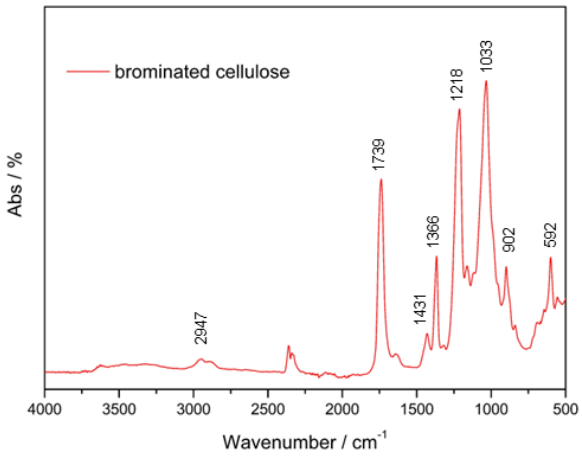

5.7.3 Synthesis of tosyl cellulose, **42**

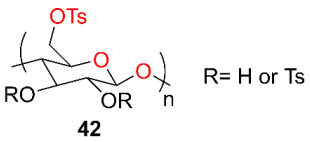

42

1.0 g of microcrystalline cellulose (AVICEL PH 101) (6 mmol of anhydroglucose unit) was dried overnight in oven at 60 °C prior to use. Then 40 mL of anhydrous DMA were added in a two neck round bottom flask equipped with a magnetic stir bar and a reflux condenser, and the mixture was heated at 130 °C for 2 h. Then, 1.0 g of LiCl was added and the mixture was stirred for another 2 h and then allowed to cool down at room temperature and stirred until a transparent and homogeneous solution was obtained. Then, 5 mL (5.5 eq.) of Et_3N were added and the reaction temperature was adjusted to 4 °C. Finally, a solution of 5.7 g (5 eq.) of Tosyl Chloride, **41** in anhydrous DMA (10 mL) was added dropwise during 1 h, and the mixture was stirred at this temperature for 48 h. The resulting mixture was added dropwise to into 1 L of cold water. The precipitate was filtered, washed with 1 L of water, then washed with 500 mL of ethanol. The precipitate was added to 500 mL of water and the resulting suspension was stirred overnight at room temperature. Then the suspension was filtered and washed again with water and finally with ethanol. The product was recovered after drying in 91% yield.

Characterization data

ATR-FTIR: $\tilde{\nu}$ = 3325, 2888, 1595, 1427, 1165, 1107, 1052, 1029 815, 664, 547 cm^{-1}

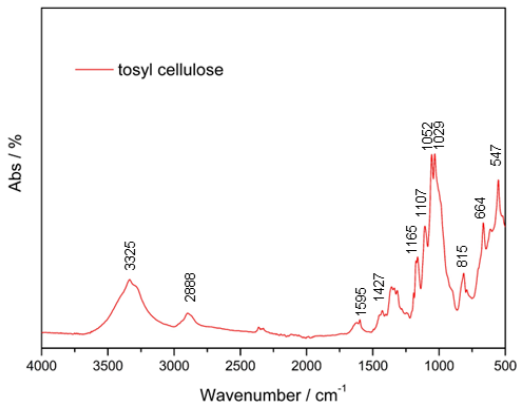

5.7.4 Polymerisation of iPOx (**11**), AmOx (**18**), and EstOx (**21**) monomers onto activated cellulose

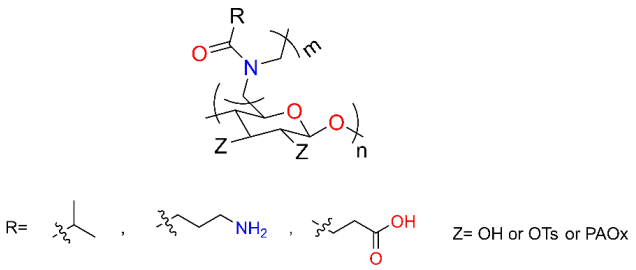

A two-neck round bottom flask equipped with an efficient reflux condenser and a magnetic stir bar was charged with monomer (**11** or **18** or **21**) (10 mmol), with 80 mg of chlorinated cellulose (**39**) or brominated cellulose (**40**) or tosyl cellulose (**42**), and anhydrous ACN (5 mL) and the reaction mixture was stirred at 90 °C from 48 to 72 h. After, the reaction was quenched by addition of 10 eq. to initiator of 1M NaOH and the resulting mixture was stirred at the same temperature for 2 h. Finally, the solvent was reduced with a rotatory evaporator and the residue was added to a solution of petroleum ether: diethyl ether (1:1). The product was recovered as a pale yellow to white precipitate, the supernatant was removed, and the product was washed twice with the petroleum ether: diethyl ether solution, then with methanol (three times) and recovered after centrifugation (5000 rpm, 10 min) in 80-120 mg yield.

Characterization data of cell-PiPOx from tosyl cellulose (42)

ATR-FTIR: $\tilde{\nu}$ = 3335, 2896, 1735,1633, 1599, 1427, 1165, 1107, 1052, 1029 815, 664, 547 cm^{-1}

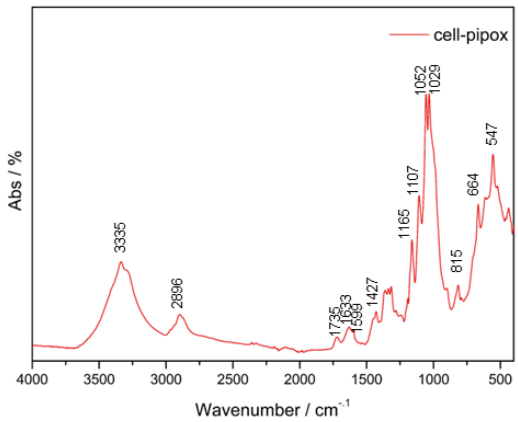

Cleavage of the amine protecting group for cellulose-pAmOx made starting with tosyl cellulose (42)

Cellulose-pAmOx (120 mg) was dissolved in dry DCM (5 mL) and then trifluoroacetic acid (80 µL) was added. The solution was stirred at room temperature overnight, and subsequently, the product was dry at reduced pressure. The crude product was redissolved in DCM and precipitated by dropping the reaction solution into petroleum ether: diethyl ether (1:1), then the product (105 mg) was washed with methanol and collected by centrifugation.

Characterization data of cell-pAmOx

ATR-FTIR: $\tilde{\nu}$ = 3330, 2891, 1679,1637, 1427, 1165, 1107, 1052, 1029 815, 664, 547 cm^{-1}

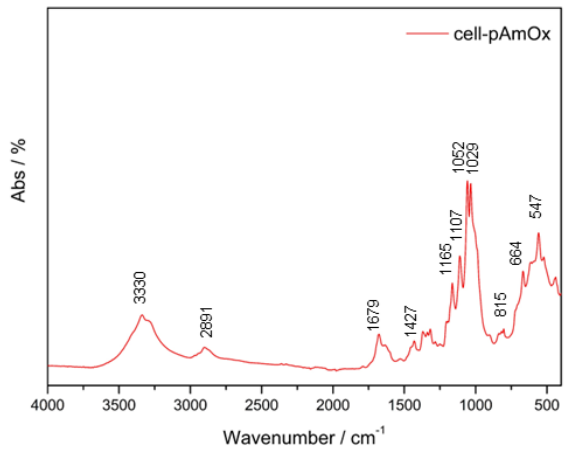

Cleavage of the carboxyl protecting group for cellulose-pEstOx made starting with tosyl cellulose (42)

Cellulose-pEstOx (120 mg) was dispersed in 5 mL mL of a 5% KOH solution and stirred overnight at room temperature. Then, ~ 425 µL of glacial acetic acid was added to neutralize residual KOH, and the product (110 mg) was washed milli-Q-grade water several times, and dried.

Characterization data of cell-pEstOx

ATR-FTIR: $\tilde{\nu}$ = 3326, 2899, 1730,1623, 1427, 1165, 1107, 1052, 1029 815, 664, 547 cm^{-1}

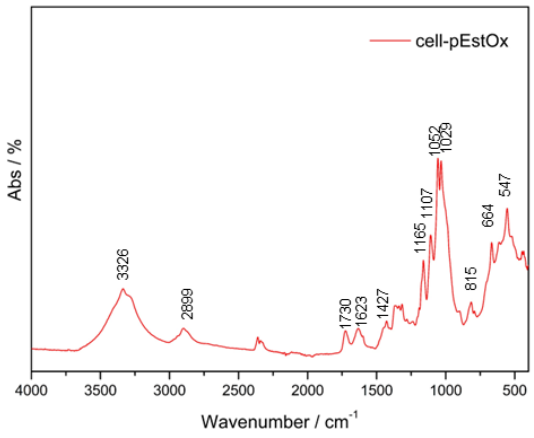

5.7.5 Heavy metal ions adsorption with cell-PiPOx, cell-pAmOx, cell-pEstOx

Inductive Coupled Plasma Emission Spectroscopy (ICP-OES) calibration curves

Calibration curves were prepared by serial dilution (with 0.5% HNO3 milli-Q-grade water) of a multi-element stock standard solution (ICP grade in 5% HNO_3), with final concentrations ranging from 1 to 60 mg L^{-1}.

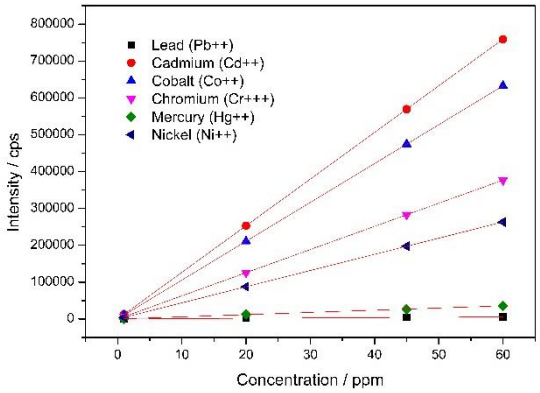

Heavy Metal	λ (nm)	Intercept Value	Slope Value	Standard Error	R2
Lead (Pb++)	266	-0.0216	97	0.006	0.999
Cadmium (Cd++)	228	-0.6200	12655	0.362	0.997
Cobalt (Co++)	238	-0.1864	10546	0.009	0.999
Chromium (Cr+++)	205	-0.5269	6283	0.300	0.998
Mercury (Hg++)	184	-0.9533	589	0.178	0.999
Nickel (Ni++)	216	-0.2401	4386	0.004	0.999

Preparation of heavy metal ions solutions

To give a cation concentration of 50 ppm, separately the proper amount of the corresponding chloride salts ($PbCl_2$, $CrCl_3$, $CdCl_2$, $CoCl_2$, $NiCl_2$, and $HgCl_2$) was weighted and transferred in a plastic volumetric flask, then HCl 0.01M milli-Q-grade water was added. After complete dissolution of salt, the solution was equilibrated at 25 °C and employed in adsorption experiments.

Adsorption experiments

Adsorption experiments were done in triplicate under batch operation conditions targeting the heavy metal ions. First, an amount of 4 mg of the cellulose, cell-PiPOx, cell-pAmOx, and cell-pEstOx were added separately into 15 mL falcon tubes. Then, 10 mL of heavy metal ion standard solutions with concentrations of 50 ppm were added. To allow homogenous adsorption the tubes were incubated in a thermostatic shaker (50 rpm for 12 h) Triplicate controls, which consisted of solutions of the corresponding heavy metal ion solution in the absence of any adsorbent and in the same conditions, were run in parallel. Finally, the supernatants were filtered using PTFE filters, additionally acidified with 1 µL of concentrated HNO_3 and analysed by ICP-OES.

5.8 Composite materials with lignin and poly(2-oxazoline)s

5.8.1 Synthesis of tosyl lignin, **43**

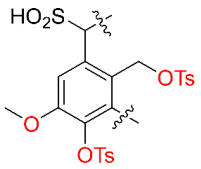

43

2.5 g of commercially available lignin (obtained by Kraft process) is stirred in water dispersion overnight at room temperature with 3.8 g (2 eq.) of *p*-toluensulfonilchloride (**41**) and 4.2 mL (3 eq.) of Et_3N. After this period, the reaction mixture was cooled down to 4 °C and filtered. The precipitate was washed with cold water, then with ethanol and recovered as brown powder in 90% yield.

Characterization data

ATR-FTIR: $\tilde{\nu}$ = 2942, 1599, 1365, 1261, 1173, 1087, 1032, 851, 809, 665, 547 cm^{-1}

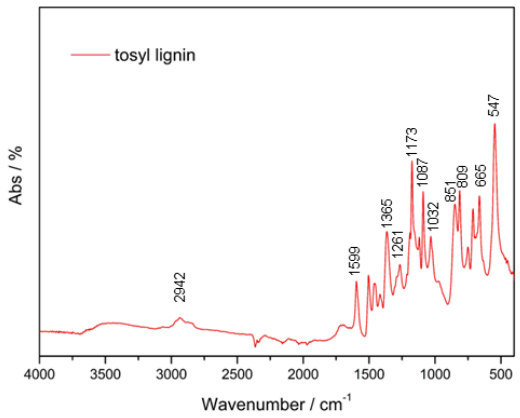

5.8.2 Synthesis of lignin-PiPOx

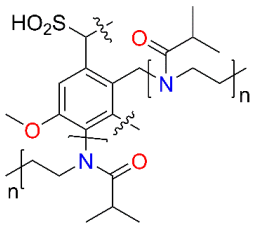

A two-neck round bottom flask equipped with an efficient reflux condenser and a magnetic stir bar was charged with monomer iPOx (**11**) (10 mmol), with 72 mg of tosyl lignin (**43**) and anhydrous ACN (5 mL) and the reaction mixtures was stirred at 90 °C for 48 h. After, the reaction was quenched by addition of 10 eq. to initiator of 1M NaOH and the resulting mixture was stirred at the same temperature for 2 h. Finally, the solvent was reduced with a rotatory evaporator and the residue was added to a solution of petroleum ether: diethyl ether (1:1). The product was recovered as a light brown precipitate, the supernatant was removed, and the product was washed twice with the petroleum ether: diethyl ether solution, then with THF and recovered after centrifugation in 85 mg yield.

Characterization data of lignin-PiPOx

ATR-FTIR: $\tilde{\nu}$ = 2967, 2929, 2870,1726,1649,1590, 1365, 1261, 1173, 1087, 1032, 851, 809, 665, 547 cm^{-1}

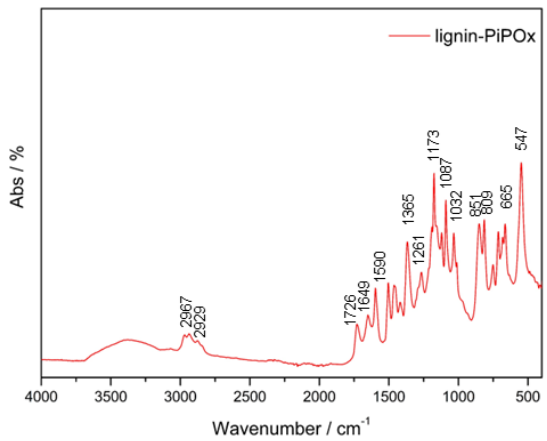

6. Bibliography

(1) Samal, K.; Mahapatra, S.; Hibzur Ali, M. Pharmaceutical Wastewater as Emerging Contaminants (EC): Treatment Technologies, Impact on Environment and Human Health. *Energy Nexus* **2022**, *6*, 100076. https://doi.org/10.1016/j.nexus.2022.100076.

(2) *Water in Crisis: A Guide to the World's Fresh Water Resources*; Gleick, P. H., Pacific Institute for Studies in Development, Environment, and Security, Stockholm Environment Institute, Pacific Institute for Studies in Development, Environment, and Security, Eds.; Oxford Univ. Press: New York, NY, **1993**.

(3) Karpińska, J.; Kotowska, U. Removal of Organic Pollution in the Water Environment. *Water* **2019**, *11*, **2017**. https://doi.org/10.3390/w11102017.

(4) OECD, Development Co-Operation Report **2012**; *Lessons in Linking Sustainability and Development*: Paris, 2012. https://doi.org/10.1787/dcr-2012-en

(5) OECD. Development Co-Operation Report 2024: *Tackling Poverty and Inequalities through the Green Transition*; **2024**. https://doi.org/10.1787/357b63f7-en.

(6) Wang, M.; Bodirsky, B. L.; Rijneveld, R.; Beier, F.; Bak, M. P.; Batool, M.; Droppers, B.; Popp, A.; van Vliet, M. T. H.; Strokal, M. A Triple Increase in Global River Basins with Water Scarcity Due to Future Pollution. *Nat. Commun.* **2024**, *15*, 880. https://doi.org/10.1038/s41467-024-44947-3.

(7) Singh, R.; Samuel, M. S.; Ravikumar, M.; Ethiraj, S.; Kumar, M. Graphene Materials in Pollution Trace Detection and Environmental Improvement. *Environ. Res.* **2024**, *243*, 117830. https://doi.org/10.1016/j.envres.2023.117830.

(8) Bernard, M. Wide Spread of Aquatic Pollution by Human Activities. *Wide Spread Aquat. Pollut. Hum. Act.* **2021**,*11*,1.

(9) Qasem, N. A. A.; Mohammed, R. H.; Lawal, D. U. Removal of Heavy Metal Ions from Wastewater: A Comprehensive and Critical Review. *Npj Clean Water* **2021**, *4*, 36. https://doi.org/10.1038/s41545-021-00127-0.

(10) Zou, Y.; Wang, X.; Khan, A.; Wang, P.; Liu, Y.; Alsaedi, A.; Hayat, T.; Wang, X. Environmental Remediation and Application of Nanoscale Zero-Valent Iron and Its Composites for the Removal of Heavy Metal Ions: A Review. *Environ. Sci. Technol.* **2016**, *50*, 7290–7304. https://doi.org/10.1021/acs.est.6b01897.

(11) Borba, C. E.; Guirardello, R.; Silva, E. A.; Veit, M. T.; Tavares, C. R. G. Removal of Nickel(II) Ions from Aqueous Solution by Biosorption in a Fixed Bed Column: Experimental and Theoretical Breakthrough Curves. *Biochem. Eng. J.* **2006**, *30*, 184–191. https://doi.org/10.1016/j.bej.2006.04.001.

(12) Taseidifar, M.; Makavipour, F.; Pashley, R. M.; Rahman, A. F. M. M. Removal of Heavy Metal Ions from Water Using Ion Flotation. *Environ. Technol. Innov.* **2017**, *8*, 182–190. https://doi.org/10.1016/j.eti.2017.07.002.

(13) García-Niño, W. R.; Pedraza-Chaverrí, J. Protective Effect of Curcumin against Heavy Metals-Induced Liver Damage. *Food Chem. Toxicol.* **2014**, *69*, 182–201. https://doi.org/10.1016/j.fct.2014.04.016.

(14) Bryce-Smith, D. Behavioural Effects of Lead and Other Heavy Metal Pollutants. *Chem. Br.* **1972**, *8*, 240–243.

(15) Chemical Speciation of Trace Metals in Airborne Particles at An Industrialized Site. *J. Environ. Sci.* **2006**, *15*, 503–511. https://doi.org/10.5322/JES.2006.15.6.503.

(16) Vincent, J. B. Chromium: Is It Essential, Pharmacologically Relevant, or Toxic? In *Interrelations between Essential Metal Ions and Human Diseases*; Sigel, A., Sigel, H., Sigel, R. K. O., Eds.; Metal Ions in Life Sciences; Springer Netherlands: Dordrecht, **2013**,*13*, pp 171–198. https://doi.org/10.1007/978-94-007-7500-8_6.

(17) Moore, J. W.; Ramamoorthy, S.; Ballantyne, E. E. *Heavy Metals in Natural Waters: Applied Monitoring and Impact Assessment*; Springer Series on environmental management; Springer: New York Heidelberg, **1984**.
(18) Bernhoft, R. A. Mercury Toxicity and Treatment: A Review of the Literature. *J. Environ. Public Health* **2012**,1–10. https://doi.org/10.1155/2012/460508.
(19) Schaider, L. A.; Rodgers, K. M.; Rudel, R. A. Review of Organic Wastewater Compound Concentrations and Removal in Onsite Wastewater Treatment Systems. *Environ. Sci. Technol.* **2017**, *51*, 7304–7317. https://doi.org/10.1021/acs.est.6b04778.
(20) Praveenkumarreddy, Y.; Vimalkumar, K.; Ramaswamy, B. R.; Kumar, V.; Singhal, R. K.; Basu, H.; Gopal, C. M.; Vandana, K. E.; Bhat, K.; Udayashankar, H. N.; Balakrishna, K. Assessment of Non-Steroidal Anti-Inflammatory Drugs from Selected Wastewater Treatment Plants of Southwestern India. *Emerg. Contam.* **2021**, *7*, 43–51. https://doi.org/10.1016/j.emcon.2021.01.001.
(21) Chopra, S.; Kumar, D. Ibuprofen as an Emerging Organic Contaminant in Environment, Distribution and Remediation. *Heliyon* **2020**, *6*, e04087. https://doi.org/10.1016/j.heliyon.2020.e04087.
(22) Tyumina, E. A.; Bazhutin, G. A.; Cartagena Gómez, A. d. P.; Ivshina, I. B. Nonsteroidal Anti-Inflammatory Drugs as Emerging Contaminants. *Microbiology* **2020**, *89*, 148–163. https://doi.org/10.1134/S0026261720020125.
(23) Feng, L.; Van Hullebusch, E. D.; Rodrigo, M. A.; Esposito, G.; Oturan, M. A. Removal of Residual Anti-Inflammatory and Analgesic Pharmaceuticals from Aqueous Systems by Electrochemical Advanced Oxidation Processes. A Review. *Chem. Eng. J.* **2013**, *228*, 944–964. https://doi.org/10.1016/j.cej.2013.05.061.
(24) Novoa-Luna, K. A.; Romero-Romero, R.; Natividad-Rangel, R.; Galar-Martínez, M.; SanJuan-Reyes, N.; García-Medina, S.; Martínez-Vieyra, C.; Neri-Cruz, N.; Gómez-Oliván, L. M. Oxidative Stress Induced in Hyalella Azteca by an Effluent from a NSAID-Manufacturing Plant in Mexico. *Ecotoxicology* **2016**, *25*, 1288–1304. https://doi.org/10.1007/s10646-016-1682-2.
(25) Selderslaghs, I. W. T.; Blust, R.; Witters, H. E. Feasibility Study of the Zebrafish Assay as an Alternative Method to Screen for Developmental Toxicity and Embryotoxicity Using a Training Set of 27 Compounds. *Reprod. Toxicol.* **2012**, *33*, 142–154. https://doi.org/10.1016/j.reprotox.2011.08.003.
(26) Estrada-Almeida, A. G.; Castrejón-Godínez, M. L.; Mussali-Galante, P.; Tovar-Sánchez, E.; Rodríguez, A. Pharmaceutical Pollutants: Ecotoxicological Impacts and the Use of Agro-Industrial Waste for Their Removal from Aquatic Environments. *J. Xenobiotics* **2024**, *14*, 1465–1518. https://doi.org/10.3390/jox14040082.
(27) Parolini, M.; Binelli, A. Sub-Lethal Effects Induced by a Mixture of Three Non-Steroidal Anti-Inflammatory Drugs (NSAIDs) on the Freshwater Bivalve Dreissena Polymorpha. *Ecotoxicology* **2012**, *21*, 379–392. https://doi.org/10.1007/s10646-011-0799-6.
(28) Fernandes, J. P.; Almeida, C. M. R.; Salgado, M. A.; Carvalho, M. F.; Mucha, A. P. Pharmaceutical Compounds in Aquatic Environments—Occurrence, Fate and Bioremediation Prospective. *Toxics* **2021**, *9*, 257. https://doi.org/10.3390/toxics9100257.
(29) Nishat, A.; Yusuf, M.; Qadir, A.; Ezaier, Y.; Vambol, V.; Ijaz Khan, M.; Ben Moussa, S.; Kamyab, H.; Sehgal, S. S.; Prakash, C.; Yang, H.-H.; Ibrahim, H.; Eldin, S. M. Wastewater Treatment: A Short Assessment on Available Techniques. *Alex. Eng. J.* **2023**, *76*, 505–516. https://doi.org/10.1016/j.aej.2023.06.054.
(30) Khopkar, S. M. *Environmental Pollution: Monitoring and Control*; New Age Internat. Publ: New Delhi, **2004**.
(31) Gupta, A.; Thakur, I. S. Treatment of Organic Recalcitrant Contaminants in Wastewater. In *Biological Wastewater Treatment and Resource Recovery*; Farooq, R., Ahmad, Z., Eds.; InTech, **2017**. https://doi.org/10.5772/66346.

(32) Rashid, R.; Shafiq, I.; Akhter, P.; Iqbal, M. J.; Hussain, M. A State-of-the-Art Review on Wastewater Treatment Techniques: The Effectiveness of Adsorption Method. *Environ. Sci. Pollut. Res.* **2021**, *28*, 9050–9066. https://doi.org/10.1007/s11356-021-12395-x.

(33) Rout, P. R.; Zhang, T. C.; Bhunia, P.; Surampalli, R. Y. Treatment Technologies for Emerging Contaminants in Wastewater Treatment Plants: A Review. *Sci. Total Environ.* **2021**, *753*, 141990. https://doi.org/10.1016/j.scitotenv.2020.141990.

(34) Fernandes, J.; Ramísio, P. J.; Puga, H. A Comprehensive Review on Various Phases of Wastewater Technologies: Trends and Future Perspectives. *Eng* **2024**, *5*, 2633–2661. https://doi.org/10.3390/eng5040138.

(35) Fernandes, J. P.; Almeida, C. M. R.; Pereira, A. C.; Ribeiro, I. L.; Reis, I.; Carvalho, P.; Basto, M. C. P.; Mucha, A. P. Microbial Community Dynamics Associated with Veterinary Antibiotics Removal in Constructed Wetlands Microcosms. *Bioresour. Technol.* **2015**, *182*, 26–33. https://doi.org/10.1016/j.biortech.2015.01.096.

(36) Rodriguez, J.; Stopić, S.; Krause, G.; Friedrich, B. Feasibility Assessment of Electrocoagulation towards a New Sustainable Wastewater Treatment. *Environ. Sci. Pollut. Res. - Int.* **2007**, *14*, 477–482. https://doi.org/10.1065/espr2007.05.424.

(37) Al-Shannag, M.; Al-Qodah, Z.; Bani-Melhem, K.; Qtaishat, M. R.; Alkasrawi, M. Heavy Metal Ions Removal from Metal Plating Wastewater Using Electrocoagulation: Kinetic Study and Process Performance. *Chem. Eng. J.* **2015**, *260*, 749–756. https://doi.org/10.1016/j.cej.2014.09.035.

(38) Hakizimana, J. N.; Gourich, B.; Chafi, M.; Stiriba, Y.; Vial, C.; Drogui, P.; Naja, J. Electrocoagulation Process in Water Treatment: A Review of Electrocoagulation Modeling Approaches. *Desalination* **2017**, *404*, 1–21. https://doi.org/10.1016/j.desal.2016.10.011.

(39) Aswathy, P.; Gandhimathi, R.; Ramesh, S. T.; Nidheesh, P. V. Removal of Organics from Bilge Water by Batch Electrocoagulation Process. *Sep. Purif. Technol.* **2016**, *159*, 108–115. https://doi.org/10.1016/j.seppur.2016.01.001.

(40) Sardari, K.; Fyfe, P.; Lincicome, D.; Wickramasinghe, S. R. Aluminum Electrocoagulation Followed by Forward Osmosis for Treating Hydraulic Fracturing Produced Waters. *Desalination* **2018**, *428*, 172–181. https://doi.org/10.1016/j.desal.2017.11.030.

(41) Tahreen, A.; Jami, M. S.; Ali, F. Role of Electrocoagulation in Wastewater Treatment: A Developmental Review. *J. Water Process Eng.* **2020**, *37*, 101440. https://doi.org/10.1016/j.jwpe.2020.101440.

(42) Judd, S.; Judd, C. *The MBR Book: Principles and Applications of Membrane Bioreactors in Water and Wastewater Treatment*; Elsevier: Amsterdam Paris, **2006**.

(43) Judd, S. The Status of Membrane Bioreactor Technology. *Trends Biotechnol.* **2008**, *26*, 109–116. https://doi.org/10.1016/j.tibtech.2007.11.005.

(44) Goswami, L.; Vinoth Kumar, R.; Borah, S. N.; Arul Manikandan, N.; Pakshirajan, K.; Pugazhenthi, G. Membrane Bioreactor and Integrated Membrane Bioreactor Systems for Micropollutant Removal from Wastewater: A Review. *J. Water Process Eng.* **2018**, *26*, 314–328. https://doi.org/10.1016/j.jwpe.2018.10.024.

(45) Liu, L.; Luo, X.-B.; Ding, L.; Luo, S.-L. Application of Nanotechnology in the Removal of Heavy Metal From Water. In *Nanomaterials for the Removal of Pollutants and Resource Reutilization*; Elsevier, **2019**; pp 83–147. https://doi.org/10.1016/B978-0-12-814837-2.00004-4.

(46) Brillas, E.; Mur, E.; Sauleda, R.; Sànchez, L.; Peral, J.; Domènech, X.; Casado, J. Aniline Mineralization by AOP's: Anodic Oxidation, Photocatalysis, Electro-Fenton and Photoelectro-Fenton Processes. *Appl. Catal. B Environ.* **1998**, *16*, 31–42. https://doi.org/10.1016/S0926-3373(97)00059-3.

(47) Cai, Q. Q.; Lee, B. C. Y.; Ong, S. L.; Hu, J. Y. Fluidized-Bed Fenton Technologies for Recalcitrant Industrial Wastewater Treatment–Recent Advances, Challenges and Perspective. *Water Res.* **2021**, *190*, 116692. https://doi.org/10.1016/j.watres.2020.116692.

(48) Xu, X.-R.; Li, X.-Y.; Li, X.-Z.; Li, H.-B. Degradation of Melatonin by UV, UV/H2O2, Fe2+/H2O2 and UV/Fe2+/H2O2 Processes. *Sep. Purif. Technol.* **2009**, *68*, 261–266. https://doi.org/10.1016/j.seppur.2009.05.013.

(49) Pignatello, J. J.; Oliveros, E.; MacKay, A. Advanced Oxidation Processes for Organic Contaminant Destruction Based on the Fenton Reaction and Related Chemistry. *Crit. Rev. Environ. Sci. Technol.* **2006**, *36*, 1–84. https://doi.org/10.1080/10643380500326564.

(50) Satyam, S.; Patra, S. Innovations and Challenges in Adsorption-Based Wastewater Remediation: A Comprehensive Review. *Heliyon* **2024**, *10*, e29573. https://doi.org/10.1016/j.heliyon.2024.e29573.

(51) Azam, K.; Shezad, N.; Shafiq, I.; Akhter, P.; Akhtar, F.; Jamil, F.; Shafique, S.; Park, Y.-K.; Hussain, M. A Review on Activated Carbon Modifications for the Treatment of Wastewater Containing Anionic Dyes. *Chemosphere* **2022**, *306*, 135566. https://doi.org/10.1016/j.chemosphere.2022.135566.

(52) Vyrides, I.; Conteras, P. A.; Stuckey, D. C. Post-Treatment of a Submerged Anaerobic Membrane Bioreactor (SAMBR) Saline Effluent Using Powdered Activated Carbon (PAC). *J. Hazard. Mater.* **2010**, *177*, 836–841. https://doi.org/10.1016/j.jhazmat.2009.12.109.

(53) Brethauer, S.; Shahab, R. L.; Studer, M. H. Impacts of Biofilms on the Conversion of Cellulose. *Appl. Microbiol. Biotechnol.* **2020**, *104*, 5201–5212. https://doi.org/10.1007/s00253-020-10595-y.

(54) Supanchaiyamat, N.; Jetsrisuparb, K.; Knijnenburg, J. T. N.; Tsang, D. C. W.; Hunt, A. J. Lignin Materials for Adsorption: Current Trend, Perspectives and Opportunities. *Bioresour. Technol.* **2019**, *272*, 570–581. https://doi.org/10.1016/j.biortech.2018.09.139.

(55) Hong, S.; Shen, X.-J.; Xue, Z.; Sun, Z.; Yuan, T.-Q. Structure–Function Relationships of Deep Eutectic Solvents for Lignin Extraction and Chemical Transformation. *Green Chem.* **2020**, *22*, 7219–7232. https://doi.org/10.1039/D0GC02439B.

(56) Xiao, X.; Jiang, J.; Wang, Y.; Wang, B.; Yuan, T.-Q.; Shi, Q.; Liao, X.; Shi, B.; Sun, R.-C. Microwave-Assisted Sulfonation of Lignin for the Fabrication of a High-Performance Dye Dispersant. *ACS Sustain. Chem. Eng.* **2021**, *9*, 9053–9061. https://doi.org/10.1021/acssuschemeng.1c02148.

(57) Kai, D.; Tan, M. J.; Chee, P. L.; Chua, Y. K.; Yap, Y. L.; Loh, X. J. Towards Lignin-Based Functional Materials in a Sustainable World. *Green Chem.* **2016**, *18*, 1175–1200. https://doi.org/10.1039/C5GC02616D.

(58) Naseem, A.; Tabasum, S.; Zia, K. M.; Zuber, M.; Ali, M.; Noreen, A. Lignin-Derivatives Based Polymers, Blends and Composites: A Review. *Int. J. Biol. Macromol.* **2016**, *93*, 296–313. https://doi.org/10.1016/j.ijbiomac.2016.08.030.

(59) Roa, K.; Oyarce, E.; Boulett, A.; ALSamman, M.; Oyarzún, D.; Pizarro, G. D. C.; Sánchez, J. Lignocellulose-Based Materials and Their Application in the Removal of Dyes from Water: A Review. *Sustain. Mater. Technol.* **2021**, *29*, e00320. https://doi.org/10.1016/j.susmat.2021.e00320.

(60) Sayyed, A. J.; Pinjari, D. V.; Sonawane, S. H.; Bhanvase, B. A.; Sheikh, J.; Sillanpää, M. Cellulose-Based Nanomaterials for Water and Wastewater Treatments: A Review. *J. Environ. Chem. Eng.* **2021**, *9*, 106626. https://doi.org/10.1016/j.jece.2021.106626.

(61) Aoudi, B.; Boluk, Y.; Gamal El-Din, M. Recent Advances and Future Perspective on Nanocellulose-Based Materials in Diverse Water Treatment Applications. *Sci. Total Environ.* **2022**, *843*, 156903. https://doi.org/10.1016/j.scitotenv.2022.156903.

(62) Zhou, Y.; Zhang, M.; Hu, X.; Wang, X.; Niu, J.; Ma, T. Adsorption of Cationic Dyes on a Cellulose-Based Multicarboxyl Adsorbent. *J. Chem. Eng. Data* **2013**, *58*, 413–421. https://doi.org/10.1021/je301140c.

(63) Zhou, Y.; Zhang, M.; Wang, X.; Huang, Q.; Min, Y.; Ma, T.; Niu, J. Removal of Crystal Violet by a Novel Cellulose-Based Adsorbent: Comparison with Native Cellulose. *Ind. Eng. Chem. Res.* **2014**, *53*, 5498–5506. https://doi.org/10.1021/ie404135y.

(64) Bonenfant, D.; Niquette, P.; Mimeault, M.; Hausler, R. Adsorption and Recovery of Nonylphenol Ethoxylate on a Crosslinked β-Cyclodextrin-Carboxymethylcellulose Polymer. *Water Sci. Technol.* **2010**, *61*, 2293–2301. https://doi.org/10.2166/wst.2010.152.
(65) Mbayachi, V. B.; Ndayiragije, E.; Sammani, T.; Taj, S.; Mbuta, E. R.; Khan, A. U. Graphene Synthesis, Characterization and Its Applications: A Review. *Results Chem.* **2021**, *3*, 100163. https://doi.org/10.1016/j.rechem.2021.100163.
(66) Dasari Shareena, T. P.; McShan, D.; Dasmahapatra, A. K.; Tchounwou, P. B. A Review on Graphene-Based Nanomaterials in Biomedical Applications and Risks in Environment and Health. *Nano-Micro Lett.* **2018**, *10*, 53. https://doi.org/10.1007/s40820-018-0206-4.
(67) Novoselov, K. S.; Jiang, D.; Schedin, F.; Booth, T. J.; Khotkevich, V. V.; Morozov, S. V.; Geim, A. K. Two-Dimensional Atomic Crystals. *Proc. Natl. Acad. Sci.* **2005**, *102*, 10451–10453. https://doi.org/10.1073/pnas.0502848102.
(68) Edwards, R. S.; Coleman, K. S. Graphene Synthesis: Relationship to Applications. *Nanoscale* **2013**, *5*, 38–51. https://doi.org/10.1039/C2NR32629A.
(69) Van Noorden, R. Production: Beyond Sticky Tape. *Nature* **2012**, *483*, S32–S33. https://doi.org/10.1038/483S32a.
(70) Hibino, H.; Kageshima, H.; Nagase, M. Graphene Growth on Silicon Carbide. *NTT Tech. Rev.* **2010**, *8*.
(71) Brownson, D. A. C.; Banks, C. E. The Electrochemistry of CVD Graphene: Progress and Prospects. *Phys. Chem. Chem. Phys.* **2012**, *14*, 8264. https://doi.org/10.1039/c2cp40225d.
(72) Brownson, D. A. C.; Banks, C. E. CVD Graphene Electrochemistry: The Role of Graphitic Islands. *Phys. Chem. Chem. Phys.* **2011**, *13*, 15825. https://doi.org/10.1039/c1cp21978b.
(73) Mahmoudi, T.; Wang, Y.; Hahn, Y.-B. Graphene and Its Derivatives for Solar Cells Application. *Nano Energy* **2018**, *47*, 51–65. https://doi.org/10.1016/j.nanoen.2018.02.047.
(74) Baraton, L.; He, Z.; Lee, C. S.; Maurice, J. L.; Cojocaru, C. S.; Lee, Y. H.; Pribat, D. Study of Graphene Growth Mechanism on Nickel Thin Films. In *GraphITA 2011*; Ottaviano, L., Morandi, V., Eds.; Carbon Nanostructures; Springer Berlin Heidelberg: Berlin, Heidelberg, **2012**; pp 1–7. https://doi.org/10.1007/978-3-642-20644-3_1.
(75) Jariwala, D.; Srivastava, A.; Ajayan, P. M. Graphene Synthesis and Band Gap Opening. *J. Nanosci. Nanotechnol.* **2011**, *11*, 6621–6641. https://doi.org/10.1166/jnn.2011.5001.
(76) Peng, W.; Li, H.; Liu, Y.; Song, S. A Review on Heavy Metal Ions Adsorption from Water by Graphene Oxide and Its Composites. *J. Mol. Liq.* **2017**, *230*, 496–504. https://doi.org/10.1016/j.molliq.2017.01.064.
(77) Khaliha, S.; Bianchi, A.; Kovtun, A.; Tunioli, F.; Boschi, A.; Zambianchi, M.; Paci, D.; Bocchi, L.; Valsecchi, S.; Polesello, S.; Liscio, A.; Bergamini, M.; Brunetti, M.; Luisa Navacchia, M.; Palermo, V.; Melucci, M. Graphene Oxide Nanosheets for Drinking Water Purification by Tandem Adsorption and Microfiltration. *Sep. Purif. Technol.* **2022**, *300*, 121826. https://doi.org/10.1016/j.seppur.2022.121826.
(78) Zaaba, N. I.; Foo, K. L.; Hashim, U.; Tan, S. J.; Liu, W.-W.; Voon, C. H. Synthesis of Graphene Oxide Using Modified Hummers Method: Solvent Influence. *Procedia Eng.* **2017**, *184*, 469–477. https://doi.org/10.1016/j.proeng.2017.04.118.
(79) Meena, J.; Gupta, A.; Ahuja, R.; Panda, A. K.; Bhaskar, S. Inorganic Particles for Delivering Natural Products. In *Sustainable Agriculture Reviews 44*; Saneja, A., Panda, A. K., Lichtfouse, E., Eds.; Sustainable Agriculture Reviews; Springer International Publishing: Cham, **2020**, pp 205–241. https://doi.org/10.1007/978-3-030-41842-7_6.
(80) Kasthuri, J.; Veerapandian, S.; Rajendiran, N. Biological Synthesis of Silver and Gold Nanoparticles Using Apiin as Reducing Agent. *Colloids Surf. B Biointerfaces* **2009**, *68*, 55–60. https://doi.org/10.1016/j.colsurfb.2008.09.021.
(81) Bazylińska, U.; Kulbacka, J.; Chodaczek, G. Nanoemulsion Structural Design in Co-Encapsulation of Hybrid Multifunctional Agents: Influence of the Smart PLGA Polymers on the Nanosystem-Enhanced

Delivery and Electro-Photodynamic Treatment. *Pharmaceutics* **2019**, *11*, 405. https://doi.org/10.3390/pharmaceutics11080405.
(82) Crini, G. Kinetic and Equilibrium Studies on the Removal of Cationic Dyes from Aqueous Solution by Adsorption onto a Cyclodextrin Polymer. *Dyes Pigments* **2008**, *77*, 415–426. https://doi.org/10.1016/j.dyepig.2007.07.001.
(83) Ko, D.; Patel, H. A.; Yavuz, C. T. Synthesis of Nanoporous 1,2,4-Oxadiazole Networks with High CO_2 Capture Capacity. *Chem. Commun.* **2015**, *51*, 2915–2917. https://doi.org/10.1039/C4CC08649J.
(84) Patel, H. A.; Karadas, F.; Byun, J.; Park, J.; Deniz, E.; Canlier, A.; Jung, Y.; Atilhan, M.; Yavuz, C. T. Highly Stable Nanoporous Sulfur-Bridged Covalent Organic Polymers for Carbon Dioxide Removal. *Adv. Funct. Mater.* **2013**, *23*, 2270–2276. https://doi.org/10.1002/adfm.201202442.
(85) Patel, H. A.; Karadas, F.; Canlier, A.; Park, J.; Deniz, E.; Jung, Y.; Atilhan, M.; Yavuz, C. T. High Capacity Carbon Dioxide Adsorption by Inexpensive Covalent Organic Polymers. *J. Mater. Chem.* **2012**, *22*, 8431. https://doi.org/10.1039/c2jm30761h.
(86) Alaba, P. A.; Oladoja, N. A.; Sani, Y. M.; Ayodele, O. B.; Mohammed, I. Y.; Olupinla, S. F.; Daud, W. M. W. Insight into Wastewater Decontamination Using Polymeric Adsorbents. *J. Environ. Chem. Eng.* **2018**, *6*, 1651–1672. https://doi.org/10.1016/j.jece.2018.02.019.
(87) Hoogenboom, R. Poly(2-Oxazoline)s: A Polymer Class with Numerous Potential Applications. *Angew. Chem. Int. Ed.* **2009**, *48*, 7978–7994. https://doi.org/10.1002/anie.200901607.
(88) Glassner, M.; Vergaelen, M.; Hoogenboom, R. Poly(2-Oxazoline)s: A Comprehensive Overview of Polymer Structures and Their Physical Properties: Poly(2-Oxazoline)s. *Polym. Int.* **2018**, *67*, 32–45. https://doi.org/10.1002/pi.5457.
(89) Lorson, T.; Lübtow, M. M.; Wegener, E.; Haider, M. S.; Borova, S.; Nahm, D.; Jordan, R.; Sokolski-Papkov, M.; Kabanov, A. V.; Luxenhofer, R. Poly(2-Oxazoline)s Based Biomaterials: A Comprehensive and Critical Update. *Biomaterials* **2018**, *178*, 204–280. https://doi.org/10.1016/j.biomaterials.2018.05.022.
(90) Cesana, S.; Auernheimer, J.; Jordan, R.; Kessler, H.; Nuyken, O. First Poly(2-oxazoline)s with Pendant Amino Groups. *Macromol. Chem. Phys.* **2006**, *207*, 183–192. https://doi.org/10.1002/macp.200500495.
(91) Adams, N.; Schubert, U. S. Poly(2-Oxazolines) in Biological and Biomedical Application Contexts. *Adv Drug Deliv. Rev* **2007**, *59*, 1504.
(92) Seeliger, W.; Aufderhaar, E.; Diepers, W.; Feinauer, R.; Nehring, R.; Thier, W.; Hellmann, H. Recent Syntheses and Reactions of Cyclic Imidic Esters. *Angew. Chem. Int. Ed. Engl.* **1966**, *5*, 875–888. https://doi.org/10.1002/anie.196608751.
(93) Kagiya, T.; Narisawa, S.; Maeda, T.; Fukui, K. Ring-opening Polymerization of 2-substituted 2-oxazolines. *J. Polym. Sci. [B]* **1966**, *4*, 441–445. https://doi.org/10.1002/pol.1966.110040701.
(94) Yön, N.; Akbulut, C.; Gunes, S.; Alsaran, M.; Olgun, U.; Kayhan, F.; Kaymak, G. Effects of Poly(2-Ethyl-2-Oxazoline) Exposure on Ovary Histology of Zebrafish (Danio Rerio). *Fresenius Environ. Bull.* **2015**, *24*, 4072–4076.
(95) Lusina, A.; Nazim, T.; Cegłowski, M. Poly(2-Oxazoline)s as Stimuli-Responsive Materials for Biomedical Applications: Recent Developments of Polish Scientists. *Polymers* **2022**, *14*, 4176. https://doi.org/10.3390/polym14194176.
(96) Meyers, A. I.; Temple, D. L.; Haidukewych, D.; Mihelich, E. D. Oxazolines. XI. Synthesis of Functionalized Aromatic and Aliphatic Acids. Useful Protecting Group for Carboxylic Acids against Grignard and Hydride Reagents. *J. Org. Chem.* **1974**, *39*, 2787–2793. https://doi.org/10.1021/jo00932a024.
(97) Fijten, M. W. M.; Haensch, C.; Van Lankvelt, B. M.; Hoogenboom, R.; Schubert, U. S. Clickable Poly(2-Oxazoline)s as Versatile Building Blocks. *Macromol. Chem. Phys.* **2008**, *209*, 1887–1895. https://doi.org/10.1002/macp.200800226.

(98) Rossegger, E.; Schenk, V.; Wiesbrock, F. Design Strategies for Functionalized Poly(2-Oxazoline)s and Derived Materials. *Polymers* **2013**, *5*, 956–1011. https://doi.org/10.3390/polym5030956.
(99) Hoogenboom, R.; Schlaad, H. Thermoresponsive Poly(2-Oxazoline)s, Polypeptoids, and Polypeptides. *Polym. Chem.* **2017**, *8*, 24–40. https://doi.org/10.1039/C6PY01320A.
(100) Huber, S.; Hutter, N.; Jordan, R. Effect of End Group Polarity upon the Lower Critical Solution Temperature of Poly(2-Isopropyl-2-Oxazoline). *Colloid Polym. Sci.* **2008**, *286*, 1653–1661. https://doi.org/10.1007/s00396-008-1942-7.
(101) Shi, J.; Votruba, A. R.; Farokhzad, O. C.; Langer, R. Nanotechnology in Drug Delivery and Tissue Engineering: From Discovery to Applications. *Nano Lett.* **2010**, *10*, 3223–3230. https://doi.org/10.1021/nl102184c.
(102) Wilson, D. S.; Dalmasso, G.; Wang, L.; Sitaraman, S. V.; Merlin, D.; Murthy, N. Orally Delivered Thioketal Nanoparticles Loaded with TNF-α–siRNA Target Inflammation and Inhibit Gene Expression in the Intestines. *Nat. Mater.* **2010**, *9*, 923–928. https://doi.org/10.1038/nmat2859.
(103) Mironov, V.; Visconti, R. P.; Kasyanov, V.; Forgacs, G.; Drake, C. J.; Markwald, R. R. Organ Printing: Tissue Spheroids as Building Blocks. *Biomaterials* **2009**, *30*, 2164–2174. https://doi.org/10.1016/j.biomaterials.2008.12.084.
(104) Koo, O. M.; Rubinstein, I.; Onyuksel, H. Role of Nanotechnology in Targeted Drug Delivery and Imaging: A Concise Review. *Nanomedicine Nanotechnol. Biol. Med.* **2005**, *1*, 193–212. https://doi.org/10.1016/j.nano.2005.06.004.
(105) Furno, F.; Morley, K. S.; Wong, B.; Sharp, B. L.; Arnold, P. L.; Howdle, S. M.; Bayston, R.; Brown, P. D.; Winship, P. D.; Reid, H. J. Silver Nanoparticles and Polymeric Medical Devices: A New Approach to Prevention of Infection? *J. Antimicrob. Chemother.* **2004**, *54*, 1019–1024. https://doi.org/10.1093/jac/dkh478.
(106) *Safety of Nanoparticles: From Manufacturing to Medical Applications*; Webster, T. J., Ed.; Nanostructure science and technology; Springer: New York, NY, **2009**.
(107) Heskins, M.; Guillet, J. E. Solution Properties of Poly(N-Isopropylacrylamide). *J. Macromol. Sci. Part - Chem.* **1968**, *2*, 1441–1455. https://doi.org/10.1080/10601326808051910.
(108) Kumar, A.; Srivastava, A.; Galaev, I. Y.; Mattiasson, B. Smart Polymers: Physical Forms and Bioengineering Applications. *Prog. Polym. Sci.* **2007**, *32*, 1205–1237. https://doi.org/10.1016/j.progpolymsci.2007.05.003.
(109) Seuring, J.; Agarwal, S. Polymers with Upper Critical Solution Temperature in Aqueous Solution. *Macromol. Rapid Commun.* **2012**, *33*, 1898–1920. https://doi.org/10.1002/marc.201200433.
(110) Southall, N. T.; Dill, K. A.; Haymet, A. D. J. A View of the Hydrophobic Effect. *J. Phys. Chem. B* **2002**, *106*, 521–533. https://doi.org/10.1021/jp015514e.
(111) Sponchioni, M.; Capasso Palmiero, U.; Moscatelli, D. Thermo-Responsive Polymers: Applications of Smart Materials in Drug Delivery and Tissue Engineering. *Mater. Sci. Eng. C* **2019**, *102*, 589–605. https://doi.org/10.1016/j.msec.2019.04.069.
(112) Halperin, A.; Kröger, M.; Winnik, F. M. Poly(*N* -isopropylacrylamide) Phase Diagrams: Fifty Years of Research. *Angew. Chem. Int. Ed.* **2015**, *54*, 15342–15367. https://doi.org/10.1002/anie.201506663.
(113) Deshmukh, S. A.; Kamath, G.; Suthar, K. J.; Mancini, D. C.; Sankaranarayanan, S. K. R. S. Non-Equilibrium Effects Evidenced by Vibrational Spectra during the Coil-to-Globule Transition in Poly(N-Isopropylacrylamide) Subjected to an Ultrafast Heating–Cooling Cycle. *Soft Matter* **2014**, *10*, 1462–1480. https://doi.org/10.1039/C3SM51750K.
(114) Belal, K.; Stoffelbach, F.; Lyskawa, J.; Fumagalli, M.; Hourdet, D.; Marcellan, A.; Smet, L. D.; de la Rosa, V. R.; Cooke, G.; Hoogenboom, R.; Woisel, P. Recognition-Mediated Hydrogel Swelling Controlled by Interaction with a Negative Thermoresponsive LCST Polymer. *Angew. Chem. Int. Ed.* **2016**, *55*, 13974–13978. https://doi.org/10.1002/anie.201605630.

(115) Amin, B.; Malekzadeh, M.; Heidari, M. R.; Hosseinzadeh, H. Effect of Crocus Sativus Extracts and Its Active Constituent Safranal on the Harmaline-Induced Tremor in Mice. *Iran. J. Basic Med. Sci.* **2015**, *18*, 449–458.
(116) Vihola, H.; Laukkanen, A.; Valtola, L.; Tenhu, H.; Hirvonen, J. Cytotoxicity of Thermosensitive Polymers Poly(N-Isopropylacrylamide), Poly(N-Vinylcaprolactam) and Amphiphilically Modified Poly(N-Vinylcaprolactam). *Biomaterials* **2005**, *26*, 3055–3064. https://doi.org/10.1016/j.biomaterials.2004.09.008.
(117) Dworak, A.; Utrata-Wesołek, A.; Oleszko, N.; Wałach, W.; Trzebicka, B.; Anioł, J.; Sieroń, A. L.; Klama-Baryła, A.; Kawecki, M. Poly(2-Substituted-2-Oxazoline) Surfaces for Dermal Fibroblasts Adhesion and Detachment. *J. Mater. Sci. Mater. Med.* **2014**, *25*, 1149–1163. https://doi.org/10.1007/s10856-013-5135-7.
(118) Verbraeken, B.; Monnery, B. D.; Lava, K.; Hoogenboom, R. The Chemistry of Poly(2-Oxazoline)s. *Eur. Polym. J.* **2017**, *88*, 451–469. https://doi.org/10.1016/j.eurpolymj.2016.11.016.
(119) Roma, E.; Corsi, P.; Willinger, M.; Leitner, N. S.; Zirbs, R.; Reimhult, E.; Capone, B.; Gasperi, T. Theoretical and Experimental Design of Heavy Metal-Mopping Magnetic Nanoparticles. *ACS Appl. Mater. Interfaces* **2021**, *13*, 1386–1397. https://doi.org/10.1021/acsami.0c17759.
(120) Lorson, T.; Lübtow, M. M.; Wegener, E.; Haider, M. S.; Borova, S.; Nahm, D.; Jordan, R.; Sokolski-Papkov, M.; Kabanov, A. V.; Luxenhofer, R. Poly(2-Oxazoline)s Based Biomaterials: A Comprehensive and Critical Update. *Biomaterials* **2018**, *178*, 204–280. https://doi.org/10.1016/j.biomaterials.2018.05.022.
(121) Stefanuto, L.; Ricci, A.; Del Galdo, S.; Rossi, C.; Pepi, S.; Giordano, E.; Capone, B.; Tofani, D.; Gasperi, T. 2-Oxazoline-Based Polymer for Pharmaceutical Products Adsorption in Aqueous Media. J. Polym. Sci. **2024**,*62*, 5656-5664, https://doi.org/10.1002/pol.20240624.
(122) Shajahan, R.; Sarang, R.; Ramakrishnan, R.; Saithalavi, A. Recent Advances in Polymer-Supported Proline-Derived Catalysts forAsymmetric Reactions. *Curr. Organocatalysis* **2023**, *10*, 81–112. https://doi.org/10.2174/2213337210666230224115814.
(123) Mahand, S. N.; Aliakbarzadeh, S.; Moghaddam, A.; Moghaddam, A. S.; Kruppke, B.; Nasrollahzadeh, M.; Khonakdar, H. A. Polyoxazoline: A Review Article from Polymerization to Smart Behaviors and Biomedical Applications. *Eur. Polym. J.* **2022**, *178*, 111484. https://doi.org/10.1016/j.eurpolymj.2022.111484.
(124) Cegłowski, M.; Marien, Y. W.; Smeets, S.; De Smet, L.; D'hooge, D. R.; Schroeder, G.; Hoogenboom, R. Molecularly Imprinted Polymers with Enhanced Selectivity Based on 4-(Aminomethyl)Pyridine-Functionalized Poly(2-Oxazoline)s for Detecting Hazardous Herbicide Contaminants. *Chem. Mater.* **2022**, *34*, 84–96. https://doi.org/10.1021/acs.chemmater.1c02813.
(125) Diehl, C.; Schlaad, H. Thermo-Responsive Polyoxazolines with Widely Tuneable LCST: Thermo-Responsive Polyoxazolines with Widely Tuneable LCST. *Macromol. Biosci.* **2009**, *9*, 157–161. https://doi.org/10.1002/mabi.200800213.
(126) Park, J.-S.; Kataoka, K. Precise Control of Lower Critical Solution Temperature of Thermosensitive Poly(2-Isopropyl-2-Oxazoline) via Gradient Copolymerization with 2-Ethyl-2-Oxazoline as a Hydrophilic Comonomer. *Macromolecules* **2006**, *39*, 6622–6630. https://doi.org/10.1021/ma0605548.
(127) Konefał, R.; Černoch, P.; Konefał, M.; Spěváček, J. Temperature Behavior of Aqueous Solutions of Poly(2-Oxazoline) Homopolymer and Block Copolymers Investigated by NMR Spectroscopy and Dynamic Light Scattering. *Polymers* **2020**, *12*, 1879. https://doi.org/10.3390/polym12091879.
(128) Zhao, J.; Hoogenboom, R.; Van Assche, G.; Van Mele, B. Demixing and Remixing Kinetics of Poly(2-Isopropyl-2-Oxazoline) (PIPOZ) Aqueous Solutions Studied by Modulated Temperature Differential Scanning Calorimetry. *Macromolecules* **2010**, *43*, 6853–6860. https://doi.org/10.1021/ma1012368.

(129) Obeid, R.; Tanaka, F.; Winnik, F. o. M. Heat-Induced Phase Transition and Crystallization of Hydrophobically End-Capped Poly(2-Isopropyl-2-Oxazoline)s in Water. *Macromolecules* **2009**, *42*, 5818.
(130) Li, T.; Tang, H.; Wu, P. Molecular Evolution of Poly(2-Isopropyl-2-Oxazoline) Aqueous Solution during the Liquid–Liquid Phase Separation and Phase Transition Process. *Langmuir* **2015**, *31*, 6870–6878. https://doi.org/10.1021/acs.langmuir.5b01009.
(131) Sun, S.; Wu, P. Conformational Changes in the Heat-Induced Crystallization of Poly(2-Isopropyl-2-Oxazoline) in the Solid State. *Phys. Chem. Chem. Phys.* **2015**, *17*, 31084–31092. https://doi.org/10.1039/C5CP05719A.
(132) Katsumoto, Y.; Tsuchiizu, A.; Qiu, X.; Winnik, F. M. Dissecting the Mechanism of the Heat-Induced Phase Separation and Crystallization of Poly(2-Isopropyl-2-Oxazoline) in Water through Vibrational Spectroscopy and Molecular Orbital Calculations. *Macromolecules* **2012**, *45*, 3531–3541. https://doi.org/10.1021/ma300252e.
(133) Diehl, C.; Černoch, P.; Zenke, I.; Runge, H.; Pitschke, R.; Hartmann, J.; Tiersch, B.; Schlaad, H. Mechanistic Study of the Phase Separation/Crystallization Process of Poly(2-Isopropyl-2-Oxazoline) in Hot Water. *Soft Matter* **2010**, *6*, 3784. https://doi.org/10.1039/c0sm00114g.
(134) Meyer, M.; Antonietti, M.; Schlaad, H. Unexpected Thermal Characteristics of Aqueous Solutions of Poly(2-Isopropyl-2-Oxazoline). *Soft Matter* **2007**, *3*, 430. https://doi.org/10.1039/b616678d.
(135) Demirel, A. L.; Meyer, M.; Schlaad, H. Formation of Polyamide Nanofibers by Directional Crystallization in Aqueous Solution. *Angew Chem* **2007**, *46*, 8622.
(136) Del Galdo, S.; De Filippo, C. A.; Stefanuto, L.; Sennato, S.; Gasperi, T.; Chiessi, E.; Capone, B. On the Nature of the Thermoresponsiveness of Poly(2-Isopropyl-2-Oxazoline) in Aqueous Solution. *J. Mol. Liq.* **2023**, *392*, 123420. https://doi.org/10.1016/j.molliq.2023.123420.
(137) Lawson, C. L.; Hanson, R. J. *Solving Least Squares Problems*, **1995**. https://doi.org/10.1137/1.9781611971217.
(138) Allen, M. P.; Tildesley, D. J. *Computer Simulation of Liquids*; Oxford university press, 2017.
(139) Eisenhaber, F.; Lijnzaad, P.; Argos, P.; Sander, C.; Scharf, M. The Double Cubic Lattice Method: Efficient Approaches to Numerical Integration of Surface Area and Volume and to Dot Surface Contouring of Molecular Assemblies. *J. Comput. Chem.* **1995**, *16*, 273–284. https://doi.org/10.1002/jcc.540160303.
(140) Luxenhofer, R.; Han, Y.; Schulz, A.; Tong, J.; He, Z.; Kabanov, A. V.; Jordan, R. Poly(2-oxazoline)s as Polymer Therapeutics. *Macromol. Rapid Commun.* **2012**, *33*, 1613–1631. https://doi.org/10.1002/marc.201200354.
(141) Oleszko, N.; Utrata-Wesołek, A.; Wałach, W.; Libera, M.; Hercog, A.; Szeluga, U.; Domański, M.; Trzebicka, B.; Dworak, A. Crystallization of Poly(2-Isopropyl-2-Oxazoline) in Organic Solutions. *Macromolecules* **2015**, *48*, 1852–1859. https://doi.org/10.1021/ma502586x.
(142) Hernández-Ramírez, A.; Hernández-Tenorio, R.; Hinojosa-Reyes, L.; Ramos-Delgado, N.; Guzmán-Mar, J. L. Determination of Pharmaceuticals Discharged in Wastewater from a Public Hospital Using LC-MS/MS Technique. *J. Mex. Chem. Soc.* **2021**, *65*. https://doi.org/10.29356/jmcs.v65i1.1439.
(143) Nakada, N.; Tanishima, T.; Shinohara, H.; Kiri, K.; Takada, H. Pharmaceutical Chemicals and Endocrine Disrupters in Municipal Wastewater in Tokyo and Their Removal during Activated Sludge Treatment. *Water Res.* **2006**, *40*, 3297–3303. https://doi.org/10.1016/j.watres.2006.06.039.
(144) Ciślak, M.; Kruszelnicka, I.; Zembrzuska, J.; Ginter-Kramarczyk, D. Estrogen Pollution of the European Aquatic Environment: A Critical Review. *Water Res.* **2023**, *229*, 119413. https://doi.org/10.1016/j.watres.2022.119413.
(145) Wojnarowski, K.; Podobiński, P.; Cholewińska, P.; Smoliński, J.; Dorobisz, K. Impact of Estrogens Present in Environment on Health and Welfare of Animals. *Animals* **2021**, *11*, 2152. https://doi.org/10.3390/ani11072152.

(146) Alcalde-Garcia, F.; Prasher, S.; Kaliaguine, S.; Tavares, J. R.; Dumont, M.-J. Desorption Strategies and Reusability of Biopolymeric Adsorbents and Semisynthetic Derivatives in Hydrogel and Hydrogel Composites Used in Adsorption Processes. *ACS Eng. Au* **2023**, *3*, 443–460. https://doi.org/10.1021/acsengineeringau.3c00022.
(147) Dreyer, D. R.; Park, S.; Bielawski, C. W.; Ruoff, R. S. The Chemistry of Graphene Oxide. *Chem Soc Rev* **2010**, *39*, 228–240. https://doi.org/10.1039/B917103G.
(148) Thakur, K.; Kandasubramanian, B. Graphene and Graphene Oxide-Based Composites for Removal of Organic Pollutants: A Review. *J. Chem. Eng. Data* **2019**, *64*, 833–867. https://doi.org/10.1021/acs.jced.8b01057.
(149) Shahriary, L.; Athawale, A. Graphene Oxide Synthesized by Using Modified Hummers Approach. *Renew Energy Env. Eng* **2014**, *2*, 58-63
(150) Arsad, I. D. N.; Surani, H.; Nasution, A.; Abd Rashid, A. R. High-Yield and Stepwise Synthesis of Graphene Oxide by Modified Hummers' Method. **2019**.*12*,413-422
(151) Xue, Y.; Liu, Y.; Lu, F.; Qu, J.; Chen, H.; Dai, L. Functionalization of Graphene Oxide with Polyhedral Oligomeric Silsesquioxane (POSS) for Multifunctional Applications. *J. Phys. Chem. Lett.* **2012**, *3*, 1607–1612. https://doi.org/10.1021/jz3005877.
(152) Ohno, K.; Zhao, C.; Nishina, Y. Polymer-Brush-Decorated Graphene Oxide: Precision Synthesis and Liquid-Crystal Formation. *Langmuir* **2019**, *35*, 10900–10909. https://doi.org/10.1021/acs.langmuir.9b01747.
(153) Wang, J. Functionalization of Graphene Oxide with Polysilicone: Synthesis, Characterization, and Its Flame Retardancy in Epoxy Resin. *Polymers* **2021**, *13*, 3857. https://doi.org/10.3390/polym13213857.
(154) Petrović, S.; Savić, S.; Zvezdanović, J.; Nikolić, L.; Stojiljković, S. Benzoic Acid Removal from Aqueous Solutions by Activated Charcoal. *Adv. Technol.* **2021**, *10*, 5–10. https://doi.org/10.5937/savteh2101005P.
(155) Chung, H.-K.; Kim, W.-H.; Park, J.; Cho, J.; Jeong, T.-Y.; Park, P.-K. Application of Langmuir and Freundlich Isotherms to Predict Adsorbate Removal Efficiency or Required Amount of Adsorbent. *J. Ind. Eng. Chem.* **2015**, *28*, 241–246. https://doi.org/10.1016/j.jiec.2015.02.021.
(156) Lesmana, S. O.; Febriana, N.; Soetaredjo, F. E.; Sunarso, J.; Ismadji, S. Studies on Potential Applications of Biomass for the Separation of Heavy Metals from Water and Wastewater. *Biochem. Eng. J.* **2009**, *44*, 19–41. https://doi.org/10.1016/j.bej.2008.12.009.
(157) Ndoun, M. C.; Elliott, H. A.; Preisendanz, H. E.; Williams, C. F.; Knopf, A.; Watson, J. E. Adsorption of Pharmaceuticals from Aqueous Solutions Using Biochar Derived from Cotton Gin Waste and Guayule Bagasse. *Biochar* **2021**, *3*, 89–104. https://doi.org/10.1007/s42773-020-00070-2.
(158) Silva Filho, E. C.; Santos Júnior, L. S.; Silva, M. M. F.; Fonseca, M. G.; Santana, S. A. A.; Airoldi, C. Surface Cellulose Modification with 2-Aminomethylpyridine for Copper, Cobalt, Nickel and Zinc Removal from Aqueous Solution. *Mater. Res.* **2012**, *16*, 79–84. https://doi.org/10.1590/S1516-14392012005000147.
(159) Fox, S. C.; Edgar, K. J. Staudinger Reduction Chemistry of Cellulose: Synthesis of Selectively *O* -Acylated 6-Amino-6-Deoxy-Cellulose. *Biomacromolecules* **2012**, *13*, 992–1001. https://doi.org/10.1021/bm2017004.
(160) Mais, U.; Binder, W. H.; Knaus, S.; Gruber, H. Synthesis and 13C CP MAS NMR Spectroscopy of Cellulose-Graft-Poly(N-Acetylethylenimine). *Macromol. Chem. Phys.* **2000**, *201*, 2115–2122.
(161) El Hamdaoui, L.; Es-said, A.; El Marouani, M.; El Bouchti, M.; Bchitou, R.; Kifani-Sahban, F.; El Moussaouiti, M. Tosylation Optimization, Characterization and Pyrolysis Kinetics of Cellulose Tosylate. *ChemistrySelect* **2020**, *5*, 7695–7703. https://doi.org/10.1002/slct.202001906.
(162) Diop, A.; Awada, H.; Zerrouki, R.; Daneault, C.; Montplaisir, D. Tosylation and Characterization of Lignin in Water. *Ind. Eng. Chem. Res.* **2014**, *53*, 16771–16776. https://doi.org/10.1021/ie502543p.

(163) Renu; Agarwal, M.; Singh, K. Heavy Metal Removal from Wastewater Using Various Adsorbents: A Review. *J. Water Reuse Desalination* **2017**, *7*, 387–419. https://doi.org/10.2166/wrd.2016.104.
(164) Heidari, A.; Younesi, H.; Mehraban, Z. Removal of Ni(II), Cd(II), and Pb(II) from a Ternary Aqueous Solution by Amino Functionalized Mesoporous and Nano Mesoporous Silica. *Chem. Eng. J.* **2009**, *153*, 70–79. https://doi.org/10.1016/j.cej.2009.06.016.
(165) Islam, Md. A.; Morton, D. W.; Johnson, B. B.; Pramanik, B. K.; Mainali, B.; Angove, M. J. Opportunities and Constraints of Using the Innovative Adsorbents for the Removal of Cobalt(II) from Wastewater: A Review. *Environ. Nanotechnol. Monit. Manag.* **2018**, *10*, 435–456. https://doi.org/10.1016/j.enmm.2018.10.003.
(166) Majigsuren, E.; Byambasuren, U.; Bat-Amgalan, M.; Mendsaikhan, E.; Kano, N.; Kim, H. J.; Yunden, G. Adsorption of Chromium (III) and Chromium (VI) Ions from Aqueous Solution Using Chitosan–Clay Composite Materials. *Polymers* **2024**, *16*, 1399. https://doi.org/10.3390/polym16101399.
(167) Aljohani, M. M.; Makki, A. A.; Alqarni, A. A.; Albalawi, K. A.; Albalawi, A. S.; Alharbi, M. J.; Al-Aoh, H. A.; Mustafa, S. K. Adsorbents Used for Removal of Mercury from Aqueous Solutions: A Review. *Int. Res. J. Pure Appl. Chem.* **2022**, 43–55. https://doi.org/10.9734/irjpac/2022/v23i130455.